Sediment fluxes dominate glacial-interglacial changes in ocean carbon inventory: results from factorial simulations over the past 780,000 years

Markus Adloff[1,2], Aurich Jeltsch-Thömmes[1,2], Frerk Pöppelmeier[1,2], Thomas F. Stocker[1,2], and Fortunat Joos[1,2]

[1]Climate and Environmental Physics, Physics Institute, University of Bern, Switzerland
[2]Oeschger Centre for Climate Change Research, University of Bern, Switzerland

Correspondence: Markus Adloff (markus.adloff@unibe.ch)

Abstract. Atmospheric CO_2 concentrations varied over ice age cycles due to net exchange fluxes of carbon between land, ocean, marine sediments, lithosphere, and the atmosphere. Marine sediments and polar ice cores archived indirect biogeochemical evidence of these carbon transfers, which resulted from poorly understood responses of the various carbon reservoirs to climate forcing. Modelling studies ~~proved~~ demonstrated the potential of several physical and biogeochemical processes to impact atmospheric CO_2 under steady-state glacial conditions. Yet, it remains unclear how much ~~they~~ these processes affected carbon cycling during transient changes of repeated glacial cycles, and what role burial and release of sedimentary organic and inorganic carbon and nutrients played. Addressing this knowledge gap, we produced a simulation ensemble ~~of~~ with various idealized physical and biogeochemical carbon cycle forcings over the repeated glacial inceptions and terminations of the last 780 kyr with the Bern3D Earth system model of intermediate complexity, which includes dynamic marine sediments. ~~This ensemble allows for assessing transient carbon cycle changes due to these different forcings and~~ The long simulations demonstrate that initiating transient glacial simulations with an interglacial geologic carbon cycle balance causes isotopic drifts that require several 100 kyr to overcome. These model drifts need to be considered when designing spin-up strategies for model experiments. Beyond this, our simulation ensemble allows for gaining a process-based understanding of the transient carbon fluxes resulting from the forcings, and the associated isotopic shifts that could serve as proxy data~~, in a continuously perturbed Earth system~~. We present results of the simulated Earth system dynamics in the non-equilibrium glacial cycles and a comparison with multiple proxy time series. From this we draw several conclusions: In our simulations, the forcings cause sedimentary perturbations that have large effects on marine and atmospheric carbon storage and carbon isotopes. Dissolved Inorganic Carbon (DIC) changes differ by a factor of up to 28 between simulations with and without interactive sediments, while CO_2 changes in the atmosphere are up to four times larger when interactive sediments are simulated. The relationship between simulated DIC (-1800–1400 GtC) and atmospheric CO_2 change (-170–190 GtC) over the last deglaciation is strongly setup-dependent, highlighting the need for considering multiple carbon reservoirs and multi-proxy analyses to more robustly quantify global carbon cycle changes during glacial cycles. ~~Finally, initiating transient simulations with an interglacial geologic carbon cycle balance causes isotopic drifts that require several 100 kyr to overcome. These model drifts need to be considered~~

~~when designing spin-up strategies.~~

1 Introduction

During the Quaternary, the Earth's carbon cycle repeatedly shifted between low atmospheric CO_2 during glacial periods and elevated mixing ratios during interglacials in orbitally-paced cycles (Petit et al., 1999; Siegenthaler et al., 2005; Lüthi et al., 2008). The reconstructed evolution of atmospheric CO_2 from Antarctic ice cores aligns closely with temperature and is lagged by ice sheet extent, suggesting a close coupling of climate and the carbon cycle (e.g. Shackleton, 2000; Bereiter et al., 2015). Yet, simulating atmospheric CO_2 changes that are consistent with reconstructed CO_2 and other proxy data is challenging because the observed carbon cycle changes were the result of complex Earth system responses to climate forcing (Schmittner, 2008).

Changing ocean chemistry is often attributed an important role in these cycles because of the considerable size of the marine carbon reservoir (Broecker, 1982a) and because reconstructions show that overall there was likely less carbon stored on land (in vegetation, permafrost, peatlands and soils) at the Last Glacial Maximum (LGM) than during the current warm period (Yu et al., 2010; Lindgren et al., 2018; Jeltsch-Thömmes et al., 2019). A multitude of physical and biogeochemical processes have been assessed for their contribution to changes in the marine carbon storage on these timescales (e.g. Kohfeld and Ridgwell, 2009; Sigman et al., 2010; Fischer et al., 2010), and their relative importance for the CO_2 difference between the LGM and the late Holocene have been tested in numerical simulations with dynamic ocean models (e.g. Brovkin et al., 2012; Menviel et al., 2012). Changes in ocean circulation and increased CO_2 solubility due to lower temperatures contributed to the lower glacial atmospheric CO_2 concentration (Broecker, 1982a; Smith et al., 1999; Brovkin et al., 2007; Sigman et al., 2010; Fischer et al., 2010), while increased salinity and surface ocean dissolved inorganic carbon (DIC) concentrations due to lowered sea levels tend to counteract this effect by stimulating CO_2 outgassing to the glacial atmosphere (Weiss, 1974; Broecker, 1982a; Brovkin et al., 2007). Furthermore, reduced CO_2 outgassing from the Southern Ocean due to a greater extent of sea ice isolating the surface ocean from the atmosphere, and enhanced stratification due to brine rejection during sea ice formation are other physical processes suggested to have affected the glacial carbon cycle (Stephens and Keeling, 2000; Bouttes et al., 2010).

Marine biogeochemical processes that lead to lower atmospheric CO_2 include a shift of organic carbon remineralization to greater depths, as well as increased export production due to increased nutrient supply ~~from~~ to the whole ocean. These processes have opposite effects on export production. Nutrient input from the weathering of emerged shelves (phosphate)~~and~~ , changes in nitrogen fixation and dentrification, and enhanced dust deposition (iron, silica) ~~and changes in Southern Ocean dynamics and nutrient utilization, which would have counteracted the effect of colder temperatures and large sea ice extent on surface ocean export production and nutrient utilization (Broecker, 1982b; Martin, 1990; Pollock, 1997; Deutsch et al., 2004)~~ . could had boosted export productivity (Broecker, 1982b; Martin, 1990; Pollock, 1997; Deutsch et al., 2004). On the other hand, a reduced return rate of nutrients from the deep ocean into the surface in response to deeper remineralization might have resulted in more efficient nutrient utilization and less export.

In a (hypothetical) closed atmosphere-ocean system, the combination of these processes results in increased marine carbon storage during glacials, but not necessarily in the open Earth system because the carbon removed from the surface ocean and atmosphere by these processes could have been sequestered ~~in the water column as DIC or particulate carbon but also~~ as particulate carbon in marine sediments ~~. Carbon can also be transferred to the land~~in addition to DIC in the water column. Constraints on glacial atmospheric CO_2 can be reconciled with increased and decreased marine DIC inventory in an open system (Jeltsch-Thömmes et al., 2019; Kemppinen et al., 2019), though reproducing reconstructed carbon isotopic changes in atmosphere and ocean seems to require elevated DIC at the LGM (Jeltsch-Thömmes et al., 2019).

It is very probable that changing sedimentary carbonate and particulate organic carbon (POC) burial played a relevant role in glacial-interglacial carbon cycle changes by altering seawater carbonate chemistry, carbonate ion concentrations, carbon isotope ratios, and oxygenation. Particularly, continental shelves have emerged from the ocean during glacial sea level low stands and provided new reef habitats and carbonate deposition environments during deglaciations and interglacials (e.g. Broecker, 1982b; Opdyke and Walker, 1992; Ridgwell et al., 2003; Brovkin et al., 2007; Menviel and Joos, 2012). Additionally, carbonate burial changes in the open ocean have been considered as amplifiers of marine carbon uptake (e.g. Archer and Maier-Reimer, 1994; Kohfeld and Ridgwell, 2009; Schneider et al., 2013; Roth et al., 2014; Kerr et al., 2017; Kobayashi et al., 2021). Organic carbon burial is also prone to vary in response to changes in the rain rate of POC sinking to the sea floor and altered oxygenation. Previous model simulations ~~, that included POC burial,~~ showed that interactive sediments including POC burial greatly affect atmospheric CO_2 and carbon isotope variations through the burial-nutrient feedback, whereby enhanced burial of organic-bound carbon and nutrients reduces export production (Tschumi et al., 2011; Roth et al., 2014; Jeltsch-Thömmes et al., 2019; Jeltsch-Thömmes and Joos, 2023). Reconstructions of marine burial changes over the last glacial cycle suggest a reduction in globally-integrated inorganic carbon burial (Cartapanis et al., 2018; Wood et al., 2023) during the last glacial period, but increased organic (Cartapanis et al., 2016) sedimentary carbon burial. The ~~extents~~ magnitudes of both changes are uncertain due to the spatial heterogeneity of sedimentary burial and the inherently local nature of marine archives, but possibly of comparable magnitude to terrestrial carbon stock changes (Cartapanis et al., 2016, 2018). These findings demonstrate that organic and inorganic sedimentary changes and imbalances with weathering fluxes need to be considered when quantifying carbon reservoir changes of the ocean, atmosphere, and land and interpreting the reconstructed changes in CO_2, carbonate ion concentrations, isotopes, and nutrients over glacial cycles.

Model-based estimates of carbon and carbon isotope inventory differences between glacial and interglacial periods are complicated by temporal carbon cycle imbalances during the continuously evolving climate of glacial cycles. This is particularly challenging when simulating dynamic elemental cycling in and burial from reactive marine sediments and the input of elements by weathering and volcanic outgassing because of long-lasting re-equilibration and memory effects in carbon and nutrient fluxes and particularly isotopic changes (Tschumi et al., 2011; Jeltsch-Thömmes and Joos, 2020). Dynamic sedimentary adjustment, i.e. the equilibration of sedimentary dissolution and remineralization to changes in bottom water which slowly diffuse into sedimentary porewater, and imbalances between the supply (weathering) and loss (sedimentary burial) of carbon and nutrients ~~also~~ increase the equilibration time of atmospheric CO_2 by a factor of up to 20 to several tens of thousands of years and the resulting $\delta^{13}C$ perturbations take hundreds of thousands of years to recover (Roth et al., 2014; Jeltsch-Thömmes

et al., 2019; Jeltsch-Thömmes and Joos, 2023). Importantly, the equilibration time scales are longer than typical interglacials in the late Pleistocene, which opens up the possibility for memory effects that span several glacial cycles.

A caveat of several modeling studies attempting to quantify carbon reservoir sizes at the LGM is that they assume a steady state carbon cycle in a closed (~~atmosphere-ocean only~~atmosphere-ocean-land, excluding interactive marine sediments) system and do not account for the history of environmental changes that pre-dated the LGM but could have introduced long-lasting memory effects. Transient simulations of an entire glacial cycle with a fully dynamic marine and sedimentary carbon cycle showed that time lags in the carbon cycle response to orbital forcing add constraints for the identification of the processes that caused glacial CO_2 changes (Menviel et al., 2012). In particular, imbalances between marine carbon burial and continental weathering and the long marine residence time of phosphate delay the CO_2 increase during the temperature rise of deglaciations. Accounting for these long-term effects in ~~their~~ the experimental design, transient simulations of more than one glacial cycle showed that reconstructed atmospheric CO_2 and benthic marine $\delta^{13}C$ changes over the last 400 kyr could be reasonably well simulated with a combination of physical (radiative and ocean volume changes) and biogeochemical processes ~~((carbonate chemistry and land carbon changes, temperature-dependent remineralization depth, additional nutrient supply during glacials,~~ (carbonate chemistry and land carbon changes, temperature-dependent remineralization depth, additional nutrient supply during glacials, s . Yet, shallow water carbonate burial was prescribed and POC burial not included in the simulations, which begs the question~~how the effect~~ : what were the effects of the considered processes on glacial-interglacial atmospheric CO_2 and carbon isotopic ratios changes if the sediments are dynamically calculated. Recently, simulations of glacial-interglacial cycles beyond the Mid-Brunhes transition (~430 ka) were run with a box model (Köhler and Munhoven, 2020) and a purely physical model (Stein et al., 2020) which are unable to capture transient and spatially heterogeneous interactive sediments. CLIMBER-2, a fully coupled intermediate-complexity Earth system model, was run stepwise over the last 3 Myr, but the results were not analysed for the carbon cycle dynamics (Willeit et al., 2019).

Here we examine systematically how the transient built-up and dissolution of marine sediments on glacial-interglacial timescales affects the carbon cycle changes produced by the various processes suggested to be relevant on these timescales, a gap left by previous studies. We consider explicitly burial of organic carbon and opal, in addition to $CaCO_3$. Instead of searching for the most likely scenario that reconciles the vast proxy evidence, we attempt to gain a more complete process understanding and overview of the proxy-relevant signals that these processes cause in the presence of weathering-burial imbalances. With this goal, we extend factorial simulations of multiple simplified physical and biogeochemical forcings in a marine sediment and isotope-enabled intermediate complexity Earth system model over the last 780 kyr and compare the resulting carbon and carbon isotopic signals to reconstructions. The long timescale is chosen to avoid biases resulting from steady state assumptions and account for the possibility of memory effects under continuously varying climate and carbon cycle that could span multiple glacial cycles. Consequently, all carbon stores are achieved dynamically rather than being prescribed. We present two sets of simulations with and without interactive sediments to distinguish the role of interactive sediments in the carbon cycle changes caused by the tested forcings over reoccurring glacial cycles of the last 780 kyr.

2 Methods

2.1 Bern3D v2.0s

We simulated the Earth system's transition through the last 780 kyr of glacial cycles with the intermediate complexity Earth system model Bern3D v2.0s, which has an irregular 41×40 grid (lowest resolution: lat×lon = 5°×10° in the North Pacific, highest resolution: lat×lon = 3°×7° in the Equatorial Atlantic) in the horizontal and 32 logarithmically spaced ocean depth layers. The model combines modules for 3D physical ocean dynamics, marine biogeochemistry, marine interactive sediments, and atmospheric energy-moisture balance.

The physical ocean component transports tracers through the ocean by advection, convection, and diffusion. Euphotic zone production depends on temperature, light, sea ice cover, and nutrient (phosphate, iron, silica) availability (Parekh et al., 2008; Tschumi et al., 2011) and explicitly calculates carbon isotope dynamics (Jeltsch-Thömmes et al., 2019). In our setup, a fraction of the particulate organic matter formed in the surface ocean is instantly remineralized following an oxygen concentration dependent version of the globally-uniform Martin curve (Battaglia and Joos, 2018) and particulate inorganic carbon and opal dissolution occurs according to globally-uniform e-folding profiles. The remaining solid particles reaching the sediment-ocean interface enter reactive sediments, where they are preserved, remineralized, or redissolved depending on dynamically calculated porewater chemistry, and mixed by bioturbation (Tschumi et al., 2011). $CaCO_3$ dissolution rates in the sediments are determined from the pore water saturation state, and POC remineralisation is parameterised by a linear dependence on porewater O_2 (Heinze et al., 1999; Tschumi et al., 2011). The model contains 10 layers of reactive sediments. As matter gets pushed downward out of the bottom layer ('sedimentary burial'), it is lost to the modelled inventories. These loss fluxes of C, ^{13}C, Alk, P, and Si are at equilibrium compensated for by a corresponding solute input flux from land into the coastal surface ocean. The (pre-industrial) land-sea mask and bathymetry are fixed throughout the spin-up and simulations.

2.2 Model spin-up with interglacial boundary conditions

We spun up the model with pre-industrial boundary conditions in three stages, sequentially coupling all modules, for computational efficiency. First, we forced the ocean circulation and then the atmosphere-ocean carbon cycle as a closed system with pre-industrial climatic conditions and prescribed CO_2 for 20 kyr. In the next step, the sediment module is coupled and terrestrial solute supply (phosphate, alkalinity, DIC, DI^{13}C and Si) to the ocean is set to dynamically balance the loss through sedimentary burial for 50 kyr. At the end of this stage, the solute input flux, hereafter named 'weathering input', required to balance sedimentary burial is diagnosed (Table S1) and kept constant for the rest of the spin up procedure and throughout our transient experiments. Until this stage, atmospheric CO_2 and δ^{13}C were prescribed. The spun up model for the pre-industrial was then run for 2000 years as an open system (freely evolving CO_2 and δ^{13}C) with radiative forcing that varied linearly from PI to the slightly different MIS19 conditions, the starting point of our experiments. The total length of the spin-up to this point was 72 kyr. To avoid large drifts in carbon isotopes and alkalinity ~~(Jeltsch-Thömmes and Joos, 2023, explained at the end of our results section)~~ (Jeltsch-Thömmes and Joos, 2023, explained at the end of section 3.5) in the simulations with the forcings that perturbed the carbon cycle the most (PO4, REMI, LAND, CO2T, BGC, ALL, described in the next section), we ran the fully-interactive

model with each respective forcing for two glacial cycles (215 kyr) before starting our experiments. We discuss the relevance of initial conditions and imbalances of the geologic carbon cycle at the end of the manuscript. Model limitations due to constant terrestrial solute supply are discussed in the supplementary material (section SI.5).

2.3 Experimental design

Data constraints on carbon cycle forcings are too sparse to know exact magnitudes and timings of the forcings that might have varied spatially and temporarily over the last eight glacial cycles. An inverse estimation of the forcings from the resulting proxy signals requires a different simulation ensemble and is beyond the scope of our study. Rather than trying to guess the most proxy consistent forcing amplitudes and patterns, we designed seven simplified forcings, each with one exemplary magnitude, to simulate the generic effects of processes that have been identified as glacial-interglacial carbon cycle drivers. Except for the orbital changes, which were calculated following Berger (1978); Berger and Loutre (1991) and the reconstructed CO_2, N_2O and CH_4 curves (Loulergue et al., 2008; Joos and Spahni, 2008; Bereiter et al., 2015; Etminan et al., 2016), which we used to calculate the radiative forcing of greenhouse gas changes, the amplitudes of the forcings were set to cause noticeable CO_2 or circulation shifts, informed by previous studies (e.g. Tschumi et al., 2011; Menviel and Joos, 2012; Menviel et al., 2012; Jeltsch-Thömmes et al., 2019; Pöppelmeier et al., 2020). We produced timeseries of these forcings by defining a maximum forcing amplitude for the LGM, a minimum for the Holocene and then modulating this amplitude by reconstructed relative changes in the temporal evolution of either Antarctic ice core δD (Jouzel et al., 2007) or benthic δ^{18}O (Lisiecki and Raymo, 2005) for each year (Fig. 1). The choice of the isotope record for calculating the instantaneous forcing depends on whether we expect the forcing to evolve synchronously with temperature like δD or have a time lag similar to δ^{18}O (see section SI.5 for a discussion of the limitations). In all simulations, we prescribed the radiative effect of CO_2 in the atmosphere, so that all simulations have the same radiative forcing from greenhouse gases despite differences in simulated CO_2.

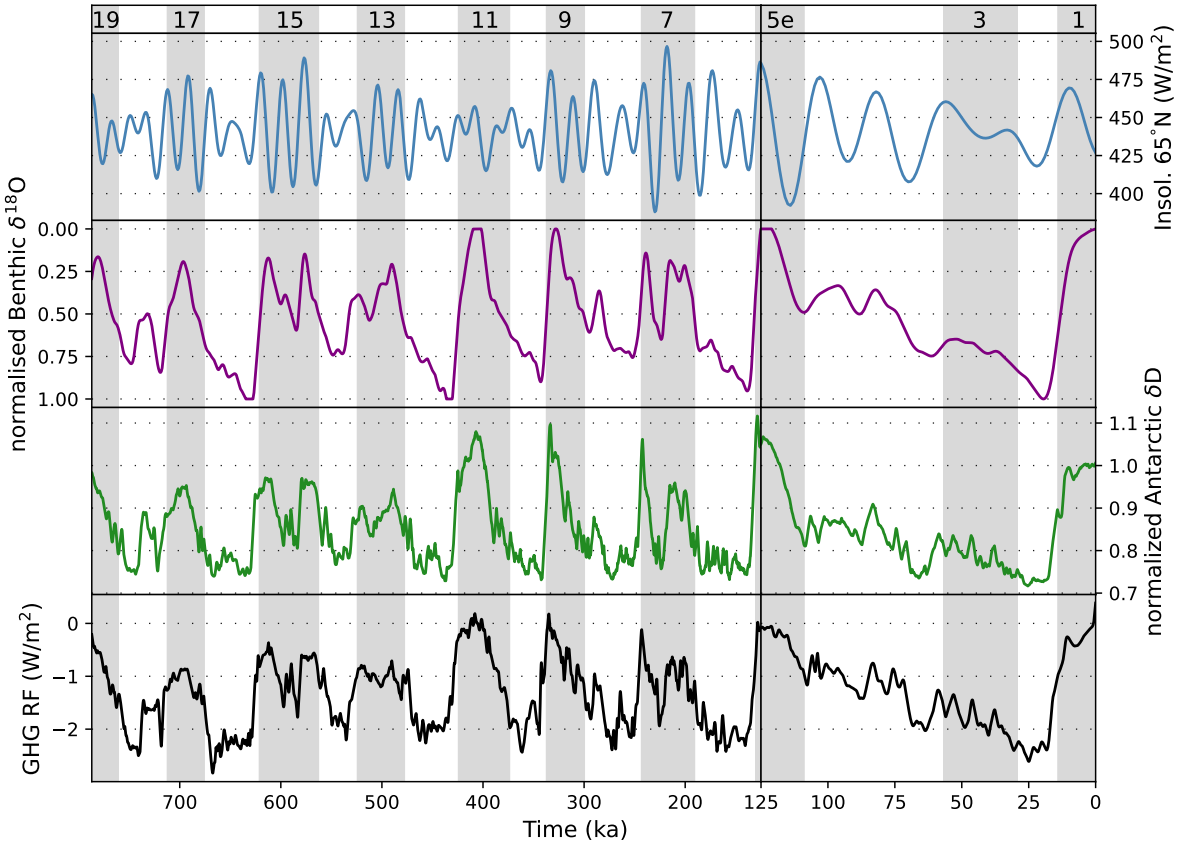

Figure 1. Forcing timeseries. Insolation changes (top panel) are calculated according to Berger (1978); Berger and Loutre (1991). The δ^{18}O forcing (second panel) is the LR04 stack (Lisiecki and Raymo, 2005), smoothed by averaging over a 10000-year moving window and normalized to the LGM-PI difference. The δD forcing (third panel) is taken from Jouzel et al. (2007) and normalized to the LGM-PI difference. The radiative forcing (RF) of CO_2, N_2O and CH_4 (~~greenhous gasses~~ greenhouse gases 'GHG', bottom panel) is calculated from Bereiter et al. (2015); Loulergue et al. (2008); Joos and Spahni (2008) following Etminan et al. (2016). Gray shading indicate uneven Marine Isotope Stages (MIS).

Specifically, we performed one 'base' run with orbital and radiative forcing only, one model run for different forcings, each added to the base forcing, and combinations of the individual forcings to study non-linear effects that appear when processes interact. All of these experiments are run once with and once without interactive sediments, to examine the effect of sediment perturbations on the results. The forcings and their rationale are described below. The experiments are summarized in Table 1.

The application of the standard forcing in simulation BASE causes temperature changes associated with orbital, albedo, and greenhouse gas changes which affect solubility, sea ice and circulation, e.g. slightly weakening AMOC (by up to 4.5 Sv, Fig. S8) and resulting in younger deep water masses in the Atlantic and Pacific during the LGM than at the PI, which is inconsistent with proxy data and thus indicates that additional Earth system changes must have occurred (Pöppelmeier et al., 2020). To achieve an older glacial deep ocean (diagnosed with an ideal age tracer), we reduced the wind stress south of 48 °S by a maximum of 40 % (simulation SOWI) temporally changing proportionately to the δD change because we assume that wind strength over the

Southern Ocean evolved without temporal lags to Antarctic temperature. As a result, the South Pacific downwelling is strengthened by up to 1.5 Sv locally in glacials, AMOC strength is further reduced by up to 1 Sv and the simulated deep ocean age is ∼100 years older in the LGM than in the PI, close to published model estimates (Schmittner, 2003). In this set-up, changing wind stress only affects the circulation, not the piston velocity of gas exchange, which is forced by a wind-speed climatology. For an independent assessment of the effect of wind speed changes on sea-air gas exchange, we performed a simulation in which we decreased the piston velocity in the Southern Ocean by a maximum of 40 % (KGAS), also following the evolution of δD. Next, we ~~tested an~~ simulated the additional negative radiative forcing due to increased ~~dust~~ aerosol loads in the glacial atmosphere ~~(e.g. Claquin et al., 2003) by~~ (AERO, e.g. Claquin et al., 2003) by further reducing the total radiative forcing by a maximum of 2.5 W/m^2 during the LGM~~to test the effects of stronger AMOC weakening (AERO)~~, modulated by the δ^{18}O record based on the reconstructed correlation between dust and δ^{18}O (Winckler et al., 2008, similar to the study of long-term circulation changes in Adloff et al. (2024)). Under this forcing, the AMOC does not shut down but weakens by up to 12 Sv relative to PI during glacial maxima ~~(the model behaviour to this forcing is described more extensively in Adloff et al., 2024) and~~ due to density changes and sea ice advance in the North Atlantic (the model behaviour under this forcing is described more extensively in Adloff e and deep North Atlantic water mass age rises to up to 1000 years~~in the deep North Atlantic as glacial deep water formation now only occurs in the Southern Ocean.~~ .

In terms of biogeochemical forcings, we mimicked five process that would have occurred during glacial cycles but are not dynamically simulated by our model. First, we added a terrestrial carbon sink/source by removing/adding 500 PgC during deglaciation/ice age inception ~~(LAND Jeltsch-Thömmes et al., 2019) and increased the~~ to simulate the marine impact of climate-driven carbon cycle changes on land (LAND Jeltsch-Thömmes et al., 2019). Second, we reduced nutrient limitation on glacial export production (PO4) with a globally-uniform addition of phosphate, the only export-limiting nutrient in our model-setup, into the surface ocean, increasing the marine phosphate inventory by 30 % during the glacial maxima~~by a globally-uniform supply of phosphate into the surface ocean (PO4)~~. The timeseries of ~~both forcings~~ LAND and PO4 are proportional to δ^{18}O changes, because we assume that both are lagging behind temperature changes due to continental ice-sheets and changing terrestrial environments. Effectively, our nutrient forcing reduces nutrient limitation globally. Rather than simulating the effects of different nutrient inputs in different regions (e.g. iron in the Southern Ocean, phosphate at shelves), we decided to group all these in one simulation with a global forcing because their net effect, increased export production, would be the same in our model, just in different regions. This is the only forcing that we did not apply to the model without interactive sediments because, while nutrients can be added to the surface ocean periodically, there is no simple way of artificially extracting nutrients from the ocean in return. ~~We also~~ Third, we reduced the speed of aerobic organic matter remineralization in the ocean to simulate temperature-driven changes in respiration rates by transitioning between the standard, pre-industrial Bern3D particle profile (Martin scaling) during interglacials and a linear profile in the first 2000 m of the water column (REMI, Fig. S9), following the δD record, since we assume that remineralization changes happened synchronously with temperature change. ~~Next~~Fourth, we reduced the PIC:POC rain ratio by 33 % in the LGM (PIPO) and similarly modulated the forcing timeseries with the δD record. ~~In addition~~ This simulation mimics the effect of an ecological shift in marine primary producers on the composition of biogenic marine particles. Fifth, we performed one run in which we let the model dynamically apply

external alkalinity (ALK) fluxes (in addition to the constant terrestrial solute supply applied in each simulation, see spin-up methodology) to restore the reconstructed atmospheric CO_2 curve (CO2T). In this simulation, the model evaluates the difference between the simulated and reconstructed CO_2 at each time step and adds or removes the marine ~~alkalinity~~ ALK required to cause the necessary compensatory air-sea carbon flux from the surface ocean. ~~Alkalinity~~ ALK changes, e.g. due to changes in shallow carbonate deposition or terrestrial weathering, are an effective lever for atmospheric CO_2 change (e.g. Brovkin et al., 2007), and this additional run shows the long-term changes in marine biochemistry if this was the dominant driver of glacial-interglacial atmospheric CO_2 change.

Table 1. Forcing scenarios. Simulations are run in two configurations: the standard setup with interactive sediments and a closed-system setup without sediments (except PO4).

ID	Description	LGM-PI amplitude	Modulating proxy
BASE	orbital changes + radiative effect of greenhouse gasses + ice sheet albedo		CO_2, CH_4, $\delta^{18}O$
SOWI	BASE + Wind stress strength over Southern Ocean (>48 °S)	-40%	δD
KGAS	BASE + gas transfer velocity in Southern Ocean	-40%	δD
AERO	BASE + Radiative forcing from dust particles	-2.5 W/m^2	$\delta^{18}O$
PHYS	BASE + all physical forcings combined		
LAND	BASE + land carbon storage	-500 PgC	$\delta^{18}O$
REMI	BASE + linear glacial remineralization profile in upper 2000m	linear	δD
PIPO	BASE + PIC:POC changes	-0.33	δD
PO4	BASE + marine PO_4 reservoir	+30%	$\delta^{18}O$
BGC	BASE + all biogeochemical forcings combined		
ALL	BASE + all forcings combined		
CO2T	BASE + restoring reconstructed atm. CO_2 concentrations	-90 ppm	CO_2

For the discussion of the simulations, we quantify the factorial effect of the simulated forcings on different carbon cycle metrics. In simulation BASE, only the standard forcing is active (see table 1), hence the factorial effect of the standard forcing is equal to the simulated change:

$$fBASE = \text{BASE}$$

In the simulations that combine the standard forcing with one other forcing, the factorial effect of the additional forcing is the difference between the respective simulation and BASE:

$$fFORC = \text{FORC} - fBASE$$

In simulations PHYS, BGC and ALL several forcings are combined. We use these simulations to determine non-linearities by calculating the difference between the results of these simulations and the linear addition of the individual effects of the active forcings:

$$nlPHYS = \text{PHYS} - (fBASE + fKGAS + fSOWI + fAERO)$$

$$nlBGC = \text{BGC} - (fBASE + fREMI + fPO4 + fPIPO + fLAND)$$

$$nlADD = \text{ALL} - \text{PHYS} - \text{BGC} + \text{BASE}$$

$$nlTOT = nlPHY + nlBGC + nlADD$$

3 Results

The general response of marine biogeochemistry to the applied forcings has been tested and described in previous studies (e.g. Tschumi et al., 2008, 2011; Menviel and Joos, 2012; Menviel et al., 2012; Jeltsch-Thömmes et al., 2019; Jeltsch-Thömmes and Joos, 2020), here we therefore just provide a brief summary and focus more extensively on their effect on the ~~sediments~~sediment fluxes. A more detailed analysis of the model behaviour under each forcing is provided in the supplementary material.

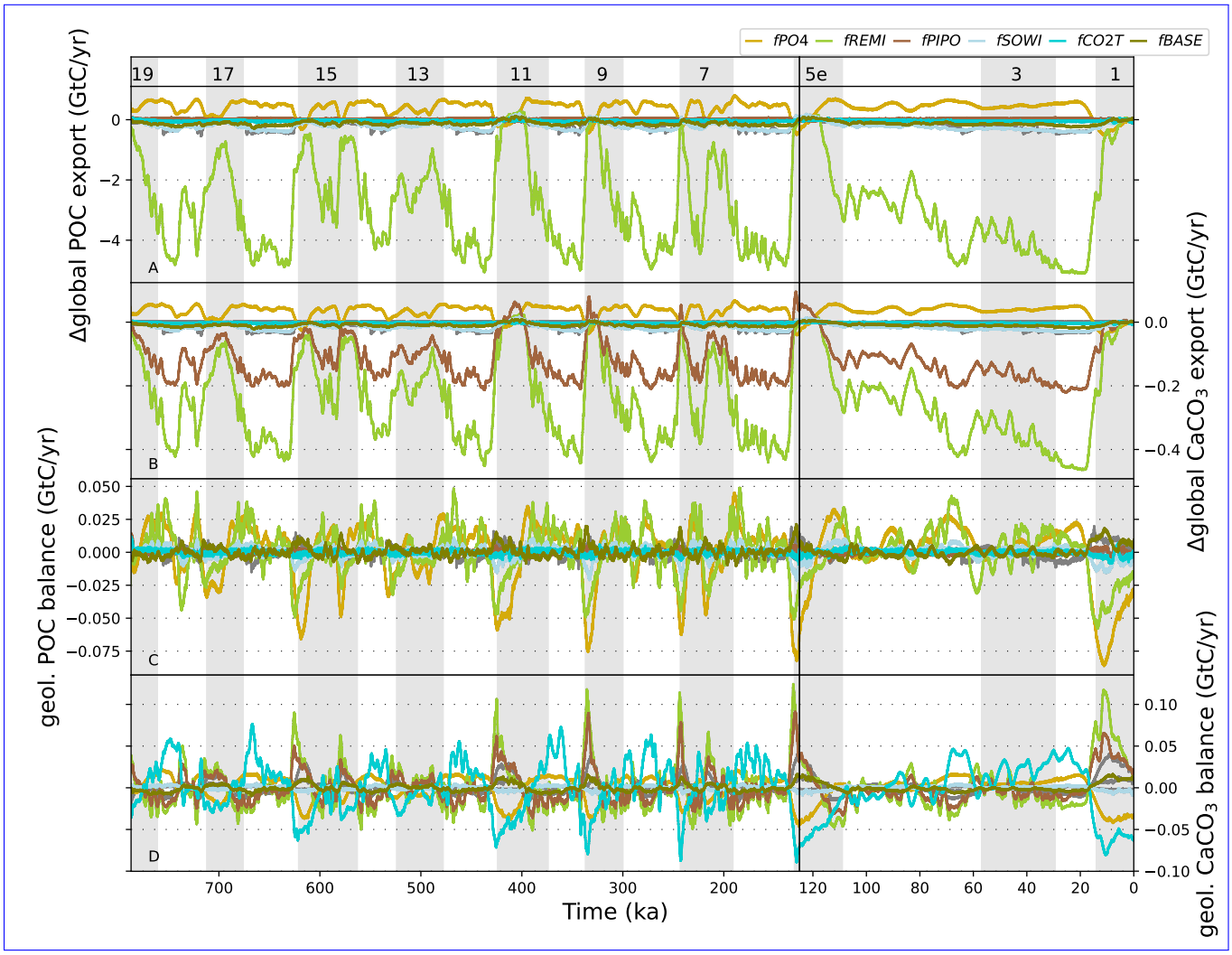

Figure 2. Transient ~~variations~~ changes of POC and $CaCO_3$ export production and geologic imbalance (i.e. the difference between accumulation of these materials in marine sediments and the lithosphere minus the constant supply into the surface ocean that mimics terrestrial weathering and volcanism in our simulations) due to the applied forcings. Shown are the factorial ~~results~~ differences from pre-industrial for each simulation. The results that are explicitly mentioned in the text are shown in colour, the others are shown in gray. Gray shading indicates uneven MIS as indicated at the top of the figure. See Fig. S10 for absolute ~~changes~~ rather than factorial differences from pre-industrial in ~~the~~ each simulations.

In our set-up, carbon exchange between the atmosphere, ocean, and sediments and the burial flux to the lithosphere reacts to climatic and biogeochemical changes while weathering input fluxes of DIC, ~~alkalinity, and~~ ALK, PO_4^{3-}, Si, and ^{13}C are constant over time. Thus, a carbon flux imbalance arises in our simulations in response to the applied forcings (Fig. 2 for factorial ~~results, see~~ differences and Fig. S10 for absolute ~~fluxes~~differences). All forcings except $fPO4$ reduce global export production during glacial phases (Fig. 2A and B), either due to cooling and expanding sea ice or increased nutrient limitation. In addition to export production, the net ~~C exchange~~ exchange of carbon and other elements between sediments and the ocean is changed

by the applied forcings via changing benthic seawater composition, either through circulation, solubility, or biogeochemical changes. Cooling (in $fBASE$) reduces global sediment accumulation rates of $CaCO_3$ and POC during glacial phases due to the ~~reductions in~~ reduced export production (~~$fBASE$~~Fig. 2C and D). In consequence, sequestration of $CaCO_3$ and POC from the reactive sediments (i.e. sedimentary burial) is also reduced in response to these forcings, since it is governed by the sedimentary mass accumulation rate. Instead, reduced ~~marine O_2, due to the deepened remineralization~~ nutrient limitation during glacial phases ($fPO4$) causes more, rather than less, export production during glacial phases. Deepening of the main remineralization depth ($fREMI$) ~~,~~ increases the preservation of sedimentary POC during glacials by reducing marine O_2. Hence, under this forcing, POC accumulation is higher during glacial than interglacial phases, while the opposite temporal change occurs for $CaCO_3$ accumulation due to reduced $CaCO_3$ export production. ~~Reduced nutrient limitation during glacial phases ($fPO4$) causes more, rather than less, export production during glacial phases.~~ Increased ALK supply in simulation CO2T causes larger sedimentary $CaCO_3$ accumulation during glacial phases when ALK input increases $CaCO_3$ stability and dissolution events during deglaciations when ALK is removed.

How do the simulated sedimentary changes in our factorial setup compare in magnitude and sign with carbon cycle proxy records?

We discuss this question first by focusing directly on changes in the carbon stored as sedimentary organic and inorganic matter and changes in the benthic carbonate system, before studying their effects on four essential carbon cycle metrics: deep ocean CO_3^{2-} atmospheric CO_2, marine DIC, and $\delta^{13}C$. Individual proxy records were selected for their resolution or length. This is not an attempt at a comprehensive compilation of proxy records, nor an attempt to understand individual records in detail. ~~Rather we aim to understand why the tested forcings do or do not reproduce prominent spatial or temporal patterns in the proxy records. It is also important to note that our~~ Our simulations are designed to constrain the potential and plausibility of major contributions of the tested forcings to the observed glacial-interglacial atmospheric CO_2 changes, rather than reproducing a full, realistic scenario. We therefore do not expect that any single simulation presented in our study captures all features of the reconstructed carbon cycle changes over glacial-interglacial cycles. Instead, we investigate ~~the isolated forcings , which~~ in isolation the forcings that would have to some extent occurred simultaneously in reality, and quantify their effects during eight consecutive glacial cycles. Comparing our results to selected proxy records, we discuss processes behind specific patterns of carbon cycle change and the role of weathering-burial imbalances in these. ~~the remaining challenges in reconciling the many carbon cycle reconstructions that are now available.~~

3.1 Sedimentary burial and CO_3^{2-} concentrations

Reconstructions of global POC burial flux changes over the last glacial cycle (Cartapanis et al., 2016) indicate that POC burial was smallest during interglacials, and gradually rose during glacial phases until it peaked during the LGM. $fSOWI$, $fREMI$ and $fPO4$ are the only effects which produce higher POC burial fluxes during glacial maxima than during interglacials (Fig. 2), and the latter two are the only ones strong enough to overprint the opposite effect due to cooling ($fBASE$, Fig. S10). However, the simulated increase in POC burial already occurs during the glacial inception, such that the highest burial rates persist throughout most of the glacial phase while in the reconstructions they remain close to the interglacial value through

MIS4. Reconstructions of global $CaCO_3$ burial changes over the last glacial cycle (Cartapanis et al., 2018) show that burial rates decreased in most ocean basins during glacial inception ~~, while they~~ but increased in the Southern Ocean, resulting in ~~only minor glacial-interglacial~~ almost no changes in the global average before MIS3. Physical forcings (e.g. $fSOWI$ in Fig. 2) do not affect global $CaCO_3$ burial rates during glacial inception, consistent with the reconstruction, while $fPO4$ and $fCO2T$ produce global burial increases and $fPIPO$ and $fREMI$ produce decreases between MIS5 and MIS3. However, the physical forcings fail to ~~decrease~~ produce lower $CaCO_3$ burial rates during MIS3 und MIS2. $fREMI$ and $fPIPO$ decrease $CaCO_3$ burial during MIS3 and MIS2 but cause much larger burial events in MIS1 than reconstructed (Fig. 2, see also Figs S2, S4, S5, S6, S7).

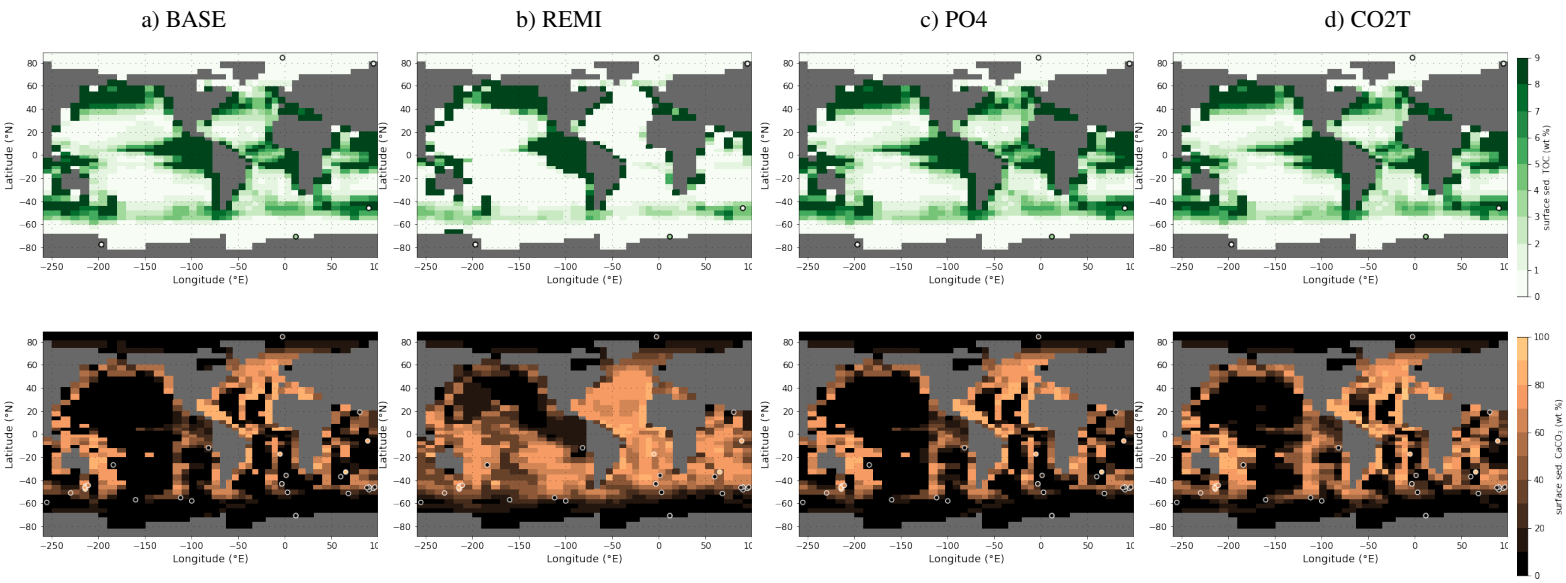

Figure 3. Sedimentary POC and $CaCO_3$ fractions during LGM ~~(Cartapanis et al., 2016; Wood et al., 2023)~~ as reconstructed ~~(circles)~~ (circles, records for POC and $CaCO_3$ are from Cartapanis et al., 2016; Wood et al., 2023, , respectively) and in simulations PHYS, REMI, PO4 and CO2T (underlying maps). Shown are only data points that fall into the local benthic grid box of the model. The root mean square errors of simulated and reconstructed values are (from left to right): 7.4 wt %, 3.3 wt %, 7.4 wt % and 6.4 wt % for POC (top row) and 33.6 wt %, 31.5 wt %, 33.3 wt % and 34.4 wt % for $CaCO_3$ (bottom row).

Most forcings increase the POC content of surface sediments (top 10 cm) during the LGM (Fig. 3 top row), the exception being $fREMI$, which decreases POC outside the East Pacific. However, too few reconstructions exist for depths that are consistent with our model bathymetry for a quantitative model-data comparison. For $CaCO_3$, a few more data points fall within our benthic ocean grid cells. The cooling-related changes ($fBASE$) included in all simulations reproduce a data-consistent carbonate compensation depth (CCD) in most of the Southern Hemisphere extra-tropics but a too high CCD in the tropical South Atlantic and Indian Ocean and a too low CCD off Peru (Fig. 3 bottom row). REMI better captures these tropical CCD changes but produces a too low extra-tropical CCD. These model-data differences indicate that different processes might explain the LGM sedimentary composition in different basins, which is not captured by our globally uniform forcings.

The model has been tuned to the pre-industrial $CaCO_3$ distribution. However, in our study late Holocene $CaCO_3$ contents are the result of almost 800 kyr of transient simulation, which result in imbalances of the geologic carbon cycle at the simulation end even though the forcing is that of the Holocene (Table S2). Differences between the dynamically-achieved and observed pre-industrial sedimentary composition add context to the size of the simulated sedimentary fluxes and memory effects. The dynamically-evolved sedimentary POC content is similar across all simulations, while the $CaCO_3$ content exhibits large-scale differences (Fig. S11, S12). Simulations with small sediment perturbations during the glacial cycle (e.g. SOWI, AERO and LAND, Fig. S12) result in $CaCO_3$ contents that are similar to Holocene estimates. In simulations REMI and PIPO, the large deglacial $CaCO_3$ burial event results in higher sedimentary $CaCO_3$ contents in the late Holocene than measured. Simulation CO2T, on the other hand, has less sedimentary $CaCO_3$ content during the late Holocene than measured. This is the result of strong dissolution due to forced ~~alkalinity~~ ALK removal from the open ocean during deglaciations, mimicking e.g. coral reef building. It is therefore less likely that sedimentary $CaCO_3$ was perturbed to the extent simulated in REMI, PIPO and CO2T.

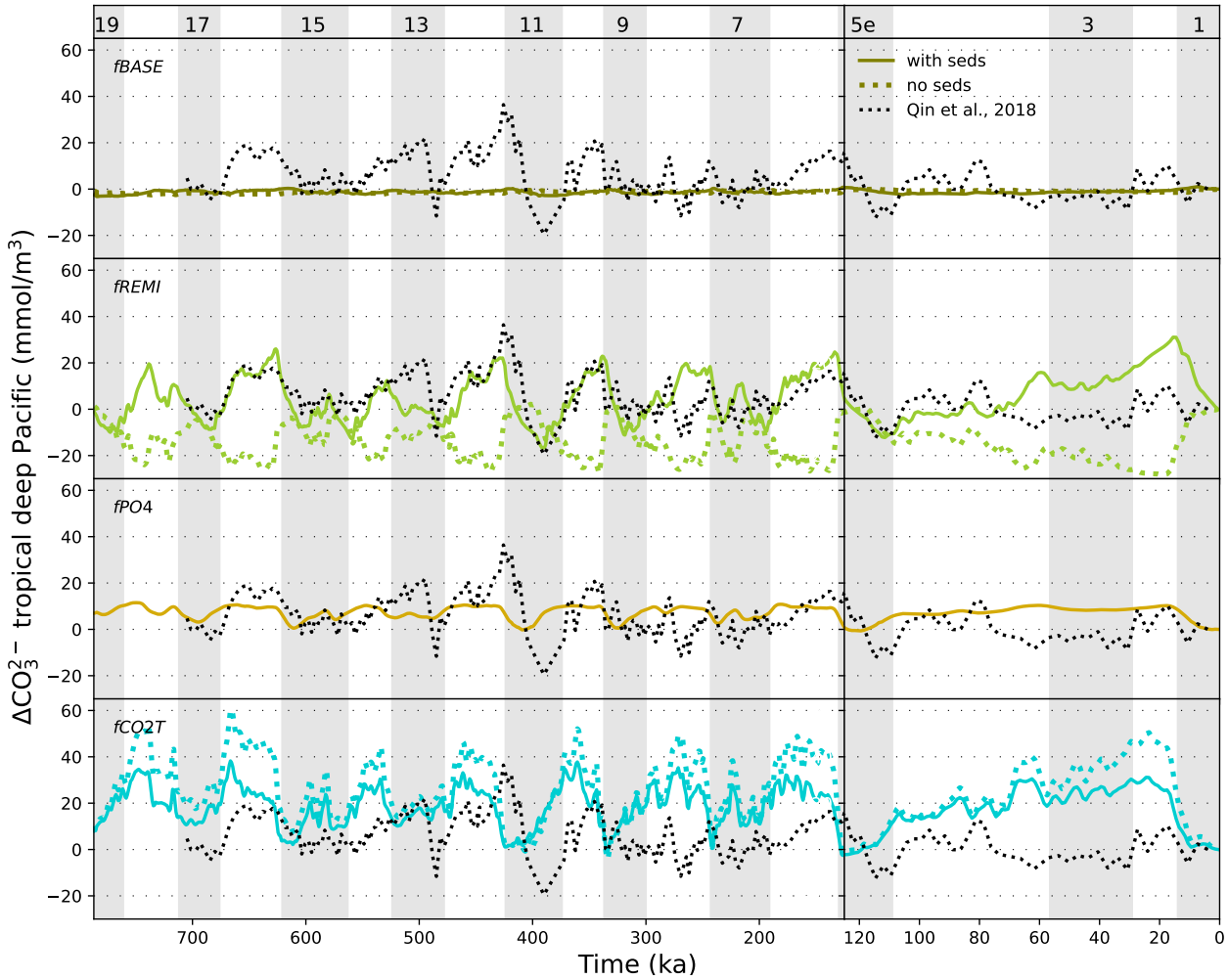

Figure 4. Evolution of CO_3^{2-} in the tropical deep Pacific as simulated for $fBASE$, $fREMI$, $fPO4$ and $fCO2T$ (from top to bottom) and reconstructed by Qin et al. (2018). The results of the other forcings are shown in Fig. S13.

Next, we address [CO_3^{2-}] changes. Kerr et al. (2017) found a repeated pattern of low benthic [CO_3^{2-}] in the tropical Pacific and Indian Ocean during interglacials and high [CO_3^{2-}] during glacials (difference of 20-55 mmol/m^3) throughout the last 500 kyrs. Qin et al. (2018) found that the same pattern extended over the last 700 kyrs, to our knowledge the longest [CO_3^{2-}] record. Physical forcings ($fBASE$, $fKGAS$, $fSOWI$, $fAERO$, $fPHYS$) and $fPO4$ have little effect on deep Pacific [CO_3^{2-}] over glacial cycles (Fig. 4, S13). Under the biogeochemical forcings ($fREMI$,$fPO4$, $fPIPO$, $fLAND$) ~~,~~ the simulated glacial-interglacial [CO_3^{2-}] difference ranges from a few mmol/m^3 to 50 mmol/m^3 ~~,~~ and is caused by invasion of CO_2 into the ocean, ALK redistributions within the ocean, and weathering-burial imbalances due to changes of the carbonate ex-

port flux and carbonate compensation ~~(Broecker and Peng, 1987, , Fig. 4 and S13)~~(Broecker and Peng, 1987, Fig. 4 and S13). $fREMI$ and $fCO2T$ cause the largest [CO_3^{2-}] changes in the deep equatorial Pacific. For the last glacial cycle, these simulated changes are larger than those reconstructed, suggesting that the forcings cause too large ALK re-distributions within the ocean or carbonate compensation during the last glacial cycle. Interestingly, however, during MIS13-MIS11 and the Mid-Brunhes transition, reconstructed [CO_3^{2-}] changes in the deep equatorial Pacific were larger than during the last glacial cycle (Qin et al., 2018, , Fig. 4). $fCO2T$ and $fREMI$, which produced larger-than-reconstructed [CO_3^{2-}] changes over the last glacial cycle, produced [CO_3^{2-}] changes more similar to those reconstructed for MIS13-MIS11. The variability of [CO_3^{2-}] amplitudes between glacial cycles in the record is not reproduced by any of our forcings~~, but~~.

While the reconstructed deep ocean [CO_3^{2-}] reservoir in the Pacific was relatively stable over the last deglaciation, a large [CO_3^{2-}] increase was reconstructed for the deep Atlantic (Qin et al., 2018; Yu et al., 2019). The different sensitivities of deep ocean [CO_3^{2-}] in the two basins is also apparent in all of our simulations (see examples in Fig. S14 and S15) and is the result of larger circulation and productivity changes in the Atlantic than Pacific. However, circulation changes produce lower [CO_3^{2-}] in the deep sub-polar North Atlantic during the LGM, while reconstructions suggest higher [CO_3^{2-}] ~~(Yu et al., 2019)~~ (Fig. S16A, Yu et al., 2019). Higher deep Atlantic [CO_3^{2-}] at the LGM requires increased nutrient supply ($fPO4$), deeper remineralization ($fREMI$) or a net ~~alkalinity~~ ALK input ($fCO2T$) ~~.~~ (Fig. S16B). These patterns appear with and without dynamic sediments in our simulations. Sediments mostly affect the amplitude and temporal evolution of deep [CO_3^{2-}] changes, not their spatial pattern (not shown).

3.2 Atmospheric CO_2

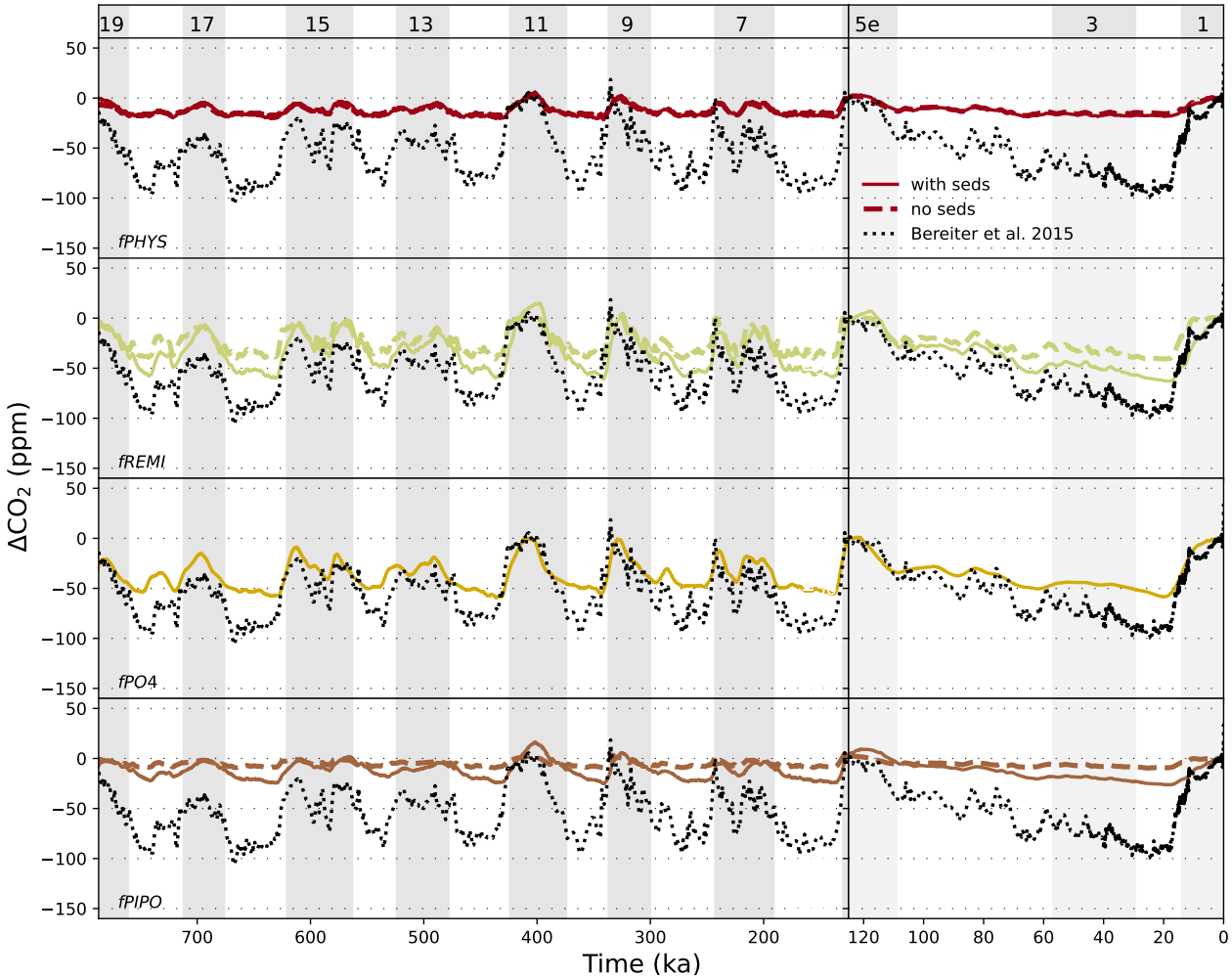

Figure 5. Transient variations of atmospheric CO_2 due to effects $fPHYS$, $fPO4$, $fREMI$, and $fPIPO$ and reconstructed by Bereiter et al. (2015). Shown is the deviation from the pre-industrial value. Gray shading indicates uneven MIS as indicated at the top of the figure. Dashed lines denote runs without sediment module (not available for PO4). The same plots for the other simulations are shown in S17.

Interactive sediments have a negligible effect on the atmospheric CO_2 changes caused by physical forcings but largely alter the CO_2 change effect of biogeochemical forcings (Fig. 5). Marine CO_2 uptake and reduced export production due to physical forcings ~~causes~~ cause a net dissolution/reduced deposition of sedimentary $CaCO_3$ during glacials and marine ~~alkalinity~~ ALK and DIC build up as a consequence. A large fraction of the glacial DIC pool is eventually incorporated into $CaCO_3$ and deposited during deglaciations with little effect on outgassing. Under ~~biogeochemcial~~ biogeochemical forcings, the larger $CaCO_3$ perturbations also have a larger effect on sea-air gas exchange. Another effect is the reduction of sedimentary organic carbon burial rates during interglacials in response to increased nutrient supply ($fPO4$) or a flattened remineralization profile ($fREMI$) during glacial phases. ~~During deglaciations, sedimentary POC deposited during glacials is remineralized, which raises DIC and further reduces~~ Sedimentary POC accumulates during glacial phases and is subsequently remineralized during

deglaciations, raising DIC and reducing ALK, both contributing to enhanced CO_2 outgassing. We explore the forcing-specific differences in more detail by focusing exemplarily on the last deglaciation.

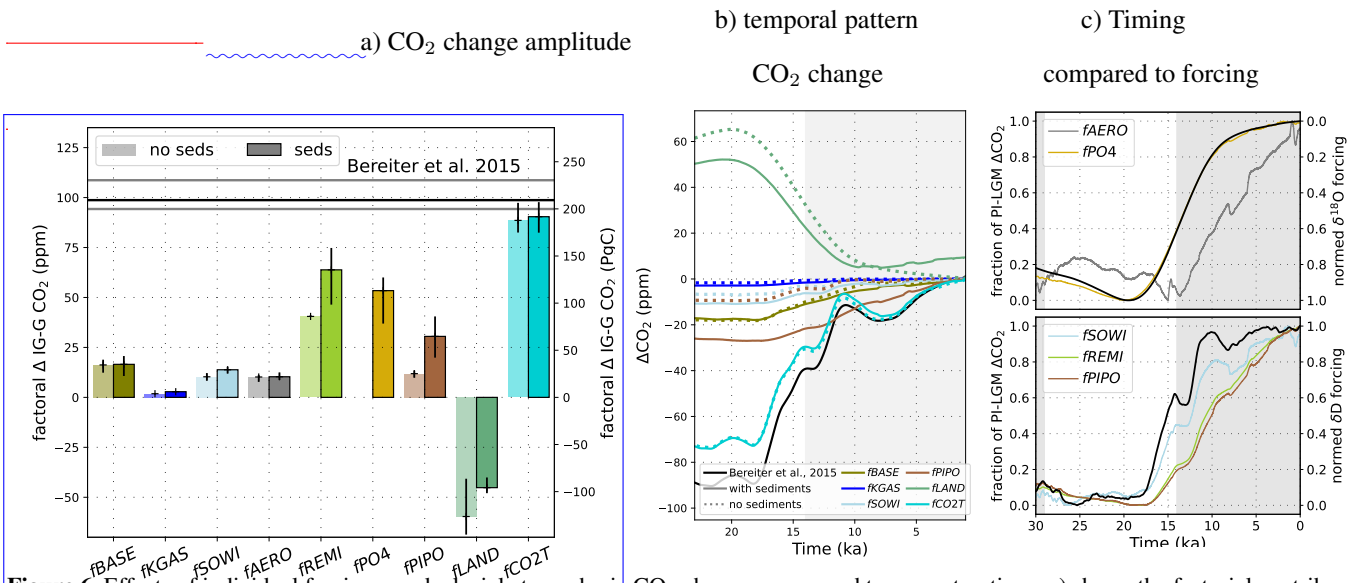

Figure 6. Effects of individual forcings on deglacial atmospheric CO_2 changes compared to reconstructions. a) shows the factorial contributions to the mean glacial-interglacial CO_2 amplitude over the last five glacial terminations (excluding terminations before the Mid-Brunhes transition), as well as the range between their minimum and maximum. Light colors indicate results without interactive sediments, full colors indicate results with interactive sediments. The mean, minimum and maximum amplitudes over the last five deglaciations in the ice core record (Bereiter et al., 2015) are shown by the black and gray horizontal lines. b) shows the factors discussed in the text transiently over the last termination. c) shows time lags between the factors and the respective forcing timeseries (black lines). The δ^{18}O and δD forcings are taken from Lisiecki and Raymo (2005) and Jouzel et al. (2007), respectively (see Methods).

By design, CO_2 restoring causes marine carbon uptake that fills the gap between dynamic atmospheric CO_2 changes of $fBASE$ and reconstructions (Fig. 6, S6, S17), so here we focus on the other forcings. Biogeochemical forcings produce the largest CO_2 differences between the LGM and PI with regard to the reconstructions (Fig. 5, 6a). The weathering-burial disequilibrium, which builds up over the glacial phase under these forcings, amplifies the deglacial CO_2 rise, particularly in $fREMI$ and $fPIPO$. In both cases, sedimentary accumulation of $CaCO_3$ spikes during deglaciation, due to increased $CaCO_3$ export as the forcings wane (Fig. 2). The corresponding ALK reduction expels more CO_2 from the surface ocean into the atmosphere. In the case of $fREMI$, this is further enhanced by a reduction in sedimentary POC accumulation during the deglaciation, which reduces the ~~C~~ carbon loss to the sediments. In both cases the sedimentary processes that amplify the deglacial CO_2 rise also reduce its speed and smooth out transient features of the δD record which are translated into transient atmospheric CO_2 changes in simulations without interactive sediments (Fig 6c). These time lags are caused by the strengthened export production, which counteracts ~~C~~ carbon degassing, and a large build-up of ~~alkalinity~~ ALK and DIC during the glacial phase (amplified by interactive sediments, Fig. S18) which is only gradually reduced by enhanced $CaCO_3$ burial during deglaciations (Fig. S19). If instead export production and sedimentary ~~C~~ carbon accumulation decrease during the deglaciations due to increased nutrient limitation ($fPO4$), the ~~C~~ carbon previously incorporated into biogenic matter is outgassed from the surface ocean and no lag

between CO_2 rise and the forcing emerges. Weathering-burial imbalances have a smaller effect on circulation-driven deglacial CO_2 degassing ($fSOWI$, $fAERO$), regarding both amplitude and timing. However, CO_2 also lags temperature in $fAERO$ (with and without interactive sediments), due to the hysteresis of the AMOC. Enhanced Southern Ocean wind stress ($fSOWI$) is the only forcing in our simulation set that is able to create fast, transient CO_2 releases despite weathering-burial imbalances. In all simulations except LAND, the lowest CO_2 values occur during the coldest interval of glacial cycles, the glacial maxima (Fig. 5, S17). In all simulations in which the deglacial CO_2 rise lags that of temperature, CO_2 keeps rising throughout the Holocene.

Interactive sediments also affect the sensitivity of the deglacial CO_2 rise to peak interglacial warmth: Only by including interactive sediments does our model simulate a shift in the MBT glacial-interglacial CO_2 amplitude comparable to the observations (Fig. S20, S21).

3.3 Marine DIC and the surface carbonate system

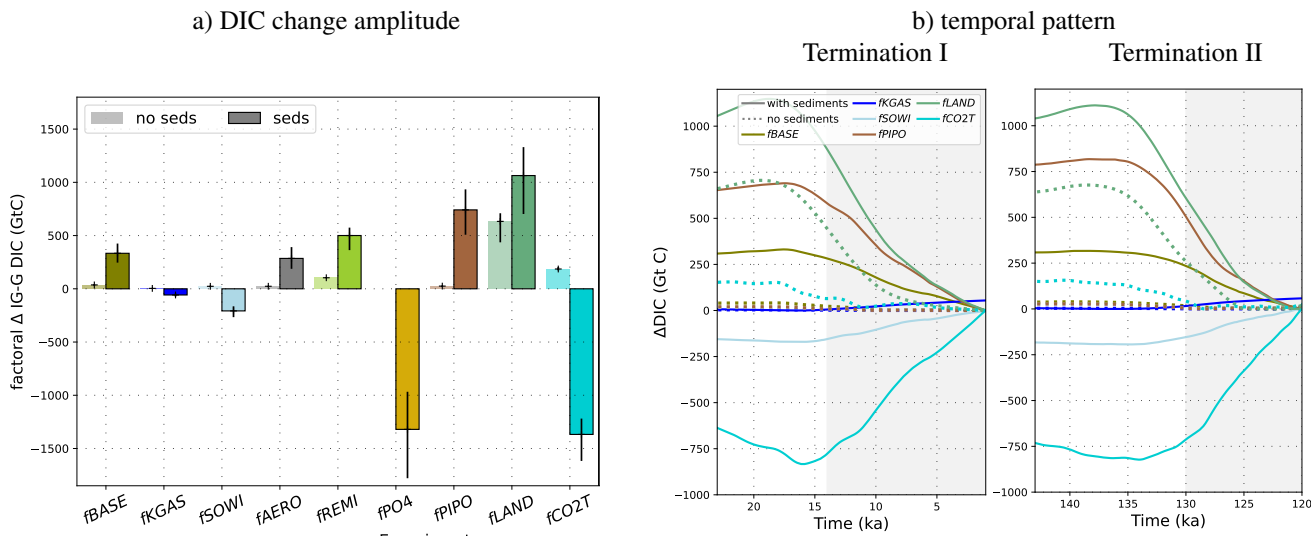

Figure 7. Factorial DIC concentration changes for each forcing over glacial cycles, from the highest or lowest DIC value during the glacial cycle, depending on which occurs earlier, to the other extreme. In a) factorial contribution of each forcing to the mean DIC amplitude over the last five glacial cycles, as well as the range between their minimum and maximum. Light colours show the without dynamic sediments, and full colours show the contributions with dynamic sediments. In b) the factorial contribution of selected forcings to the temporal DIC evolutions across two terminations is shown with and without interactive sediments.

Due to interactive sediments in our simulations, increased uptake or release of carbon in the surface ocean does not linearly correlate with DIC changes because marine carbon storage is also affected by changes in the deposition and dissolution fluxes of particulate carbon at the ocean-sediment interface. Interactive sediments affect marine carbon, ~~alkalinity~~ALK, and nutrient concentrations in two important ways: Firstly, sediments form a large dynamic reservoir which can store and release large amounts of carbon and nutrients for hundreds to tens of thousands of years. Secondly, sedimentary mass accumulation, dissolution, and remineralization rates control sedimentary burial, the only permanent sink for carbon and nutrients in our simulations

and the only mechanism by which environmental change can create imbalances with the prescribed constant solute flux from land. Fluxes into and out of the sediments respond to environmental change, in some cases on the timescale of water mass replacement or regional productivity changes. Carbon fluxes from the sediments directly affect the ocean, but not the atmosphere, which causes different amplitudes in the simulated DIC and atmospheric CO_2 changes and different timings of carbon accumulation in ocean and atmosphere. With interactive sediments, $fBASE$, $fAERO$, $fREMI$, $fPIPO$ and $fLAND$ produce highest DIC during glacial maxima and lowest DIC during interglacials as altered air-sea gas exchange and sediment accumulation result in a net influx of carbon into the ocean during glacial phases. However, while altered air-sea gas exchange still draws down atmospheric CO_2 under $fKGAS$, $fSOWI$ and $fPO4$, larger changes to the sediment fluxes remove carbon from the glacial ocean (Fig. 2) and store excess carbon as carbonate and organic carbon in sediments instead of as DIC in the ocean. Consequently, the lowest DIC occurs during glacial maxima rather than during interglacials under these effects (Fig. S4, S5). $fCO2T$ alters sedimentary carbonate preservation such that DIC extremes do not occur at the same time as atmospheric CO_2 extremes, but in between, i.e. the DIC maximum occurs during glaciation and the minimum during deglaciation (Fig. S6). Furthermore, the onset of the deglacial CO_2 rise in simulations with sediments does not always coincide with the onset of the deglacial DIC change, as is the case in simulations without sediments. This is simulated e.g. for terminations I and II due to $fLAND$ and $fCO2T$ (Fig. S23), and for terminations I, II, III and IV due to $fPO4$ and $fALL$ (Fig. S22). Across the tested processes, the corresponding ocean DIC inventory changes from glacial to interglacial are -1800–1400 GtC (Fig. 7) while the atmospheric inventory changes by -170–190 GtC (Fig. 6) over the the same period. For individual proceses, DIC changes differ by a factor of up to 28 between simulations with and without interactive sediments, while CO_2 changes in the atmosphere are maximally four times larger when interactive sediments are considered (Figs 7, 6).

The magnitude of these DIC changes depends on the forcing strength, which varies between glacial cycles. The lukewarm interglacials of the first 350 kyr of our simulations do not restore the export fluxes and sedimentary $CaCO_3$ preservation required to compensate the prescribed solute influx, and so marine DIC concentrations are persistently higher during 800-450 ka than at PI. Interglacials of the last 450 kyr of the simulation reduce DIC in the long-term because they are warm and long enough for increased carbon transfer into sediments and sediment burial.

3.4 δ^{13}C in the atmosphere and ocean

δ^{13}C in the atmosphere and ocean is also affected by weathering-burial imbalances. Ice cores preserve the δ^{13}C signature of atmospheric CO_2 (Friedli et al., 1984), which showed large fluctuations during the last glacial cycle (Fig. 8), such as fluctuations of $\sim$0.5 ‰ during MIS 4 (71-57 ka) and during the last deglaciation ($\sim$ 18-8 ka) (Eggleston et al., 2016). They also show a long-term ~~trend of lower~~ increase of atmospheric δ^{13}C ~~during the Eemian than the Holocene~~ across the last glacial cycle (Schneider et al., 2013; Eggleston et al., 2016). Reconstructions of δ^{13}C changes in marine DIC show different trajectories in different ocean basins and water masses (Oliver et al., 2010; Peterson and Lisiecki, 2018). The δ^{13}C signature of marine DIC in a given location and atmospheric CO_2 is influenced by processes which affect the whole marine carbon reservoir (e.g. changes in the ~~size~~ amplitude and composition of marine carbon input or output fluxes), as well as by changes in water mass distribution, export production, and isotopic fractionation during sea-air gas exchange and primary production (Jeltsch-

Thömmes et al., 2019; Jeltsch-Thömmes and Joos, 2023), with any signal diluted by the ~~4-box~~ land biosphere. None of the forcings that we applied here produce all of the reconstructed features. However, they show the importance of considering weathering-burial imbalances in their interpretation.

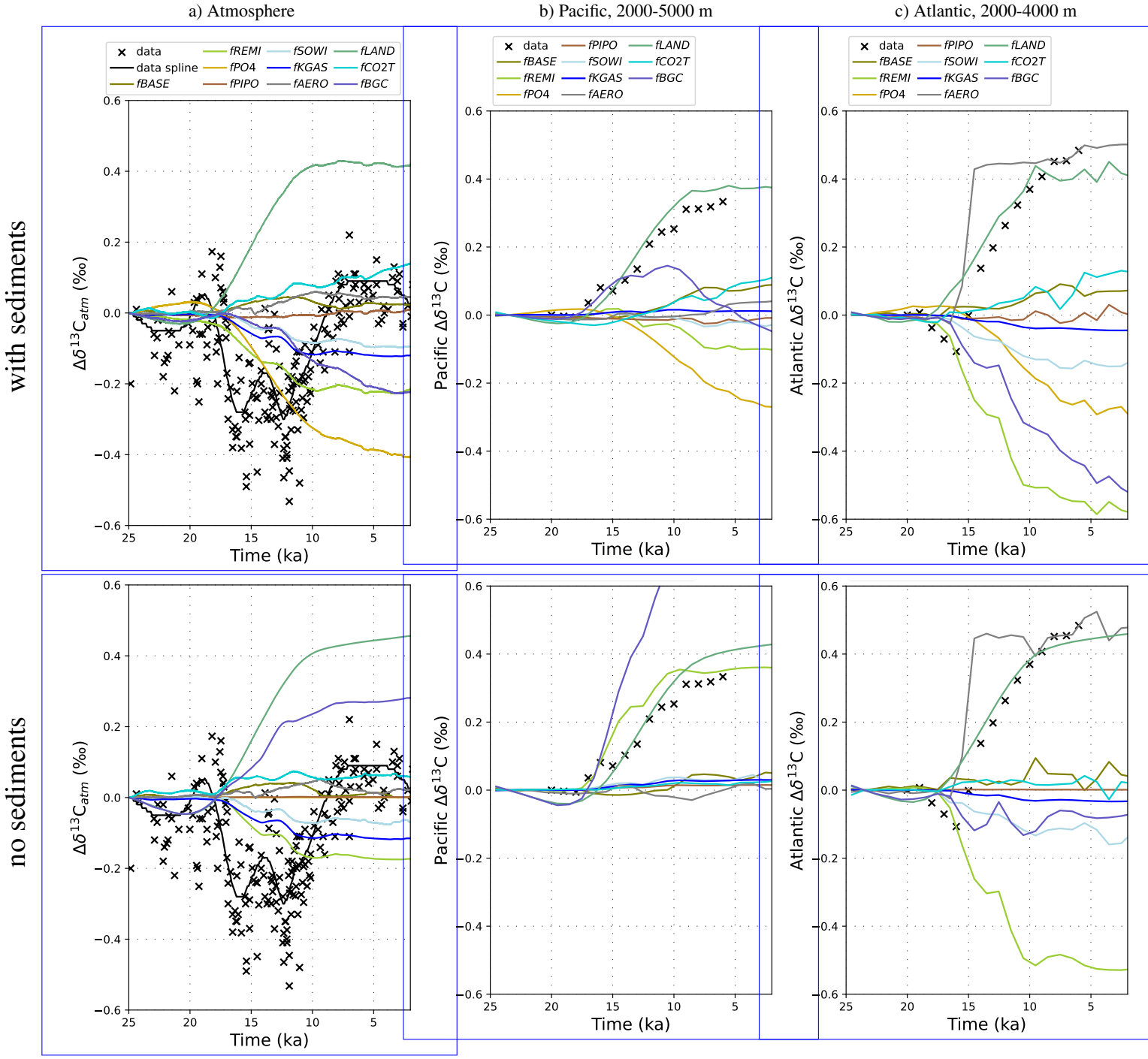

Figure 8. δ^{13}C over the last deglaciation in (a) the atmosphere, (b) deep Pacific (120–266°E, -35–55°N) and (c) deep Atlantic (0–65°N) ocean. Lines are simulation results. Crosses are reconstructions from Schmitt et al. (2012), Eggleston et al. (2016) and Peterson and Lisiecki (2018). All results are shown as differences from 24 ka. Results with interactive sediments are shown in the top row and results without sediments are shown in the bottom row.

Fig. 8 shows the factorial effects of the different forcings on atmospheric and marine δ^{13}C across the last deglaciation in comparison to the reconstructed isotopic shifts in these reservoirs. Under $fLAND$, δ^{13}C changes are driven by the simulated release of isotopically light land carbon (-24 ‰) during glacial inceptions and throughout the glacial, resulting in δ^{13}C minima in all reservoirs during glacial maxima and large δ^{13}C increases during deglaciation in response to land carbon uptake, with and without interactive sediments (Fig. 8). This whole ocean shift is the dominant signal in δ^{13}C records of the deep Pacific. In simulations without interactive sediments, $fREMI$ also causes a similar shift in the deep Pacific, yet the shift is of opposite sign in simulations with interactive sediments due to the negative ~~geologic~~ geological POC balance during the deglaciation (Fig. 2). $fPO4$ has a similar isotopic effect on the ocean as $fREMI$ with sediments because it also leads to the release of sedimentary organic carbon during the deglaciation. Since the processes that affect $\delta^{13}C_{CO_2}$ and $\delta^{13}C_{DIC}$ are different, and $\delta^{13}C_{DIC}$ varies between ocean basins, the forcings which best reproduce reconstructed evolution of δ^{13}C also vary between atmosphere and ocean, and specific water masses (Oliver et al., 2010). This indicates that different processes were likely the dominant controls on δ^{13}C regionally, even if they were not necessarily the dominant drivers of atmospheric CO_2. The impact of interactive sediments also varies between water masses. For example, in the deep Pacific accumulation of isotopically light δ^{13}C as in $fLAND$ likely dominated (Fig. 8b) but must have over-compensated the sediment-enhanced isotopic effects of $fREMI$ and $fPO4$, and cannot explain the reconstructed CO_2 rise (Fig. 6). In the deep North Atlantic, the magnitude of the δ^{13}C shift can also be reproduced by additional radiative cooling and the resulting AMOC shoaling due to $fAERO$ (Fig. 8c) and the simulated isotopic shifts are less affected by interactive sediments.

In the atmosphere, the largest δ^{13}C variability (up to $\pm$0.5 ‰) is also produced by $fLAND$, with and without interactive sediments, and by $fREMI$ and $fPO4$ in simulations with interactive sediments. In fact, the gradual trend of reconstructed atmospheric δ^{13}C over the last glacial cycle (+$\sim$0.5 ‰ from inception to LGM) is only achieved in $fPO4$, the forcing with the biggest effect on sedimentary organic carbon storage (Fig. 2). $fLAND$ causes similar long-term changes but of the opposite sign. No simulation captures the large millennial-scale fluctuations in the reconstructions (Fig. 8). Given our smoothed forcing and the absence of freshwater forcings, our simulations do not contain realistic millennial-scale circulation changes, which would likely be required to simulate these fluctuations (Tschumi et al., 2011; Schmitt et al., 2012; Menviel et al., 2015). It is well-established that a complex combination of processes is required to explain the atmospheric δ^{13}C record (e.g. Menviel et al., 2015) but a simulation over the last glacial period or the deglaciation accurately reproducing the reconstructions has not yet been achieved, and reconciling reconstructed with simulated atmospheric δ^{13}C remains a major challenge for future work. However, our simulations show that interactive sediments change the δ^{13}C signals of Earth system changes on deglacial time scales and need to be considered in such future work, despite challenges associated with model spin-up as discussed next.

3.5 Long isotopic drifts due to weathering-burial imbalances

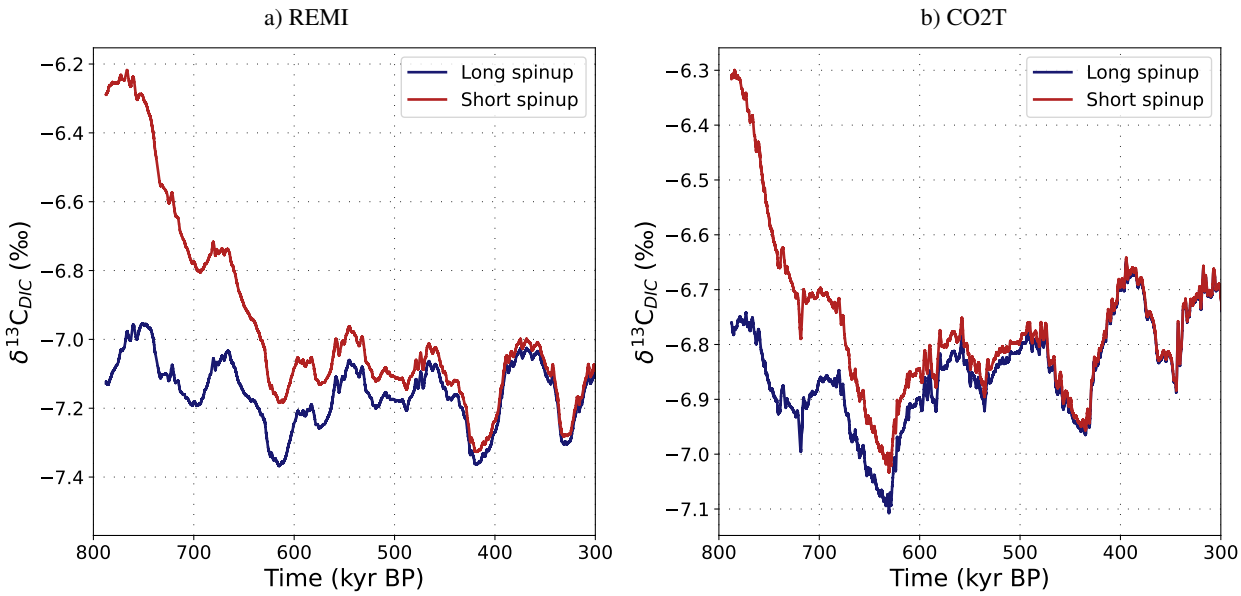

Figure 9. Comparison of simulated atmospheric δ^{13}C in simulations REMI and CO2T when started from a 'short spinup', i.e. a 70 kyr PI spinup followed by a 2 kyr adjustment to MIS19 conditions, and a 'long spinup', i.e. the short spinup plus 215 kyr of transiently simulated MIS19-MIS15.

An important technical lesson of our simulations is that the long adjustment timescale in the geologic carbon cycle also presents an initialization problem, especially for carbon isotopes (Jeltsch-Thömmes and Joos, 2023). We started our experiments from MIS19, which was a colder interglacial than the the Holocene, and Holocene conditions were not reached during the lukewarm interglacials of the first 400 kyr of the simulations. In simulations with interactive sediments, the initial imbalance between weathering inputs derived from the pre-industrial spin-up and burial fluxes adjusting to the colder lukewarm interglacials and glacial states caused δ^{13}C drifts during the first glacial cycles (Fig. 9). Consequently, the simulated glacial-interglacial δ^{13}C signal over this period is altered by the long-term adjustment of the geologic carbon cycle. We addressed this issue by transiently simulating two full glacial cycles before starting the experiments. The magnitude of the initial imbalance in the geologic carbon cycle, and hence isotopic drift, depended on the simulated forcing and was largest in simulations REMI, PIPO and CO2T. Importantly, the drift is a result of perturbing the sediment-weathering balance. The drift can therefore not be corrected for with a control simulation without forcing, because it only appears in the perturbed system. Instead, to avoid a drift, the experiment needs to start from an isotopically balanced geologic carbon cycle, which most commonly will require a long spin-up with a fully-coupled, open system, ideally over several glacial cycles especially when simulating large changes of the biological pump or marine carbonate system. We suggest that the size of the transient imbalance of the geologic carbon cycle, and thus the length of the required spin-up, could be minimized by balancing the geologic carbon cycle not for an interglacial state but for the mean burial fluxes over a full glacial cycle.

Table 2. Quantified metrics of the carbon cycle according to reconstructions and model responses in our set of simulations with sediments. Shown are the factorial effects of the tested forcings and their non-linearites in comparison with reconstructed differences (LGM minus Holocene) over the last deglaciation (specific times of the comparisons vary slightly by proxy record, depending on temporal resolution and record length, and are indicated in the table header) in various proxy systems. The data references are provided at the bottom of the table. The direction of each arrow indicates whether a difference is positive (pointing upwards, teal-coloured) or negative (pointing downwards, brown-coloured). The width of the arrows shows the size of the difference relative to the reconstruction in the uppermost row "Data". For POM export only qualitative reconstructions exist. Hence, the arrows showing simulated effects are normed by the biggest effect of any forcing.

	$\Delta[CO_2]$ (ppm)	ΔpH	ΔPOM_{export} (g/m^2/yr)			$\Delta\delta^{13}C$ (‰)			$\Delta[CO_3^{2-}]$ (μmol/kg)
loc.	global	Eq. Atl.	Iber. Marg.	Eq. Atl.	polar SO	intm. NA	deep NA	deep Pac.	deep Pac.
time	20 - 6 ka	22 - 4 ka	20 - 5 ka			20 - 6 ka			20 - 6 ka
Data	↓	↑	↑	↑	↓	↓	↓	↓	↓
Factorial Results									
$fBASE$	↓	↑	↑	↑	↓	↑	↓	↓	↓
$fKGAS$	↓	↑	↓	↓	o	↑	↑	↓	↑
$fSOWI$	↓	↑	↑	↓	o	↑	↑	↑	↑
$fAERO$	↓	↑	↓	↓	↓	↓	↓	↓	↓
$fREMI$	↓	↑	↓	↓	↑	↑	↑	↑	↑
$fPO4$	↓	↑	↑	↑	↑	↑	↑	↑	↑
$fPIPO$	↓	↑	↑	↑	↑	↓	↑	↑	↑
$fLAND$	↑	↓	↑	↑	↑	↓	↓	↓	↓
$fCO2T$	↓	↑	↑	↑	↑	↓	↑	↓	↑
Non-Linearities									
$nlPHYS$	↑	o	↑	↓	↑	↑	↓	o	↓
$nlBGC$	↑	↓	↓	↓	↓	↑	↑	o	↓
$nlALL$	↑	↓	↑	↑	↓	↓	↓	↑	↓
$nlTOT$	↑	↓	↑	↓	↓	↑	↓	↑	↓
Data ref	Bereiter 2015	Hönisch & Hemming 2005	Kohfeld 2005			Peterson 2018			Yu 2013

Table 2 provides an overview of different proxy signals that are produced in by our factorial forcings, and the non-linearities that arise when they are combined, with interactive sediments over the last deglaciation. The first row shows the reconstructed direction of LGM - Holocene differences, and the next lines show the direction and relative size (compared to the proxy signal) of changes induced by the various tested forcings. The last four rows show the direction and relative size of non-linearities caused by three different combinations of the forcings above. For many of the considered proxies, the signals are strongly amplified by the dynamic weathering-burial imbalances, and also the non-linearities are larger with than without interactive sediments. However, the non-linearities are still small compared to the effect of individual ~~biogeochemcial~~ biogeochemical forcings, and for some proxies of similar size as the effect of physical forcings. Hence, in most cases, proxy changes provide a first-order constraint on the plausibility of large changes in individual processes. $fBASE$, the effect of temperature changes due to orbital, albedo and greenhouse gas changes, moves almost all proxy systems in the reconstructed direction (the directions of the arrows match), but almost never to the reconstructed extent (the widths of the arrows do not match). It is only sufficient to explain strongly reduced export production in the polar Southern Ocean at the LGM, which in our model is predominantly driven by surface cooling and sea ice expansion regardless of which other processes also occurred.

We identified two processes by which weathering-burial imbalances most effectively raise atmospheric CO_2 during deglaciations in our simulations: ~~Alkalinity~~ ALK removal and organic carbon remineralization. Under $fPIPO$ and $fREMI$ the combination of high ~~alkalinity~~ ALK at the end of glacial phases and increased $CaCO_3$ export production during deglaciation causes large transient $CaCO_3$ deposition events in the open ocean (Fig. 2) which remove the excess glacial ~~alkalinity~~ ALK and thus drive a large but slow continuous CO_2 rise compared to the reconstruction. The marine DIC and ~~alkalinity~~ ALK that built up over the previous glacial phase are too large to be removed instantly, and the resulting large deposition of $CaCO_3$ during the deglaciation persists far into the interglacial. In consequence, these forcings produce poorer model-data matches for Holocene $CaCO_3$. We also showed that the resulting δ^{13}C and [CO_3^{2-}] signals in the deep Pacific are not consistent with reconstructions. $fCO2T$ shows the effect of forced ~~alkalinity removal during galciations~~ ALK removal during glaciations to reproduce the reconstructed atmospheric CO_2 record, and can serve to study the effect of ~~alkalinity~~ ALK removal through means other than deep ocean $CaCO_3$ burial (e.g. shallow deposition, coral reef growth, reduced terrestrial input) on other proxy systems. This forcing causes deep ocean $CaCO_3$ dissolution and increasing marine DIC during the deglaciation, moving δ^{13}C in the deep Pacific in the proxy-consistent direction but still producing a large mismatch in [CO_3^{2-}]. $fPO4$ results in a deglacial CO_2 rise due to a reduction in export production and increased remineralization of sedimentary organic matter which accumulated during the previous glacial period under reduced benthic O_2 concentrations. The resulting CO_2 increase is of similar amplitude as that due to $fREMI$ but happens faster, more consistent with the reconstruction. In addition, deep Pacific [CO_3^{2-}] is less perturbed by this effect than by $fREMI$ or $fCO2T$, yet deep ocean δ^{13}C is shifted in the wrong direction. Future work will have to test which combinations of these processes are most consistent with the wide range of available proxy data.

It is well established that cooling and circulation changes altered sea-air gas exchange and increased deep ocean carbon storage by isolating it from the surface during glacial phases (e.g. Brovkin et al., 2007). Combined, these effects contribute to changes in atmospheric CO_2 in our simulations that are comparable to Brovkin et al. (2012) (26 ppm compared to 30 ppm).

Isolating the deep Pacific through reduced Southern Ocean wind forcing (effect $fSOWI$) caused a glacial CO_2 decline by ~13 ppm, the biggest CO_2 draw-down on top of the effect orbital cooling ($fBASE$) of any isolated physical forcing that we tested. Tschumi et al. (2011) showed that this effect also has the potential to cause larger CO_2 draw-down with sedimentary amplification than simulated here. The idealised, strong reductions in wind speeds over the Southern Ocean prescribed by Tschumi et al. (2011) as a tuning knob for producing old deep ocean waters are unrealistic, but other processes could have contributed to increased isolation of the deep Pacific. Bouttes et al. (2011) showed that during glacial stages enhanced brine rejection during sea ice formation can isolate abyssal waters and cause atmospheric CO_2 and δ^{13}C changes that are similar to those reconstructed. Enhanced brine rejection could thus have provided an additional physical process that increased the glacial marine carbon storage. The strength of this process, however, is only poorly constrained, and Ganopolski and Brovkin (2017) showed that, at a sufficient strength to significantly affect deep ocean carbon storage, this process creates bigger Δ^{14}C anomalies in the deep ocean than reconstructed. Following Menviel et al. (2011), they also argue that the timing of increased sea ice formation and atmospheric CO_2 changes during the last deglaciation (Roberts et al., 2016) are not entirely consistent with a strong control of brine formation rates on marine carbon storage.

In further agreement with other modelling studies, e.g. Buchanan et al. (2016) and Morée et al. (2021), we find that changing the efficiency of the biological pumps ($fREMI$) is an efficient mechanism to achieve glacial-interglacial atmospheric CO_2 changes similar to those reconstructed from ice cores. However, because of its large effects on deep Pacific [CO_3^{2-}] and $CaCO_3$ accumulation during deglaciation it was unlikely the dominant carbon cycle change over the last glacial cycle.

A relevant role of marine sediments, particularly sedimentary $CaCO_3$, in glacial-interglacial carbon cycle dynamics has long been discussed (e.g. Broecker, 1982b; Broecker and Peng, 1987; Opdyke and Walker, 1992; Archer and Maier-Reimer, 1994; Raven and Falkowski, 1999) and shown in numerical experiments of differing physical and biogeochemical complexities (Ridgwell et al., 2003; Joos et al., 2004; Tschumi et al., 2011; Menviel et al., 2012; Roth et al., 2014; Wallmann et al., 2016; Ganopolski and Brovkin, 2017; Jeltsch-Thömmes et al., 2019; Köhler and Munhoven, 2020; Stein et al., 2020; Kobayashi et al., 2021). In agreement with other studies (e.g. Ganopolski and Brovkin, 2017; Köhler and Munhoven, 2020), we find that changing marine ~~alkalinity~~ ALK can produce large CO_2 changes. Organic carbon storage is less often considered in modelling studies, although it also showed significant changes across the last glacial cycle (Cartapanis et al., 2016). Out of the forcings we tested, reduced nutrient limitation during glacial phases ($fPO4$) produces temporal and regional organic carbon deposition changes that were most consistent with the reconstructions. In this simulation, marine sediments turn into a strong carbon sink during cold phases. The simulated increased organic carbon deposition during glacial phases reproduces the reconstructed long-term trends in atmospheric and surface ocean δ^{13}C during glacials, but is not sufficient in isolation to reproduce the reconstructed deep ocean δ^{13}C changes in the Pacific and Atlantic. Thus, while sedimentary organic carbon burial could have provided a carbon sink during glacial phases, it must have been operating alongside other processes to allow for the reconstructed benthic δ^{13}C evolution. Interestingly, processes that increase organic carbon burial during glacial phases ($fPO4$, $fREMI$) show that some of the deposited organic carbon can be returned to the ocean during deglaciations with a large potential to contribute to a fast post-glacial rise in atmospheric CO_2. In addition to carbon, nutrients are also removed from the ocean when organic matter is buried (Roth et al., 2014). Tschumi et al. (2011) demonstrated in their steady

state experiments that increased organic nutrient burial enhances nutrient limitation on export production and reduces $CaCO_3$ export, which increases surface ~~alkalinity~~ ALK and amplifies the CO_2 drawdown caused by the increased burial of organic carbon. Under $fREMI$, this process operates transiently. Given the reconstructed increased organic carbon burial rates during glacial maxima, this could have been a relevant process over the last glacial cycles, though it might have been reduced in its efficiency by reductions in the PIC:POC of export production during glacial phases (Dymond and Lyle, 1985; Sigman and Boyle, 2000). Finally, sedimentary organic carbon oxidation can also regulate marine ~~alkalinity~~ ALK by affecting sedimentary $CaCO_3$ dissolution (Emerson and Bender, 1981; Sigman and Boyle, 2000), but this effect is not directly quantified in our setup. However, we can assess that increased sedimentary organic matter remineralization on a global scale during glacial phases does not occur due to any of our tested forcings. On the contrary, the effects ($fPO4$, $fREMI$) that increase organic carbon burial during glacial maxima, a prominent feature of the reconstructions, decrease globally-averaged sedimentary remineralization rates during glacial times.

A close relationship between DIC and Δ^{14}C(DIC) is found in modern deep ocean waters and this relationship has been used to reconstruct past DIC changes from radiocarbon reconstructions (Sarnthein et al., 2013). Sedimentary carbon fluxes can de-couple deep ocean Δ^{14}C from DIC (Dinauer et al., 2020) and change DIC without altering sea-air carbon transfer, meaning that DIC changes do not necessarily imply a comparable CO_2 change in the atmosphere. In all of our simulations with interactive sediments, the DIC inventory change over a glacial cycles is larger than the simultaneous atmospheric CO_2 inventory perturbation because of changes in carbon reservoirs in sediments and weathering-burial imbalances. Changes in the simulated sedimentary burial fluxes result in net transfers of up to 2000 PgC between the carbon pools of the ocean and sediments throughout a glacial cycle, while the net loss of atmospheric ~~C~~ carbon to reproduce the reconstructed glacial CO_2 is roughly 200 PgC (Sigman and Boyle, 2000; Yu et al., 2010), and the net loss of terrestrial ~~C~~ carbon is on the order of 500-1000 PgC (Jeltsch-Thömmes et al., 2019). The carbon cycle impact of glacial cycles was thus likely larger in the ocean than in the atmosphere (Roth et al., 2014; Buchanan et al., 2016), due to changes in sedimentary carbon storage. In some of our simulations, large DIC changes are produced by big sustained weathering-burial imbalances during glacials that cannot be compensated during the relatively short deglaciations and cause interglacial carbonate preservation patterns that are not consistent with observations (Fig. S11, S12). While such simulated scenarios are thus unrealistic, it does not generically preclude the possibility of large transient weathering-burial imbalances during glacial phases. Testing a wider range of forcing magnitudes and combinations with the same model but different set-up, Jeltsch-Thömmes et al. (2019) (the DIC results of which are published in the Appendix of Morée et al. (2021)) found a larger DIC change between the pre-industrial and LGM than simulated here (3900$\pm$550 GtC compared to a maximum of 1100$\pm$300 GtC in Fig. 7) that is consistent with carbonate system proxy constraints. Combinations of the tested forcings thus allow for larger transient weathering-burial imbalances than produced by our simulation ensemble that can still be reconciled with carbon cycle proxies. Some of the tested forcings also show lower glacial than inter-glacial DIC ($fPO4$, $fCO2T$) showing that CO_2 removal from the atmosphere in theory does not need to result in increased DIC in the ocean. Instead, these biogeochemical forcings cause sedimentary changes that can store large amounts of carbon in inorganic and organic sedimentary matter. Kemppinen et al. (2019) and Jeltsch-Thömmes et al. (2019) previously showed and discussed the possibility of a negative glacial DIC anomaly due to increased sedimentary

storage. As found by Jeltsch-Thömmes et al. (2019), organic carbon burial extensive enough to cause a negative glacial DIC anomaly (e.g. $fPO4$) produces large δ^{13}C signals of opposite sign than reconstructed, and thus seems unlikely. In the study by Jeltsch-Thömmes et al. (2019), a negative glacial DIC anomaly due to ~~alkalinity-driven~~ ALK-driven $CaCO_3$ accumulation is also inconsistent with the proxy record of the last 25 kyr. Consistently, we find that reconstructed deep Pacific [CO_3^{2-}] changes make a large-scale ~~alkalinity-driven~~ ALK-driven ($fCO2T$) glacial $CaCO_3$ accumulation, which reduces atmospheric CO_2 while also reducing DIC, which is unlikely because it causes larger deep Pacific [CO_3^{2-}] changes than reconstructed over the last deglaciation (Table 2). The isotopic signal of such large $CaCO_3$ deposition, however, is smaller than that of POC burial changes and could more likely be overprinted by other processes (e.g. terrestrial carbon release and export production changes) to yield proxy-consistent evolutions (Table 2).

It has long been suggested that sedimentary imbalances also contributed to the reconstructed interglacial sedimentary changes and CO_2 rises after deglaciations (Broecker et al., 1999; Ridgwell et al., 2003; Joos et al., 2004; Broecker and Stocker, 2006; Elsig et al., 2009; Menviel et al., 2012; Brovkin et al., 2016). Consistently we find that CO_2 degassing from the ocean persisted throughout deglaciations and into interglacials (e.g. Brovkin et al., 2012), and that the carbon cycle does not reach a new equilibrium before the next glacial inception (e.g. supply-burial imbalances in the late Holocene in Table S2). In our simulations AMOC hysteresis, sedimentary changes, and delayed temperature responses, e.g. due to ice sheets (mimicked by scaling most forcings to the δ^{18}O record), introduce memory effects which buffer deglacial carbon cycle reorganizations and cause continued CO_2 rise throughout interglacials. For example, in PO4, BGC and ALL, the simulations which best align with the reconstructed glacial-interglacial organic carbon burial changes, not all glacial organic matter is remineralised and carbonate dissolution continued throughout the interglacials.

5 Conclusions

In response to different simulated carbon cycle forcings over the repeated glacial-interglacial cycles of the past 780 kyr in the Bern3D model, we found large sedimentary changes which substantially alter marine carbon and nutrient concentrations and spatial distributions. Our simulations show that biogeochemical forcings are required to perturb the sediments sufficiently to reproduce reconstructed burial changes and CO_3^{2-} variations, yet compensating processes (e.g. shallow carbonate deposition) must have operated to reduce the buffering impact of this sedimentary perturbation on the deglacial carbon cycle re-organization in order to match the speed of the associated carbon release. ~~Our~~ These results have implications for model experiment design and the interpretation of δ^{13}C proxy data: We showed that the long timescales of ocean-sediment interactions and the weathering-burial cycle pose substantial challenges for model spin up because imbalances in the geologic carbon cycle can cause isotopic drifts at the beginning of simulations and which are not present in a control run. Depending on the initial isotopic imbalance, it takes up to 200 kyr for the drift to subside and the signal of the applied forcing to dominate the simulated transient δ^{13}C changes. Further studies are needed to test whether δ^{13}C can be spun up in more computationally-expensive models by combining them with lower-complexity models. In the absence of such a spin up strategy, open system simulations

of glacial δ^{13}C are likely strongly affected by these initial drifts severely hampering interpretation of results. These long adjustment timescales also pose challenges for separating long-term from short-term signals in the proxy records.

In terms of glacial carbon cycle dynamics, our set of factorial simulations ~~further~~ leads to the following conclusions:

Firstly, ocean-sediment interactions and related weathering-burial imbalances, including fluxes of nutrients, alkalinity, organic and inorganic carbon, tend to amplify glacial-interglacial CO_2 change.

Secondly, the relationship between marine DIC and atmospheric CO_2 changes is not linear across the different forcings and strongly influenced by sediment fluxes. For example, the potential addition of phosphate from exposed continental shelves causes a decrease in atmospheric CO_2 and marine DIC by increasing sedimentary carbon storage. Factorial simulations yield changes in the ocean DIC inventory between -1340 to +1400 GtC and in the atmospheric CO_2 inventory between -96 and 180 GtC (-45 and 80 ppm) over the last five deglaciations in response to individual prescribed physical and biogeochemical forcings. This suggests that approaches utilizing the relationship between radiocarbon and DIC from modern data to reconstruct the ocean's glacial DIC inventory and the postulated corresponding CO_2 change from glacial radiocarbon data may be biased.

Thirdly, ocean-sediment interactions strongly impact the evolution of important carbon cycle parameters such as δ^{13}C(DIC) and $\delta^{13}C_{CO_2}$, CO_3^{2-}, export production, $CaCO_3$ and POM burial fluxes, preformed and remineralized nutrient concentrations, and oxygen. The interpretation of the proxy records without consideration of weathering-burial imbalances and ocean-sediment interactions for both organic and inorganic carbon may lead to erroneous conclusions.

~~We also showed that the long timescales of ocean-sediment interactions and the weathering-burial cycle pose substantial challenges for model spin-up because imbalances in the geologic carbon cycle can cause isotopic drifts at the beginning of simulations and which are not present in a control run. Depending on the initial isotopic imbalance, it takes up to 200 kyr for the drift to subside and the signal of the applied forcing to dominate the simulated transient δ^{13}C changes. Further studies are needed to test whether δ^{13}C can be spun up in more computationally-expensive models by combining them with lower-complexity models. In the absence of such a spin up strategy, open system simulations of glacial δ^{13}C are likely strongly affected by these initial drifts.~~

Data availability. All simulation output necessary to produce the figures in this manuscript are available at https://doi.org/10.5281/zenodo.11385608

.

Author contributions. FP and AJT designed the simulations. AJT ran the simulations. MA processed the model output and drafted the manuscript. MA, AJT, FP, FJ and TFS interpreted the results and edited the manuscript.

Competing interests. The authors declare that they have no conflict of interest.

Acknowledgements. This research has been supported by the Schweizerischer Nationalfonds zur Förderung der Wissenschaftlichen Forschung (grant nos. 200020-200511 and 200020-200492) and Horizon 2020 (grant nos. 101023443 and 40 820970).

References

Adloff, M., Pöppelmeier, F., Jeltsch-Thömmes, A., Stocker, T. F., and Joos, F. (2024). Multiple thermal Atlantic Meridional Overturning Circulation thresholds in the intermediate complexity model Bern3D. *Climate of the Past*, 20(6):1233–1250.

Archer, D. and Maier-Reimer, E. (1994). Effect of deep-sea sedimentary calcite preservation on atmospheric CO_2 concentration. *Nature*, 367(6460):260–263.

Battaglia, G. and Joos, F. (2018). Marine N_2O emissions from nitrification and denitrification constrained by modern observations and projected in multimillennial global warming simulations. *Global Biogeochemical Cycles*, 32(1):92–121.

Bereiter, B., Eggleston, S., Schmitt, J., Nehrbass-Ahles, C., Stocker, T. F., Fischer, H., Kipfstuhl, S., and Chappellaz, J. (2015). Revision of the EPICA Dome C CO_2 record from 800 to 600 kyr before present. *Geophysical Research Letters*, 42(2):542–549.

Berger, A. (1978). Long-term variations of caloric insolation resulting from the Earth's orbital elements. *Quaternary research*, 9(2):139–167.

Berger, A. and Loutre, M.-F. (1991). Insolation values for the climate of the last 10 million years. *Quaternary science reviews*, 10(4):297–317.

Börker, J., Hartmann, J., Amann, T., Romero-Mujalli, G., Moosdorf, N., and Jenkins, C. (2020). Chemical weathering of loess and its contribution to global alkalinity fluxes to the coastal zone during the Last Glacial Maximum, Mid-Holocene, and Present. *Geochemistry, Geophysics, Geosystems*, 21(7):e2020GC008922.

Bouttes, N., Paillard, D., and Roche, D. (2010). Impact of brine-induced stratification on the glacial carbon cycle. *Climate of the Past*, 6(5):575–589.

Bouttes, N., Paillard, D., Roche, D. M., Brovkin, V., and Bopp, L. (2011). Last Glacial Maximum CO_2 and $\delta^{13}C$ successfully reconciled. *Geophysical Research Letters*, 38(2).

Broecker, W. S. (1982a). Glacial to interglacial changes in ocean chemistry. *Progress in Oceanography*, 11(2):151–197.

Broecker, W. S. (1982b). Ocean chemistry during glacial time. *Geochimica et cosmochimica acta*, 46(10):1689–1705.

Broecker, W. S., Clark, E., McCorkle, D. C., Peng, T.-H., Hajdas, I., and Bonani, G. (1999). Evidence for a reduction in the carbonate ion content of the deep sea during the course of the Holocene. *Paleoceanography*, 14(6):744–752.

Broecker, W. S. and Peng, T.-H. (1987). The role of $CaCO_3$ compensation in the glacial to interglacial atmospheric CO_2 change. *Global Biogeochemical Cycles*, 1(1):15–29.

Broecker, W. S. and Stocker, T. F. (2006). The Holocene CO_2 rise: Anthropogenic or natural? *Eos, Transactions American Geophysical Union*, 87(3):27–27.

Brovkin, V., Brücher, T., Kleinen, T., Zaehle, S., Joos, F., Roth, R., Spahni, R., Schmitt, J., Fischer, H., Leuenberger, M., et al. (2016). Comparative carbon cycle dynamics of the present and last interglacial. *Quaternary Science Reviews*, 137:15–32.

Brovkin, V., Ganopolski, A., Archer, D., and Munhoven, G. (2012). Glacial CO_2 cycle as a succession of key physical and biogeochemical processes. *Climate of the Past*, 8(1):251–264.

Brovkin, V., Ganopolski, A., Archer, D., and Rahmstorf, S. (2007). Lowering of glacial atmospheric CO_2 in response to changes in oceanic circulation and marine biogeochemistry. *Paleoceanography*, 22(4).

Buchanan, P. J., Matear, R. J., Lenton, A., Phipps, S. J., Chase, Z., and Etheridge, D. M. (2016). The simulated climate of the Last Glacial Maximum and insights into the global marine carbon cycle. *Climate of the Past*, 12(12):2271–2295.

Cartapanis, O., Bianchi, D., Jaccard, S. L., and Galbraith, E. D. (2016). Global pulses of organic carbon burial in deep-sea sediments during glacial maxima. *Nature communications*, 7(1):10796.

Cartapanis, O., Galbraith, E. D., Bianchi, D., and Jaccard, S. L. (2018). Carbon burial in deep-sea sediment and implications for oceanic inventories of carbon and alkalinity over the last glacial cycle. *Climate of the Past*, 14(11):1819–1850.

Claquin, T., Roelandt, C., Kohfeld, K., Harrison, S., Tegen, I., Prentice, I., Balkanski, Y., Bergametti, G., Hansson, M., Mahowald, N., et al. (2003). Radiative forcing of climate by ice-age atmospheric dust. *Climate Dynamics*, 20(2):193–202.

Deutsch, C., Sigman, D. M., Thunell, R. C., Meckler, A. N., and Haug, G. H. (2004). Isotopic constraints on glacial/interglacial changes in the oceanic nitrogen budget. *Global Biogeochemical Cycles*, 18(4).

Dinauer, A., Adolphi, F., and Joos, F. (2020). Mysteriously high Δ^{14}C of the glacial atmosphere: influence of 14 C production and carbon cycle changes. *Climate of the Past*, 16(4):1159–1185.

Dymond, J. and Lyle, M. (1985). Flux comparisons between sediments and sediment traps in the eastern tropical Pacific: Implications for atmospheric C02 variations during the Pleistocene 1. *Limnology and Oceanography*, 30(4):699–712.

Edwards, N. R., Willmott, A. J., and Killworth, P. D. (1998). On the role of topography and wind stress on the stability of the thermohaline circulation. *Journal of physical oceanography*, 28(5):756–778.

Eggleston, S., Schmitt, J., Bereiter, B., Schneider, R., and Fischer, H. (2016). Evolution of the stable carbon isotope composition of atmospheric CO_2 over the last glacial cycle. *Paleoceanography*, 31(3):434–452.

Elsig, J., Schmitt, J., Leuenberger, D., Schneider, R., Eyer, M., Leuenberger, M., Joos, F., Fischer, H., and Stocker, T. F. (2009). Stable isotope constraints on Holocene carbon cycle changes from an Antarctic ice core. *Nature*, 461(7263):507–510.

Emerson, S. and Bender, M. (1981). Carbon fluxes at the sediment-water interface of the deep-sea: calcium carbonate preservation.

Etminan, M., Myhre, G., Highwood, E. J., and Shine, K. P. (2016). Radiative forcing of carbon dioxide, methane, and nitrous oxide: A significant revision of the methane radiative forcing. *Geophysical Research Letters*, 43(24):12–614.

Fischer, H., Schmitt, J., Lüthi, D., Stocker, T. F., Tschumi, T., Parekh, P., Joos, F., Köhler, P., Völker, C., Gersonde, R., et al. (2010). The role of Southern Ocean processes in orbital and millennial CO_2 variations–A synthesis. *Quaternary Science Reviews*, 29(1-2):193–205.

Friedli, H., Moor, E., Oeschger, H., Siegenthaler, U., and Stauffer, B. (1984). ^{13}C/^{12}C ratios in CO_2 extracted from Antarctic ice. *Geophysical research letters*, 11(11):1145–1148.

Frings, P. J. (2019). Palaeoweathering: how do weathering rates vary with climate? *Elements: An International Magazine of Mineralogy, Geochemistry, and Petrology*, 15(4):259–265.

Ganopolski, A. and Brovkin, V. (2017). Simulation of climate, ice sheets and CO_2 evolution during the last four glacial cycles with an Earth system model of intermediate complexity. *Climate of the Past*, 13(12):1695–1716.

Griffies, S. M. (1998). The Gent–McWilliams skew flux. *Journal of Physical Oceanography*, 28(5):831–841.

Hayes, C. T., Costa, K. M., Anderson, R. F., Calvo, E., Chase, Z., Demina, L. L., Dutay, J.-C., German, C. R., Heimbürger-Boavida, L.-E., Jaccard, S. L., et al. (2021). Global ocean sediment composition and burial flux in the deep sea. *Global biogeochemical cycles*, 35(4):e2020GB006769.

Heinze, C., Maier-Reimer, E., Winguth, A. M., and Archer, D. (1999). A global oceanic sediment model for long-term climate studies. *Global Biogeochemical Cycles*, 13(1):221–250.

Jeltsch-Thömmes, A., Battaglia, G., Cartapanis, O., Jaccard, S. L., and Joos, F. (2019). Low terrestrial carbon storage at the Last Glacial Maximum: constraints from multi-proxy data. *Climate of the Past*, 15(2):849–879.

Jeltsch-Thömmes, A. and Joos, F. (2020). Modeling the evolution of pulse-like perturbations in atmospheric carbon and carbon isotopes: The role of weathering–sedimentation imbalances. *Climate of the Past*, 16(2):423–451.

Jeltsch-Thömmes, A. and Joos, F. (2023). Carbon Cycle Responses to Changes in Weathering and the Long-Term Fate of Stable Carbon Isotopes. *Paleoceanography and paleoclimatology*, 38(2):e2022PA004577.

Jones, I. W., Munhoven, G., Tranter, M., Huybrechts, P., and Sharp, M. J. (2002). Modelled glacial and non-glacial HCO_3^-, Si and Ge fluxes since the LGM: little potential for impact on atmospheric CO2 concentrations and a potential proxy of continental chemical erosion, the marine Ge/Si ratio. *Global and Planetary Change*, 33(1-2):139–153.

Joos, F., Gerber, S., Prentice, I., Otto-Bliesner, B. L., and Valdes, P. J. (2004). Transient simulations of Holocene atmospheric carbon dioxide and terrestrial carbon since the Last Glacial Maximum. *Global Biogeochemical Cycles*, 18(2).

Joos, F. and Spahni, R. (2008). Rates of change in natural and anthropogenic radiative forcing over the past 20,000 years. *Proceedings of the National Academy of Sciences*, 105(5):1425–1430.

Jouzel, J., Masson-Delmotte, V., Cattani, O., Dreyfus, G., Falourd, S., Hoffmann, G., Minster, B., Nouet, J., Barnola, J., Chappellaz, J., et al. (2007). EPICA Dome C ice core 800kyr deuterium data and temperature estimates. *IGBP PAGES/World Data Center for Paleoclimatology data contribution series*, 91.

Kalnay, E., Kanamitsu, M., Kistler, R., Collins, W., Deaven, D., Gandin, L., Iredell, M., Saha, S., White, G., Woollen, J., et al. (1996). The NCEP/NCAR 40-year reanalysis project. *Bulletin of the American meteorological Society*, 77(3):437–472.

Kemppinen, K., Holden, P. B., Edwards, N. R., Ridgwell, A., and Friend, A. D. (2019). Coupled climate–carbon cycle simulation of the Last Glacial Maximum atmospheric CO_2 decrease using a large ensemble of modern plausible parameter sets. *Climate of the Past*, 15(3):1039–1062.

Kerr, J., Rickaby, R., Yu, J., Elderfield, H., and Sadekov, A. Y. (2017). The effect of ocean alkalinity and carbon transfer on deep-sea carbonate ion concentration during the past five glacial cycles. *Earth and Planetary Science Letters*, 471:42–53.

Kobayashi, H., Oka, A., Yamamoto, A., and Abe-Ouchi, A. (2021). Glacial carbon cycle changes by Southern Ocean processes with sedimentary amplification. *Science Advances*, 7(35):eabg7723.

Kohfeld, K. E. and Ridgwell, A. (2009). Glacial-interglacial variability in atmospheric CO_2. *Surface ocean-lower atmosphere processes*, 187:251–286.

Köhler, P. and Munhoven, G. (2020). Late Pleistocene carbon cycle revisited by considering solid Earth processes. *Paleoceanography and Paleoclimatology*, 35(12):e2020PA004020.

Krakauer, N. Y., Randerson, J. T., Primeau, F. W., Gruber, N., and Menemenlis, D. (2006). Carbon isotope evidence for the latitudinal distribution and wind speed dependence of the air–sea gas transfer velocity. *Tellus B: Chemical and Physical Meteorology*, 58(5):390–417.

Kukla, G., An, Z., Melice, J., Gavin, J., and Xiao, J. (1990). Magnetic susceptibility record of Chinese loess. *Earth and Environmental Science Transactions of the Royal Society of Edinburgh*, 81(4):263–288.

Lindgren, A., Hugelius, G., and Kuhry, P. (2018). Extensive loss of past permafrost carbon but a net accumulation into present-day soils. *Nature*, 560(7717):219–222.

Lisiecki, L. E. and Raymo, M. E. (2005). A Pliocene-Pleistocene stack of 57 globally distributed benthic δ18O records. *Paleoceanography*, 20(1).

Loulergue, L., Schilt, A., Spahni, R., Masson-Delmotte, V., Blunier, T., Lemieux, B., Barnola, J.-M., Raynaud, D., Stocker, T. F., and Chappellaz, J. (2008). Orbital and millennial-scale features of atmospheric CH4 over the past 800,000 years. *Nature*, 453(7193):383–386.

Lüthi, D., Le Floch, M., Bereiter, B., Blunier, T., Barnola, J.-M., Siegenthaler, U., Raynaud, D., Jouzel, J., Fischer, H., Kawamura, K., et al. (2008). High-resolution carbon dioxide concentration record 650,000–800,000 years before present. *nature*, 453(7193):379–382.

Martin, J. H. (1990). Glacial-interglacial CO_2 change: The iron hypothesis. *Paleoceanography*, 5(1):1–13.

Menviel, L. and Joos, F. (2012). Toward explaining the Holocene carbon dioxide and carbon isotope records: Results from transient ocean carbon cycle-climate simulations. *Paleoceanography*, 27(1).

Menviel, L., Joos, F., and Ritz, S. (2012). Simulating atmospheric CO_2, ^{13}C and the marine carbon cycle during the Last Glacial–Interglacial cycle: possible role for a deepening of the mean remineralization depth and an increase in the oceanic nutrient inventory. *Quaternary Science Reviews*, 56:46–68.

Menviel, L., Mouchet, A., Meissner, K. J., Joos, F., and England, M. H. (2015). Impact of oceanic circulation changes on atmospheric $\delta^{13}CO_2$. *Global Biogeochemical Cycles*, 29(11):1944–1961.

Menviel, L., Timmermann, A., Timm, O. E., and Mouchet, A. (2011). Deconstructing the Last Glacial termination: the role of millennial and orbital-scale forcings. *Quaternary Science Reviews*, 30(9-10):1155–1172.

Morée, A. L., Schwinger, J., Ninnemann, U. S., Jeltsch-Thömmes, A., Bethke, I., and Heinze, C. (2021). Evaluating the biological pump efficiency of the Last Glacial Maximum ocean using $\delta^{13}C$. *Climate of the Past*, 17(2):753–774.

Müller, S., Joos, F., Edwards, N., and Stocker, T. (2006). Water mass distribution and ventilation time scales in a cost-efficient, three-dimensional ocean model. *Journal of Climate*, 19(21):5479–5499.

Müller, S. A., Joos, F., Plattner, G.-K., Edwards, N. R., and Stocker, T. F. (2008). Modeled natural and excess radiocarbon: Sensitivities to the gas exchange formulation and ocean transport strength. *Global Biogeochemical Cycles*, 22(3).

Munhoven, G. (2002). Glacial–interglacial changes of continental weathering: estimates of the related CO_2 and HCO_3^- flux variations and their uncertainties. *Global and Planetary Change*, 33(1-2):155–176.

Najjar, R., Orr, J., Sabine, C., and Joos, F. (1999). Biotic-HowTo. *Internal OCMIP Report, LSCE/CEA Saclay, Gifsur-Yvette, France*.

Oliver, K. I., Hoogakker, B. A., Crowhurst, S., Henderson, G., Rickaby, R. E., Edwards, N., and Elderfield, H. (2010). A synthesis of marine sediment core $\delta^{13}C$ data over the last 150 000 years. *Climate of the Past*, 6(5):645–673.

Opdyke, B. N. and Walker, J. C. (1992). Return of the coral reef hypothesis: Basin to shelf partitioning of $CaCO_3$ and its effect on atmospheric CO_2. *Geology*, 20(8):733–736.

Orr, J. and Epitalon, J.-M. (2015). Improved routines to model the ocean carbonate system: mocsy 2.0. *Geoscientific Model Development*, 8(3):485–499.

Orr, J., Najjar, R., Sabine, C., and Joos, F. (1999). Abiotic-HowTo. *Internal OCMIP Report, LSCE/CEA Saclay, Gifsur-Yvette, France*, 1999.

Orr, J. C., Najjar, R. G., Aumont, O., Bopp, L., Bullister, J. L., Danabasoglu, G., Doney, S. C., Dunne, J. P., Dutay, J.-C., Graven, H., et al. (2017). Biogeochemical protocols and diagnostics for the CMIP6 Ocean Model Intercomparison Project (OMIP). *Geoscientific Model Development*, 10(6):2169–2199.

Parekh, P., Joos, F., and Müller, S. A. (2008). A modeling assessment of the interplay between aeolian iron fluxes and iron-binding ligands in controlling carbon dioxide fluctuations during Antarctic warm events. *Paleoceanography*, 23(4).

Peterson, C. D. and Lisiecki, L. E. (2018). Deglacial carbon cycle changes observed in a compilation of 127 benthic $\delta^{13}C$ time series (20–6 ka). *Climate of the Past*, 14(8):1229–1252.

Petit, J.-R., Jouzel, J., Raynaud, D., Barkov, N. I., Barnola, J.-M., Basile, I., Bender, M., Chappellaz, J., Davis, M., Delaygue, G., et al. (1999). Climate and atmospheric history of the past 420,000 years from the Vostok ice core, Antarctica. *Nature*, 399(6735):429–436.

Pollock, D. E. (1997). The role of diatoms, dissolved silicate and Antarctic glaciation in glacial/interglacial climatic change: a hypothesis. *Global and Planetary Change*, 14(3-4):113–125.

Pöppelmeier, F., Scheen, J., Jeltsch-Thömmes, A., and Stocker, T. F. (2020). Simulated stability of the AMOC during the Last Glacial Maximum under realistic boundary conditions. *Climate of the Past Discussions*, 2020:1–28.

Qin, B., Li, T., Xiong, Z., Algeo, T., and Jia, Q. (2018). Deep-Water Carbonate Ion Concentrations in the Western Tropical Pacific Since the Mid-Pleistocene: A Major Perturbation During the Mid-Brunhes. *Journal of Geophysical Research: Oceans*, 123(9):6876–6892.

Raven, J. A. and Falkowski, P. G. (1999). Oceanic sinks for atmospheric CO_2. *Plant, Cell & Environment*, 22(6):741–755.

Ridgwell, A. J., Watson, A. J., Maslin, M. A., and Kaplan, J. O. (2003). Implications of coral reef buildup for the controls on atmospheric CO_2 since the Last Glacial Maximum. *Paleoceanography*, 18(4).

Roberts, J., Gottschalk, J., Skinner, L. C., Peck, V. L., Kender, S., Elderfield, H., Waelbroeck, C., Vázquez Riveiros, N., and Hodell, D. A. (2016). Evolution of South Atlantic density and chemical stratification across the last deglaciation. *Proceedings of the National Academy of Sciences*, 113(3):514–519.

Roth, R., Ritz, S., and Joos, F. (2014). Burial-nutrient feedbacks amplify the sensitivity of atmospheric carbon dioxide to changes in organic matter remineralisation. *Earth System Dynamics*, 5(2):321–343.

Sarnthein, M., Schneider, B., and Grootes, P. M. (2013). Peak glacial ^{14}C ventilation ages suggest major draw-down of carbon into the abyssal ocean. *Climate of the Past*, 9(6):2595–2614.

Schmitt, J., Schneider, R., Elsig, J., Leuenberger, D., Lourantou, A., Chappellaz, J., Köhler, P., Joos, F., Stocker, T. F., Leuenberger, M., et al. (2012). Carbon isotope constraints on the deglacial CO_2 rise from ice cores. *Science*, 336(6082):711–714.

Schmittner, A. (2003). Southern Ocean sea ice and radiocarbon ages of glacial bottom waters. *Earth and Planetary Science Letters*, 213(1-2):53–62.

Schmittner, Andreas Galbraith, E. D. (2008). Glacial greenhouse-gas fluctuations controlled by ocean circulation changes. *Nature*, 546.

Schneider, R., Schmitt, J., Köhler, P., Joos, F., and Fischer, H. (2013). A reconstruction of atmospheric carbon dioxide and its stable carbon isotopic composition from the penultimate glacial maximum to the last glacial inception. *Climate of the Past*, 9(6):2507–2523.

Shackleton, N. J. (2000). The 100,000-year ice-age cycle identified and found to lag temperature, carbon dioxide, and orbital eccentricity. *Science*, 289(5486):1897–1902.

Siegenthaler, U., Stocker, T. F., Monnin, E., Luthi, D., Schwander, J., Stauffer, B., Raynaud, D., Barnola, J.-M., Fischer, H., Masson-Delmotte, V., et al. (2005). Stable carbon cycle climate relationship during the Late Pleistocene. *Science*, 310(5752):1313–1317.

Sigman, D. M. and Boyle, E. A. (2000). Glacial/interglacial variations in atmospheric carbon dioxide. *Nature*, 407(6806):859–869.

Sigman, D. M., Hain, M. P., and Haug, G. H. (2010). The polar ocean and glacial cycles in atmospheric CO_2 concentration. *Nature*, 466(7302):47–55.

Smith, H. J., Fischer, H., Wahlen, M., Mastroianni, D., and Deck, B. (1999). Dual modes of the carbon cycle since the Last Glacial Maximum. *Nature*, 400(6741):248–250.

Stein, K., Timmermann, A., Kwon, E. Y., and Friedrich, T. (2020). Timing and magnitude of Southern Ocean sea ice/carbon cycle feedbacks. *Proceedings of the National Academy of Sciences*, 117(9):4498–4504.

Stephens, B. B. and Keeling, R. F. (2000). The influence of Antarctic sea ice on glacial–interglacial CO_2 variations. *Nature*, 404(6774):171–174.

Tschumi, T., Joos, F., Gehlen, M., and Heinze, C. (2011). Deep ocean ventilation, carbon isotopes, marine sedimentation and the deglacial CO_2 rise. *Climate of the Past*, 7(3):771–800.

Tschumi, T., Joos, F., and Parekh, P. (2008). How important are Southern Hemisphere wind changes for low glacial carbon dioxide? A model study. *Paleoceanography*, 23(4).

Von Blanckenburg, F., Bouchez, J., Ibarra, D. E., and Maher, K. (2015). Stable runoff and weathering fluxes into the oceans over Quaternary climate cycles. *Nature Geoscience*, 8(7):538–542.

Wallmann, K., Schneider, B., and Sarnthein, M. (2016). Effects of eustatic sea-level change, ocean dynamics, and nutrient utilization on atmospheric pCO_2 and seawater composition over the last 130 000 years: a model study. *Climate of the Past*, 12(2):339–375.

Wanninkhof, R. (2014). Relationship between wind speed and gas exchange over the ocean revisited. *Limnology and Oceanography: Methods*, 12(6):351–362.

Weiss, R. (1974). Carbon dioxide in water and seawater: the solubility of a non-ideal gas. *Marine chemistry*, 2(3):203–215.

Willeit, M., Ganopolski, A., Calov, R., and Brovkin, V. (2019). Mid-Pleistocene transition in glacial cycles explained by declining CO_2 and regolith removal. *Science Advances*, 5(4):eaav7337.

Winckler, G., Anderson, R. F., Fleisher, M. Q., McGee, D., and Mahowald, N. (2008). Covariant glacial-interglacial dust fluxes in the equatorial Pacific and Antarctica. *science*, 320(5872):93–96.

Wood, M., Hayes, C. T., and Paytan, A. (2023). Global Quaternary Carbonate Burial: Proxy-and Model-Based Reconstructions and Persisting Uncertainties. *Annual review of marine science*, 15:277–302.

Yu, J., Menviel, L., Jin, Z., Thornalley, D., Foster, G. L., Rohling, E., McCave, I., McManus, J., Dai, Y., Ren, H., et al. (2019). More efficient North Atlantic carbon pump during the last glacial maximum. *Nature communications*, 10(1):2170.

Yu, Z., Loisel, J., Brosseau, D. P., Beilman, D. W., and Hunt, S. J. (2010). Global peatland dynamics since the last glacial maximum. *Geophysical research letters*, 37(13).

Supplementary Information for Adloff et al. 2024

Physical model parameterisations

The geostrophic-frictional balance ocean circulation is calculated explicitly (Edwards et al., 1998; Müller et al., 2006), and parameterizations are included to represent the effects of dia- and isopycnal diffusion and eddy-induced transport (Griffies, 1998). The NCEP/NCAR monthly wind stress climatology (Kalnay et al., 1996) is used to prescribe wind stress at the ocean surface. Atmosphere-ocean gas exchange and carbonate chemistry are simulated according to the OCMIP-2 protocols (Najjar et al., 1999; Orr et al., 1999, 2017; Wanninkhof, 2014; Orr and Epitalon, 2015), and gas transfer velocities are linearly scaled with wind speed instead to quadratic (Krakauer et al., 2006). The global mean sea-air gas exchange was then reduced by 19% to achieve agreement with pre-bomb testing radiocarbon distribution estimates and 20th century observations (Müller et al., 2008). This is a standard adjustment in Bern3D and accounts for the fact that Δ14C in the surface ocean is overestimated by the gas transfer velocities calculated from wind speed.

Model limitations

There are several ways in which the amplitude or regional pattern of the simulated changes might be biased by our experiment design. Firstly, by design our forcings are smooth in time and spatially uniform, which is a stark simplification. For example, the PO4 forcing ties nutrient supply to the δ^{18}O record. The correlation between dust (iron source to the open ocean) concentrations in the EPICA Dome C ice core and benthic δ^{18}O is of first order only and varies over the glacial cycle (Winckler et al., 2008). Several macro- and micronutrients were likely supplied to varying parts of the glacial ocean (Broecker, 1982b; Martin, 1990; Pollock, 1997; Deutsch et al., 2004) and while dust flux changes seem to correlate globally (Kukla et al., 1990; Winckler et al., 2008), the timings and rates of other nutrient fluxes might in reality have varied temporally and spatially. Similarly, our other forcings might change more slowly over the deglaciation than the real processes they mimic. A more detailed analysis of non-linear interactions between the tested forcings would require an additional simulation ensemble that tests all possible forcing combinations and ideally also with varying forcing magnitudes.

Another simplification in our experiment design is that the majority of our simulations assume temporally constant terrestrial solute inputs although in reality these fluxes are climate sensitive (Munhoven, 2002). It is unlikely that removing this simplification would substantially alter the simulated global carbon fluxes and reservoir size changes because it is estimated that global weathering rate changes during glacial cycles were small despite large local variability, possibly because they canceled out in the global mean (Jones et al., 2002; Von Blanckenburg et al., 2015; Frings, 2019; Börker et al., 2020). It was estimated that glacial-interglacial weathering flux changes altered atmospheric CO_2 by a maximum of 20 ppm (Köhler and Munhoven, 2020). Yet, the resulting δ^{13}C perturbation could be larger because a global balance in carbon flux changes does not imply a balance in carbon isotope fluxes (Jeltsch-Thömmes and Joos, 2023). Additionally, there might have been non-linear changes in isotopic input fluxes during the simulated time period.

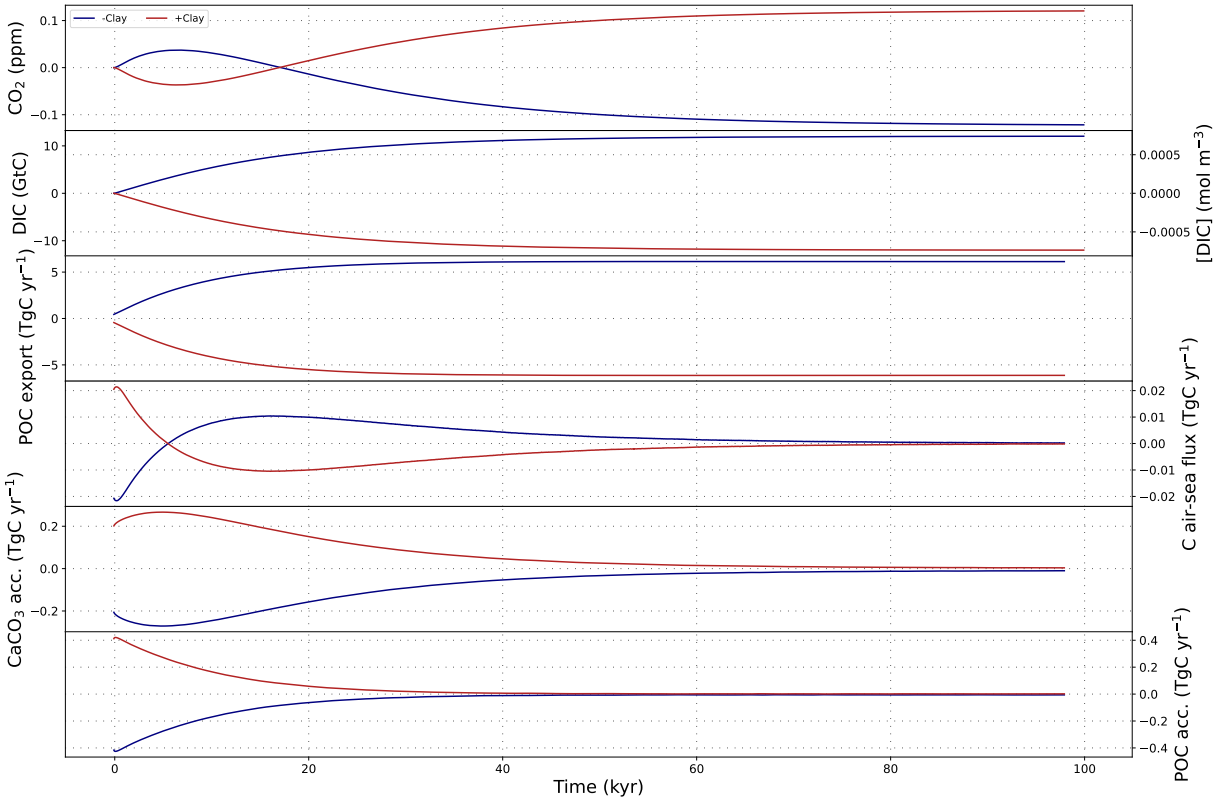

Figure S1. The effect of step changes of plus or minus 30% of the prescribed clay flux on atmospheric CO_2 concentrations, DIC and carbon fluxes over 100 kyr.

Finally, the imbalance between weathering and burial fluxes is also shaped by the sedimentation rate. In our simulations, sedimentation rates vary due to changes in biogenic export, yet accumulation of non-biogenic material was kept constant. This omission, however, is not a large error source, given that a separately prescribed step-wise 30% increase and decrease of the non-biogenic flux in the PI steady state had only marginal effects on atmospheric CO_2, DIC and sedimentary accumulation of biogenic particles (Fig. S1).

Effects of orbital, insolation and albedo changes on carbon fluxes

In the following, we examine the underlying glacial-interglacial carbon cycle changes and the effect of interactive sediments under each forcing. First we focus on the standard forcing, before discussing the effects of additional forcings.

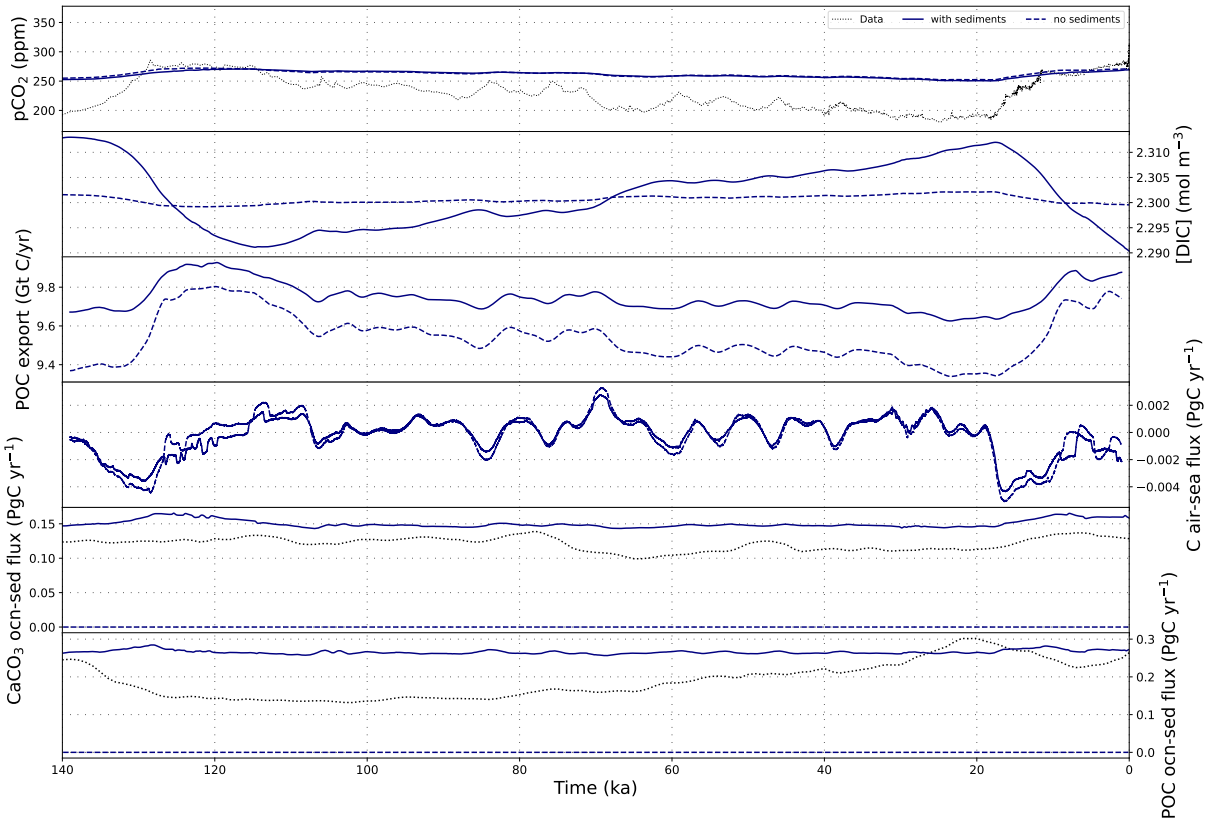

Figure S2. Atmospheric CO_2 concentrations, DIC and carbon fluxes over the most recent full glacial cyle in simulation BASE with and without dynamic sediments.

The dynamic circulation and climate affect the partitioning of carbon between the interactive carbon reservoirs in the model (atmosphere, ocean, reactive sediments and lithosphere). The applied forcings vary the CO_2 concentration gradient between air and seawater by modifying CO_2 solubility and surface ocean DIC and alkalinity concentrations. Without dynamic sediments (Fig S2), carbon in response moves between the atmosphere, the marine DIC and, to a lesser extent, DOC reservoirs in the ocean. With the standard forcing, CO_2 and O_2 solubilities increase during glacial phases because of the cooling surface ocean, leading to a steady marine uptake of carbon and oxygen from the atmosphere from peak interglacial through to the glacial maximum. The cooling reduces deep water formation rates in the North Atlantic and increases deep water formation in the Southern Ocean. These circulation changes increase the marine uptake of CO_2 while expanding sea ice prevents outgassing of marine CO_2 in the Southern Ocean. Overall POC and $CaCO_3$ export fluxes decrease during glaciation despite increased primary productivity in mid-latitudes and sub-tropics due to reduced export production in the high latitudes, predominantly due to sea ice growth, in places also because of reduced nutrient supply and lower temperatures. These export fluxes changes, particularly in the Southern Ocean, alter phosphate cycling: In interglacial states, high export fluxes effectively transfer phosphate from the photic zone to the intermediate ocean, where most exported POC is remineralized. Upwelling of intermediate water

masses returns phosphate to the surface ocean. In glacial states, less of the phosphate upwelling in the Southern Ocean is incorporated into POC and exported to intermediate ocean depths. Instead, it is downwelled and incorporated into bottom waters. In consequence, the glacial deep ocean is enriched in preformed phosphate, while phosphate concentrations at intermediate depth decrease due to climate-driven export reduction. In the surface, reduced upwelling of nutrients and reduced nutrient uptake result in almost no net change of nutrient concentrations. During deglaciation, surface and deep waters warm and upwelling as well as export fluxes are restored. Hence, decreases in atmospheric CO_2 concentration during the onsets of glaciations are directly mirrored by increases in marine DIC and decreases in marine DOC, and the inverse occurs during deglaciation.

When interactive sediments are included in the simulations, export production and ocean chemistry changes alter sediment burial and dissolution fluxes, resulting in more than 10x larger DIC fluctuations over a glacial cycle than in the closed system. Changes in net sea-air gas exchange across the glacial cycle ($\sim$0.007 PgC/yr) are smaller than changes in each POC and $CaCO_3$ burial rates ($\sim$0.02 PgC/yr). $CaCO_3$ burial is predominantly driven by productivity changes and peaks during interglacials. In glacials, $CaCO_3$ burial is reduced below areas with reduced euphotic zone $CaCO_3$ export, e.g. in the high latitudes, but additionally where $CaCO_3$ becomes unstable due lower temperatures or reduced pH due to increased sedimentary POC oxydation rates. The standard forcing is not sufficient to cause wide-spread O_2 depletion in the glacial deep ocean, hence under the standard forcing POC burial rates are driven by export production rates, with less/more burial in areas with reduced/increased POC export production, respectively. The exception is the upwelling zone in the Equatorial East Pacific and parts of the Indian Ocean, where increased POC export depletes benthic and sediment pore water O_2 during glacial phases. During deglaciations, sea ice recedes, ocean ventilation increases and the surface and intermediate oceans warm, fostering increased primary productivity. While productivity and POC burial increase quickly in the subpolar regions, POC burial rates in the Eastern Equatorial Pacific respond more slowly to the warming: Long turnover timescales of pore water O_2 in sediments and remineralisation of previously deposited POC delay the return of interglacial POC remineralisation rates relative to export rates from the surface ocean. Therefore, deglaciations are marked by faster productivity increases in the surface ocean than sedimentary POC remineralisation. This results in a 'sweet spot' during glacial terminations, when tropical POC burial is still higher than in the interglacial while extratropical POC export and burial has already recovered to interglacial levels, particularly during the last 400 kyr which show larger glacial-interglacial temperature contrasts and faster warming rates during deglaciations. This 'sweet spot' causes the maximum of global POC burial to occur during deglaciation, before the full interglacial.

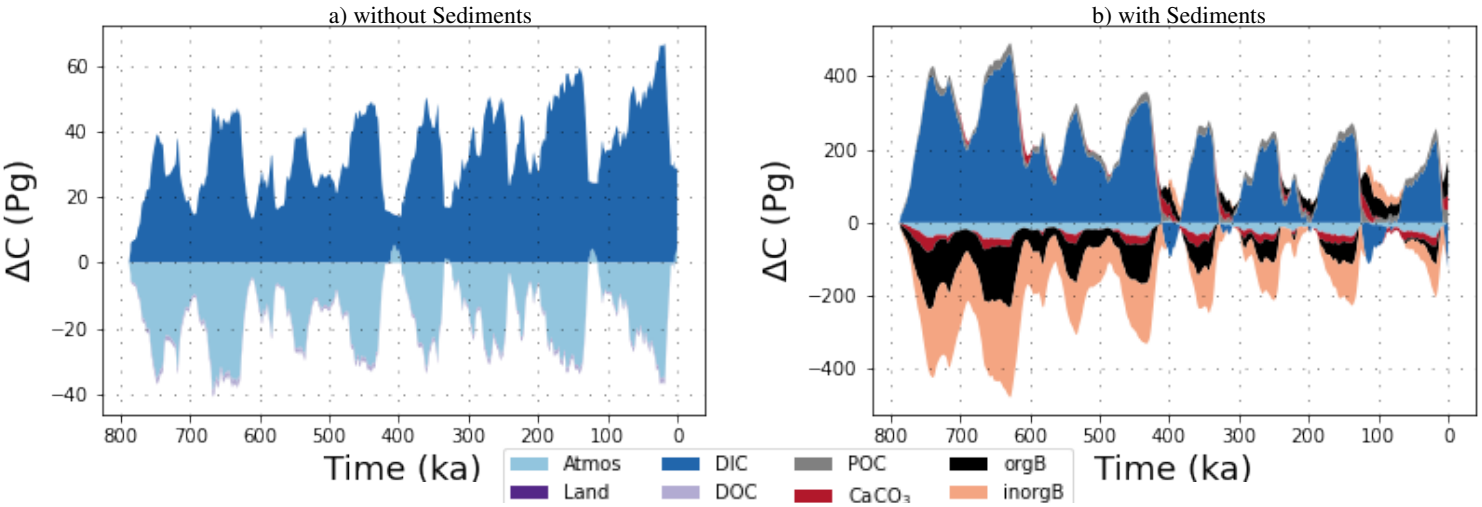

Figure S3. Transient carbon reservoir size changes across the last 780kyr as simulated in simulations with the standard (orbital, radiation and albedo) forcings in simulation BASE with and without dynamic marine sediments. Shown are the size changes of atmospheric, terrestrial, marine (DIC and DOC), sedimentary (POC and $CaCO_3$) and lithospheric (organic and inorganic) carbon storage. Note that the y-axis scale is an order of magnitude larger in b) than in a).

Introducing sediments (and a constant weathering flux) also changes carbon cycle dynamics over multiple glacial cycles. Fig S3 shows the transient changes in the simulated carbon reservoirs in simulation BASE over the entire simulated time period. In our set-up, carbon exchange between the atmosphere, ocean and sediments reacts to climatic and biogeochemical changes while weathering input fluxes of DIC, alkalinity and PO_4^{3-} are constant over time. A carbon flux imbalance arises during glacial phases in this open system. Under purely physical forcings, export fluxes from the photic zone decrease during glacial phases. Despite locally increased sedimentary POC preservation, global sediment accumulation rates decrease. In consequence, sequestration of $CaCO_3$ and POC from the reactive sediments (i.e. sediment burial) is reduced as well, since it is governed by the mass accumulation rate. The carbon which would have otherwise been buried instead accumulates as DIC in the ocean. Acceleration of sediment mass accumulation rates during glacial terminations increases sediment burial, which reduces marine DIC. The strength of these carbon cycle responses depends on the forcing strength, which varies between glacial cycles. The lukewarm interglacials of the first 350 kyr of our simulations do not restore the export fluxes and sedimentary $CaCO_3$ preservation required to re-balance the geologic carbon cycle, and so marine DIC concentrations are persistently higher during 800-450ka than at PI. Interglacials of the last 450kyr of the simulation reduce DIC in the long-term because they are warm and long enough for increased carbon transfer into sediments and sediment burial.

Effects of additional forcings and Earth system changes on carbon fluxes

The previously described carbon cycle changes vary when further forcings and Earth system changes are applied.

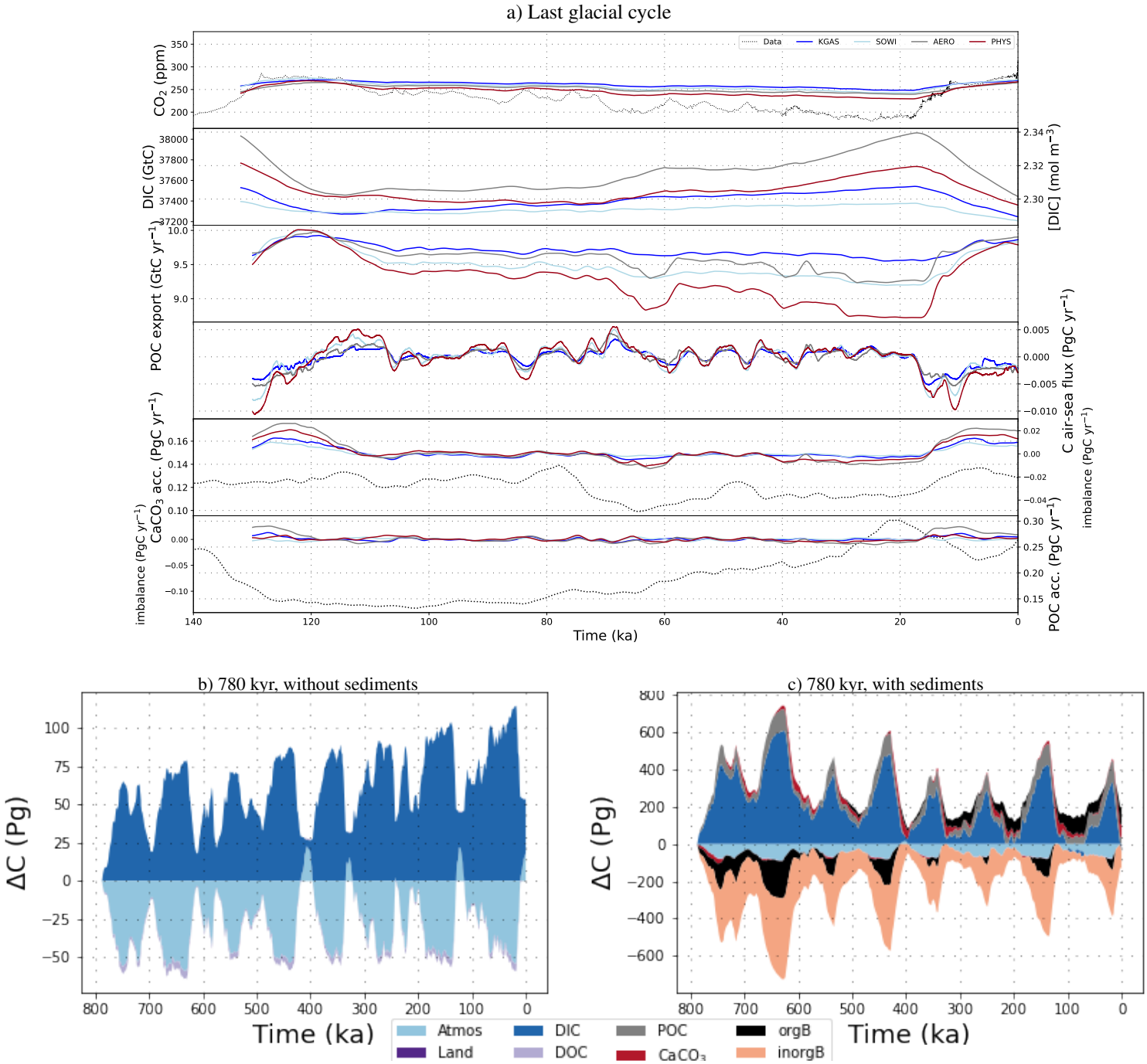

Figure S4. a) Atmospheric CO_2 concentrations, DIC and carbon fluxes over the most recent full glacial cyle in simulations with additional physical forcings in an open system. b) Transient carbon reservoir size changes across the last 780 kyr as simulated with all additional physical forcings combined in a closed system and c) in an open system. Shown are the size changes of atmospheric, terrestrial, marine (DIC and DOC), sedimentary (POC and $CaCO_3$) and lithospheric (organic and inorganic) carbon storage. Reservoir changes for individual forcings are displayed in Fig S24. Flux timeseries for simulations in a closed system are displayed in Fig S25.

Additional physical forcings result in roughly 1.5x larger carbon fluxes (Fig. S4), partially by amplifying the processes under the standard forcing and partially by introducing additional ones. Additional reduction of wind stress in the Southern Ocean (simulation SOWI) leads to a stronger isolation of deep Pacific water masses, reducing benthic oxygen levels. With dynamic sediments, more organic matter and $CaCO_3$ reaching the sediments is preserved due to the reduced oxygen concentrations, particularly in Pacific upwelling zones. This results in a larger net removal of nutrients and carbon from the ocean during glacial times which would have otherwise been released at intermediate depth. In consequence, wind stress forcing over the Southern Ocean reduces the carbon content of Pacific deep water when dynamic sediments are considered, despite an increase in water mass age. The re-ventilation of the deep Pacific during glacial termination leads to rising benthic oxygen concentrations. Due to the lower storage of dissolved nutrients and carbon in the glacial deep ocean, the potential to upwell nutrients during deglaciation is reduced, suppressing the spike in POC burial during terminations seen under the standard forcing and reducing PIC burial during these transition phases.

Reducing the transfer velocity of CO_2 in the Southern Ocean during glacials (simulation KGAS) also reduces CO_2 outgassing in the Southern Ocean which increases DIC in the deep Pacific but leaves ocean circulation unaffected, which reduces its global impact and, unlike the wind forcing, does not trap nutrients in the deep Pacific.

The AMOC slow-down in simulations with an additional reduction of incoming radiation during glacial phases and especially glacial maxima (e.g. via aerosol dimming, simulation AERO) creates an old, nutrient-rich and O_2-poor bottom water mass in the glacial Atlantic. Unlike with a vigorous AMOC, nutrients are not returned as quickly to the surface Atlantic but accumulate in the deep. The additional cooling combined with reduced nutrient supply reduces POC and $CaCO_3$ export in the Atlantic. In the North, where sea ice extent is increased and temperatures drop the most, they cease entirely. Globally, the additional cooling increases CO_2 and O_2 solubility. Overall these effects increase glacial carbon storage in the deep ocean. With dynamic sediments, the reduced $CaCO_3$ export in the North Atlantic raises the local lysocline, causing dissolution and increased marine DIC concentrations. The sudden shift in water masses when AMOC resumes during deglaciation amplifies the spike in burial rates observed under the standard forcing.

The different carbon and nutrient fluxes under these forcings change the total carbon and nutrient inventories in simulations with an open system, resulting in different DIC and nutrient concentrations at the start of the last glacial cycle and at the end of the runs.

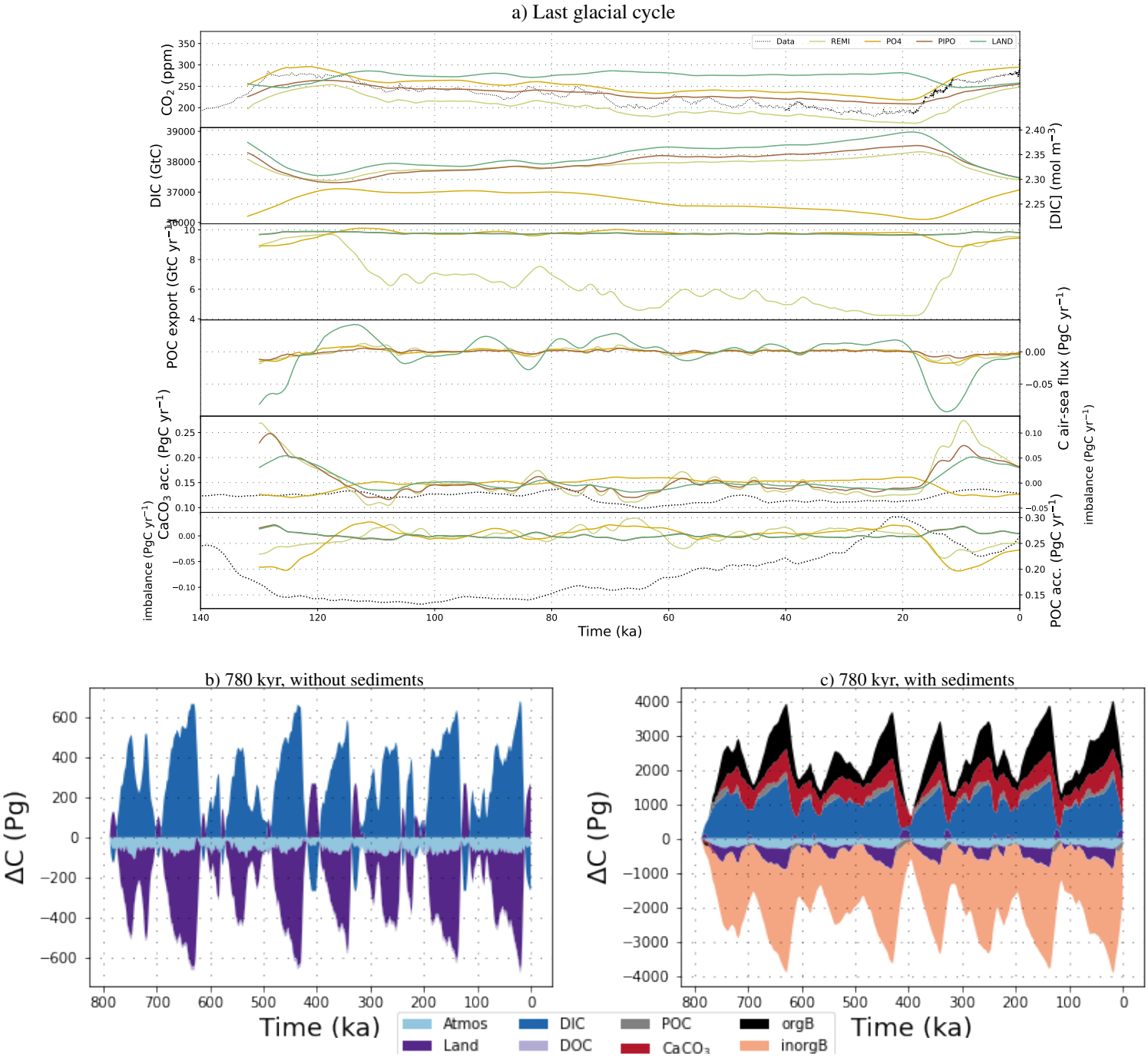

Figure S5. a) Atmospheric CO_2 concentrations, DIC and carbon fluxes over the most recent full glacial cyle in simulations with additional biogeochemical forcings in an open system. b) Transient carbon reservoir size changes across the last 780 kyr as simulated with all additional biogeochemical forcings combined in a closed system and c) in an open system. Shown are the size changes of atmospheric, terrestrial, marine (DIC and DOC), sedimentary (POC and $CaCO_3$) and lithospheric (organic and inorganic) carbon storage. Reservoir changes for individual forcings are displayed in Fig S26 and S27. Flux timeseries for simulations in a closed system are displayed in Fig S28.

Biogeochemical forcings affect carbon transfer primarily through the biological pump and the size of the terrestrial carbon sink. Nutrient inputs during glacial phases in simulation PO4 increase POC and $CaCO_3$ export, and sedimentary burial rates through increased sedimentary mass accumulation and lower O_2 concentrations in the deep ocean (Fig S5). During glacial termination, the prescribed nutrient supply to the surface ocean stops before the deep ocean is fully re-ventilated and the nutrients that accumulated in intermediate and deep water masses have returned to the surface. This delay results in low nutrient concentrations in the surface ocean, a transient drop in POC export, and consequentially burial fluxes. The reduced carbon burial raises DIC and increases the net carbon transfer from surface waters to the atmosphere during deglaciation. In consequence, when nutrients are added to a glacial ocean with responsive sediments, glacial phases become the dominant periods of organic and inorganic ~~C~~ carbon sediment burial, reducing the accumulation of marine DIC and increasing the marine uptake of atmospheric CO_2 during glacial phases. This simulation PO4 yields the temporal CO_2 evolution which most closely resembles reconstructions from ice cores.

Reducing the PIC:POC ratio of export production during glacial phases (simulation PIPO) increases alkalinity in the surface ocean which enhances marine carbon uptake from the atmosphere, resulting in an additional CO_2 drawdown of up to $\sim$10ppm without sediments. This effect is enhanced by 20ppm when dynamic sediments are considered. When the export production is tilted towards organic matter production in an ocean with interactive sediments, reduced $CaCO_3$ export during inceptions and glacial periods translate into reduced $CaCO_3$ burial rates. This leads to a shoaling of the carbonate compensation depth, a build-up of alkalinity in the ocean and increased carbon transfer from the atmosphere to the ocean. The reduced sedimentary carbonate accumulation reduces the total mass flux to the sediments. On extratropical continental slopes, the reduced mass accumulation slows organic carbon burial, retaining more nutrients in the ocean and decreasing O_2 concentrations through continued remineralization instead. On continental slopes under upwelling areas with high productivity, the reduced O_2 expands the O_2 minimum zones, an effect which outweighs the local reduction of carbonate export and results in higher POC burial rates despite less carbonate deposition. Restoration of the interglacial PIC:POC ratio during deglaciation then enhances sedimentary carbonate deposition in benthic waters with higher pH and larger O_2 minimum zones than under the standard forcing, increasing the temporal spikes in carbonate and POC burial. Reduced glacial PIC:POC increases $CaCO_3$ burial events during glacial terminations.

Lowering the remineralization depth of organic matter in the glacial water column (simulation REMI) leads to a net carbon and nutrient transfer from the surface ocean to intermediate and deep water masses, where more O_2 is consumed. Without dynamic sediments, the increased DIC concentrations in the deep ocean increases the carbon storage of the glacial ocean. In addition, the reduced dissolution of POC in the upper water column during glacials increases surface ocean pH and CO_2 uptake by the ocean. With dynamic sediments, the resulting reduction in deep ocean O_2 concentration increases POC preservation in sediments below high productivity zones, e.g. tropical continental margins and upwelling areas. Where the larger flux of POC reaching the sediments is not preserved, it is remineralized, reducing the stability of sedimentary $CaCO_3$. Glacial inceptions are then characterized by increased POC and POP fluxes into the sediments and reduced $CaCO_3$ burial. During glacial terminations, POC is increasingly remineralized at shallower depth again, leading to reduced POC fluxes into the deep ocean and POC burial compared to the glacial phase. Surface ocean pH decreases and ~~C~~ carbon is returned to the atmosphere. Compared to the

standard forcing, lowering the remineralization depth thus shifts the timing of maximal POC burial rates from the interglacial to the glacial and amplifies the transient spike in $CaCO_3$ burial as increased nutrient supply during glacials does, but it also increases sedimentary $CaCO_3$ dissolution during glacial phases.

Land carbon release to the atmosphere during glacial phases (simulation LAND) invades and acidifies the ocean due to increased atmospheric concentrations, growing the marine DIC reservoir during glacials with and without dynamic sediments, resulting in the biggest glacial marine DIC reservoirs across our simulations. When interactive sediments are considered, this marine carbon uptake reduces $CaCO_3$ preservation and leads to a shoaling of the lysocline. During termination, as the external carbon addition subsides, the ocean vents carbon back into the atmosphere, transiently allowing for increased $CaCO_3$ burial.

The previous paragraphs show that varying biogenic particle production in the surface ocean is only a relevant control on marine carbon storage changes when interactive sediments are simulated. Instead, lowering the main remineralization depth (simulation REMI) and adding terrestrial carbon release during glaciation (simulation LAND) strongly influence marine carbon storage with and without dynamic sediments. Without dynamic sediments, they double the marine carbon uptake during glacial periods. When including interactive sediments, all biogeochemical forcings have substantially larger effects on the carbon cycle than physical changes, with 5-10x larger carbon fluxes than under the standard forcing (Fig S5).

CO_2 restoring and non-linear effects of combined forcings on carbon fluxes

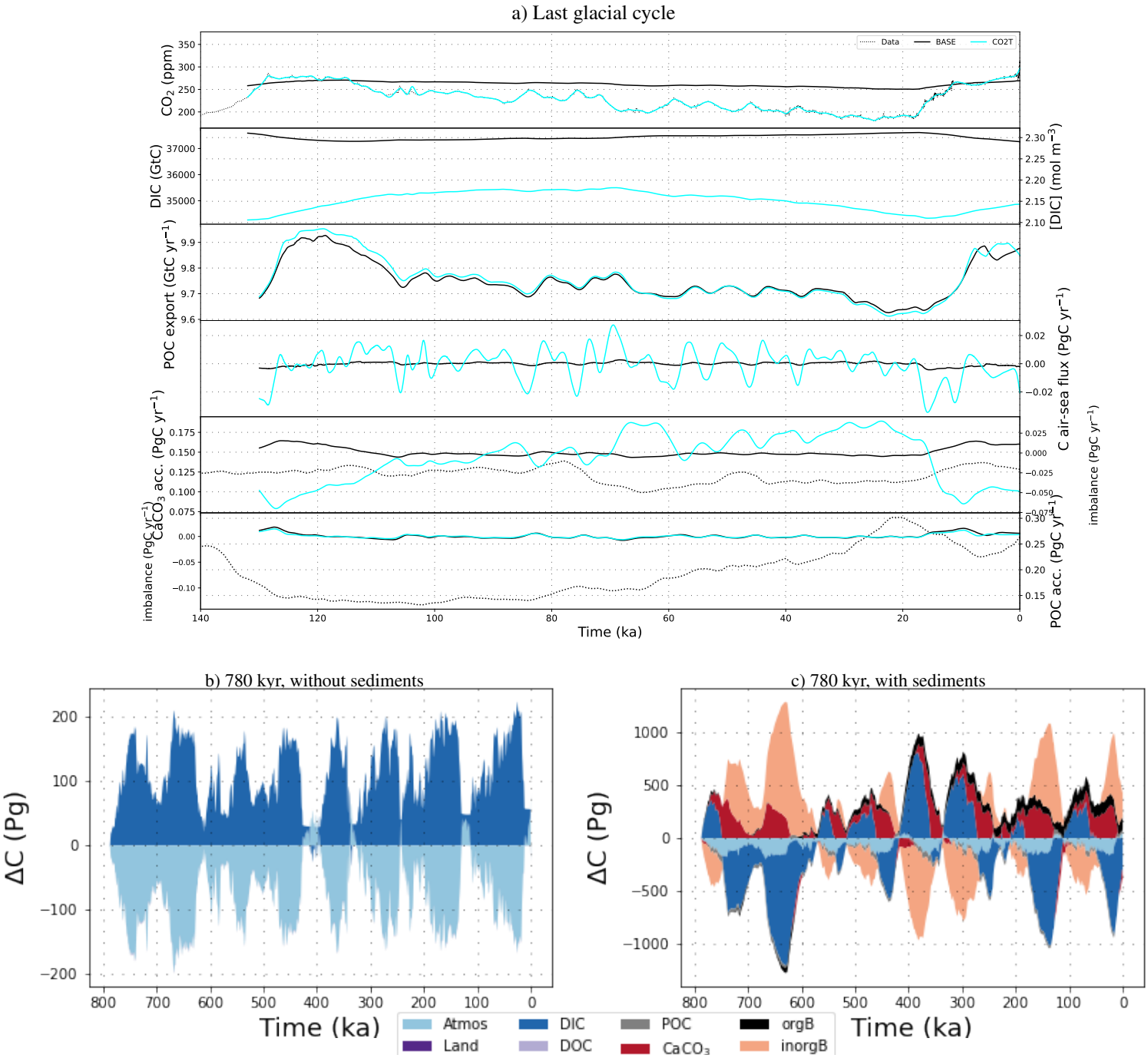

Figure S6. a) Atmospheric CO_2 concentrations, DIC and carbon fluxes over the most recent full glacial cyle in simulations BASE and CO2T in an open system. b) Transient carbon reservoir size changes across the last 780 kyr as simulated with alkalinity nudging in a closed system and c) in an open system. Shown are the size changes of atmospheric, terrestrial, marine (DIC and DOC), sedimentary (POC and $CaCO_3$) and lithospheric (organic and inorganic) carbon storage.

By design, the applied alkalinity nudging causes marine carbon uptake and release that shape atmospheric CO_2 in line with observations (Fig S6). As a consequence, the surface ocean is more alkaline in glacial times and more acidic during terminations than in the standard forcing, enabling increased marine carbon uptake. In simulations with dynamic sediments, $CaCO_3$ burial during cold phases is increased but the burial spike during terminations suppressed.

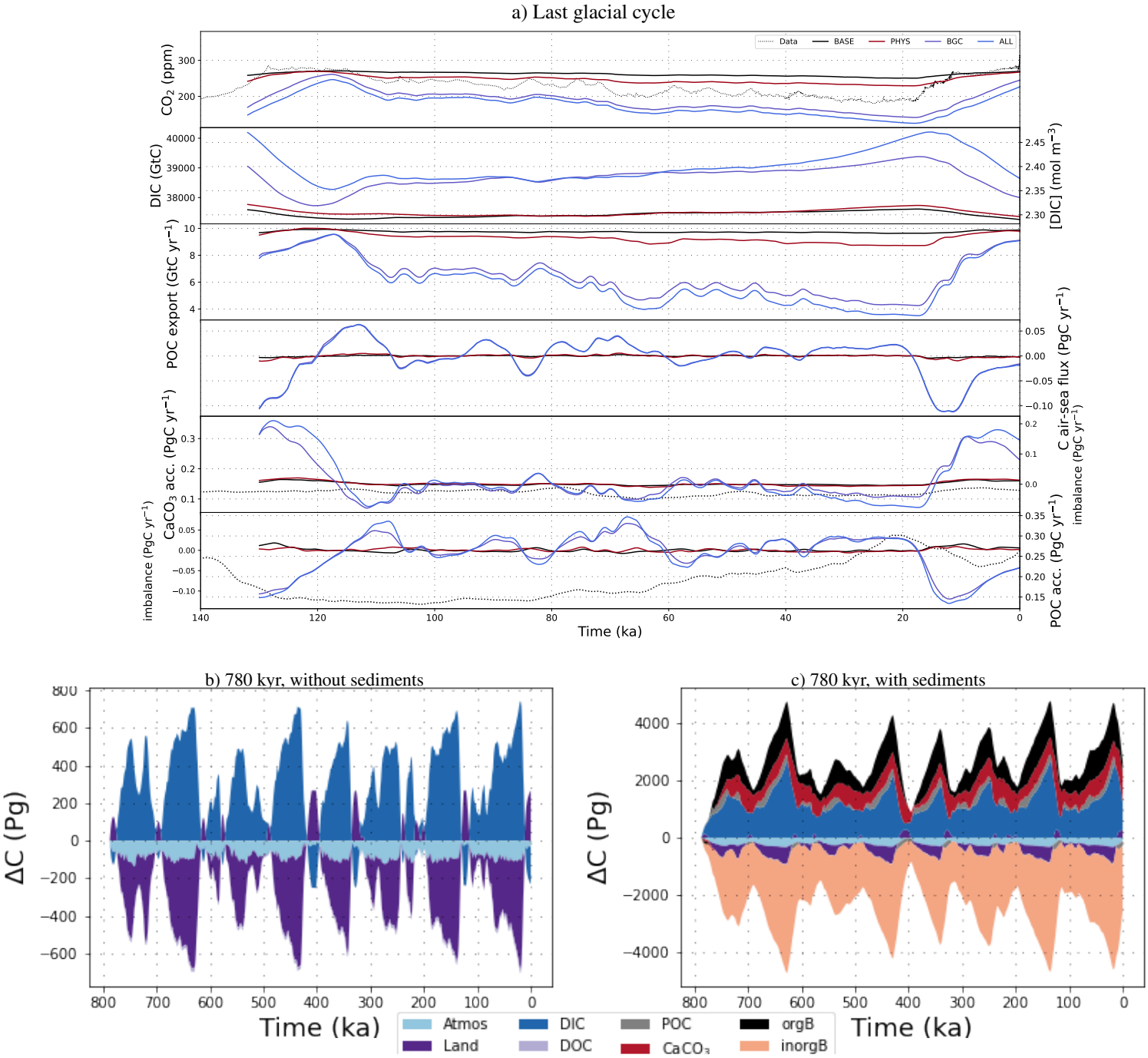

Figure S7. a) Atmospheric CO_2 concentrations, DIC and carbon fluxes over the most recent full glacial cyle in simulations with different combinations of additional forcings in an open system. b) Transient carbon reservoir size changes across the last 780 kyr as simulated with all additional forcings combined in a closed system and c) in an open system. Shown are the size changes of atmospheric, terrestrial, marine (DIC and DOC), sedimentary (POC and $CaCO_3$) and lithospheric (organic and inorganic) carbon storage. Flux timeseries for simulations in a closed system are displayed in Fig S29.

The three tested physical forcings combine almost linearly in their effect on atmospheric CO_2. Circulation change is dominated by radiation reductions, with strong AMOC weakening during glacials and some reduction of the PMOC, but less than in simulation SOWI because of increased sea ice cover in the Southern Ocean which limits the effect of wind stress changes. In consequence, the glacial deep ocean holds more nutrients when all forcings are combined: it has a large Atlantic reservoir due to sluggish overturning and a larger Pacific reservoir than in SOWI due to less organic carbon burial. During deglaciation, the release of these nutrients back into the surface ocean creates a larger productivity spike than when the forcings are applied individually, reducing marine $[O_2]$ further but causing only a minimal temporary reduction of <5 ppm in atmospheric CO_2 (Fig. S7). In simulations with interactive sediments, additional radiative forcing (AERO) and Southern Ocean wind forcing (SOWI) shift sedimentary $CaCO_3$ and POC accumulation rates in opposite directions. Yet, their effects on nutrient, temperature and oxygen distributions are almost additive.

While physical effects on carbon concentrations combine almost linearly, the combination of biogeochemical forcings is non-linear because they directly alter production and dissolution patterns in opposing ways. Acidification of benthic water masses through external nutrient (PO4) and carbon (LAND) supply during glacials counteracts the benthic pH increase under a deepened remineralisation depth (REMI). When all biogeochemical forcings are combined, net $CaCO_3$ fluxes into marine sediments are reduced during glacial maxima and increased during terminations, but the burial peak is delayed. Biogeochemical forcings dominate the carbon cycle response when all forcings are combined, except for the North Atlantic where circulation changes cause the biggest perturbation. The magnitude of the non-linearities that occur when all forcings are combined is similar to the combined effect of only the physical forcings.

Additional Figures

Table S1. Prescribed constant solute input into the surface ocean to balance steady-state interglacial sedimentary burial fluxes.

	DIC (GtC/yr)	ALK (Tmol eq/yr)	PO_4^{3-} (Tmol P/yr)	SiO (Tmol Si/yr)	$DI^{13}C$ (GtC/yr/$^{13}C_{std}$)
BASE	0.414	21.61	0.19	4.52	0.409

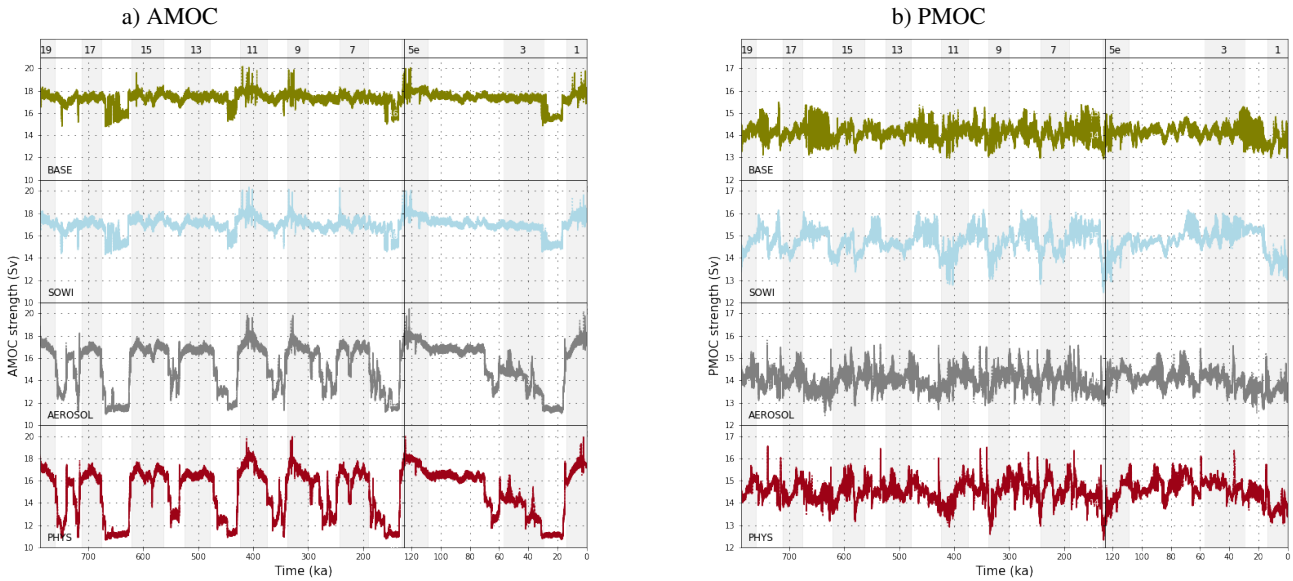

Figure S8. Transient variations of AMOC and PMOC strengths in simulations with different physcial forcings.

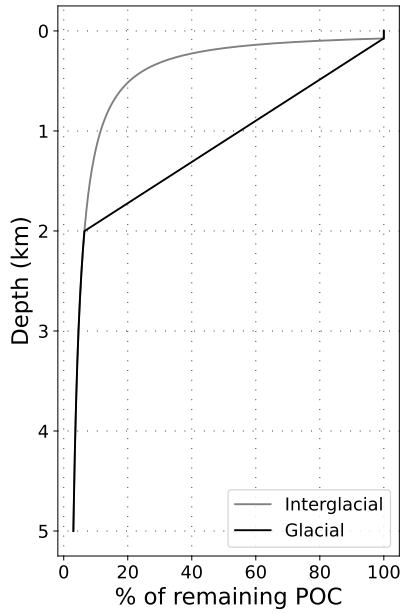

Figure S9. Comparison of the interglacial and glacial end-members of the prescribed remineralization profiles.

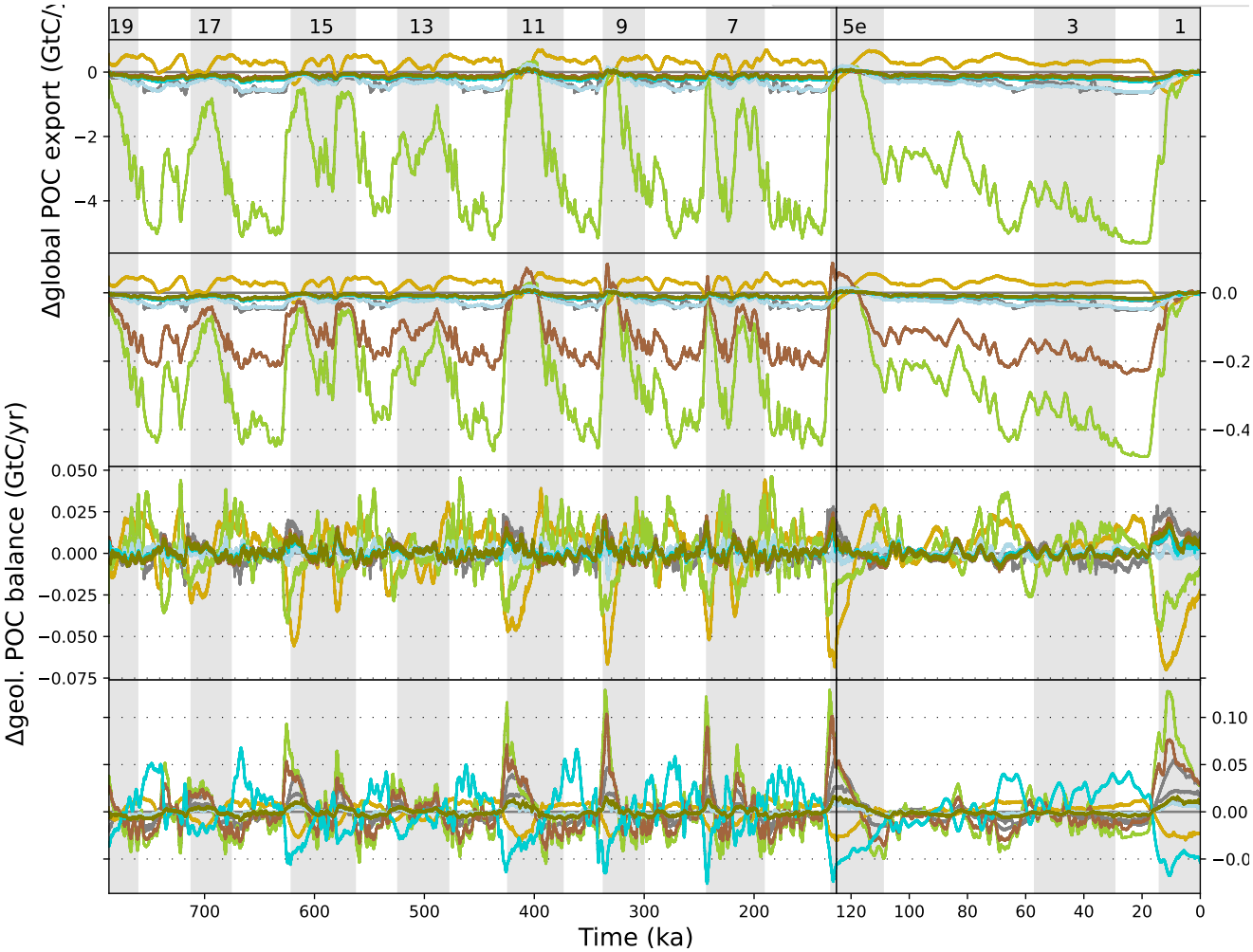

Figure S10. Transient variations of POC and $CaCO_3$ export production and geologic imbalance (i.e. the difference between accumulation of these materials in marine sediments and the constant supply into the surface ocean that mimics terrestrial weathering in our simulations) due to the applied forcings. Shown are the absolute results for each simulation. The results that are explicitly mentioned in the text are shown in colour, the others are shown in gray. Gray shading indicates uneven MIS as indicated at the top of the figure.

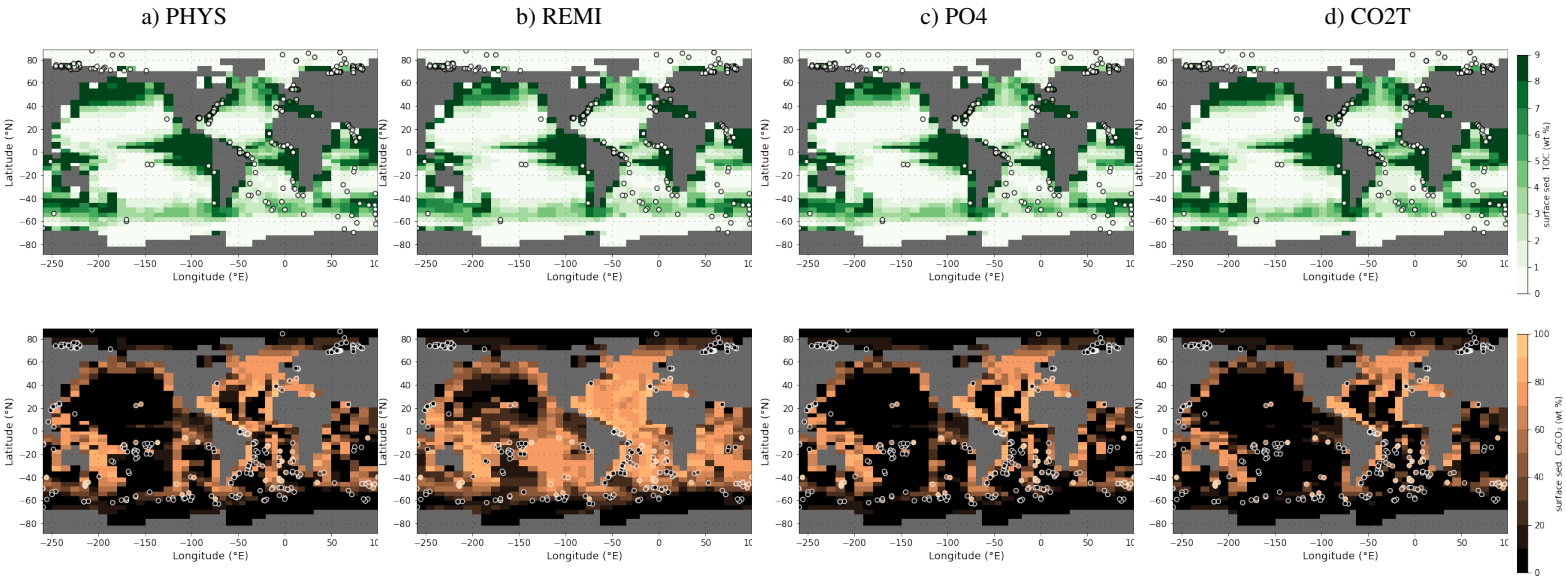

Figure S11. Sedimentary POC and $CaCO_3$ fractions during the late Holocene (Hayes et al., 2021) as reconstructed (circles) and in simulations PHYS, REMI, PO4 and CO2T (underlying maps). Shown are only data points that fall into the local benthic grid box of the model. The root mean square errors of simulated and reconstructed values are (from left to right): 7.6 %, 7.0 %, 7.6 % and 8.2 % for POC (top row) and 27.5 %, 25.7 %, 29.4 % and 31.4 % for $CaCO_3$ (bottom row).

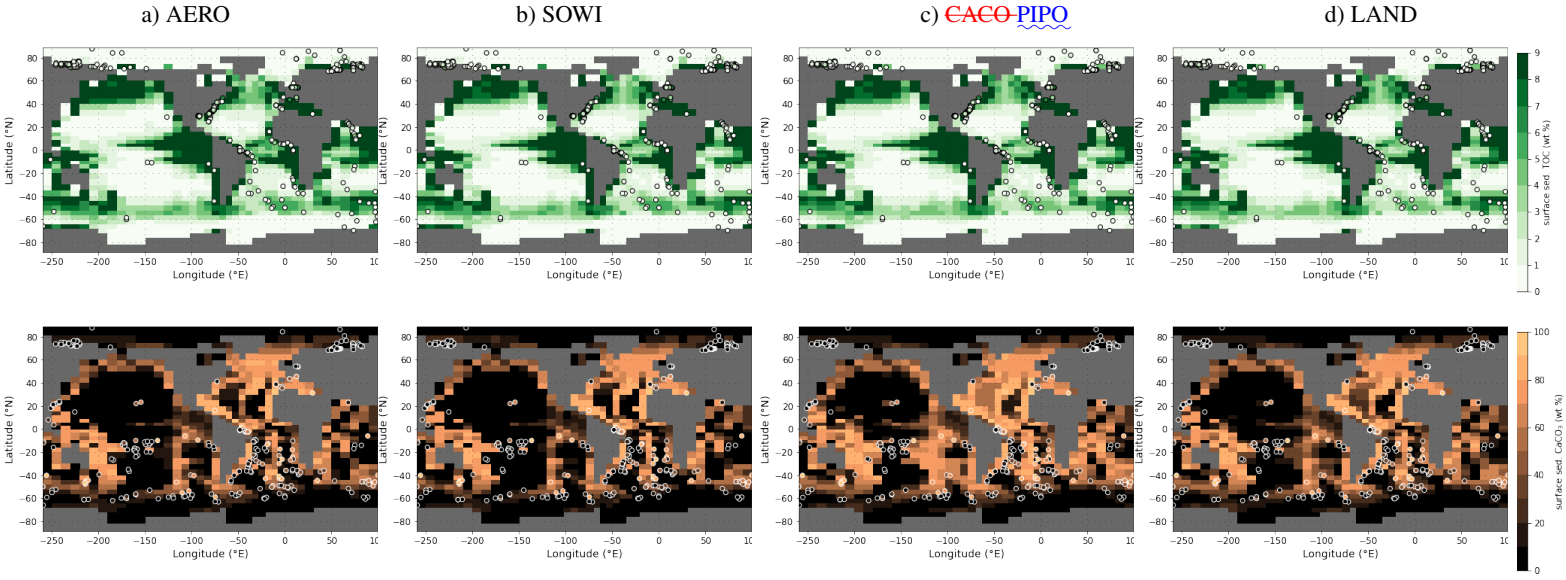

Figure S12. Sedimentary POC and $CaCO_3$ fractions during the late Holocene (Hayes et al., 2021) as reconstructed (circles) and in simulations AERO, SOWI, CACO and LAND (underlying maps). Shown are only data points that fall into the local benthic grid box of the model. The root mean square errors of simulated and reconstructed values are (from left to right): 8.8 %, 9.4 %, 7.6 % and 7.6 % for POC (top row) and 27.2 %, 27.8 %, 26.2 % and 26.6 % for $CaCO_3$ (bottom row).

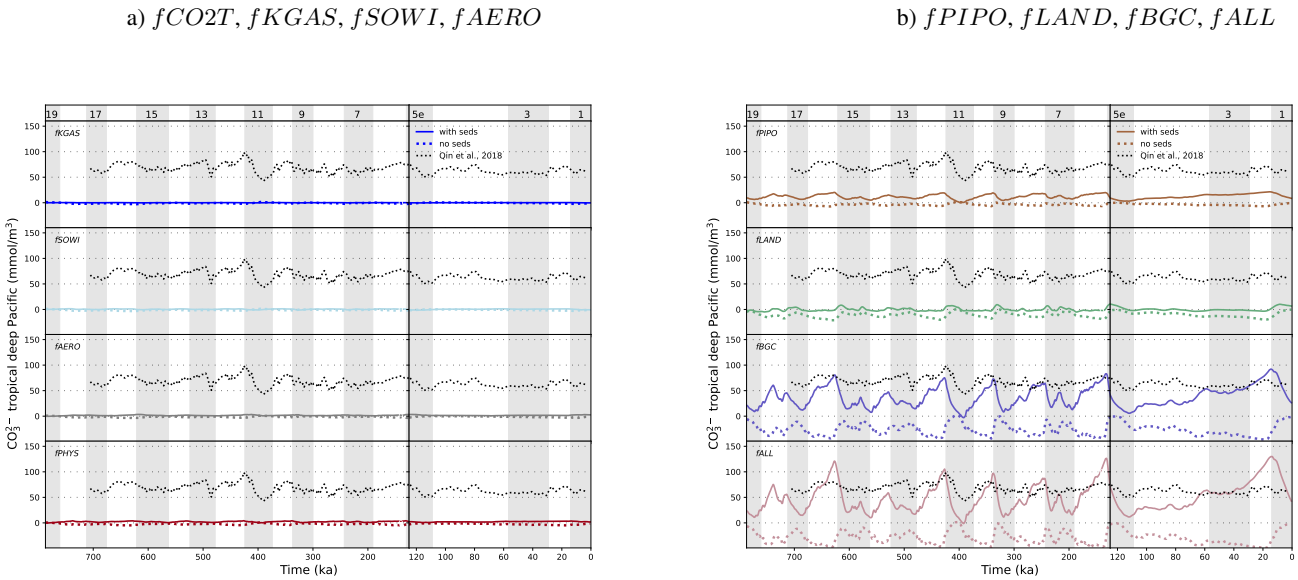

Figure S13. Transient variations of CO_3^{2-} in the tropical deep Pacific as simulated ~~in simulations~~ and reconstructed by Qin et al. (2018).

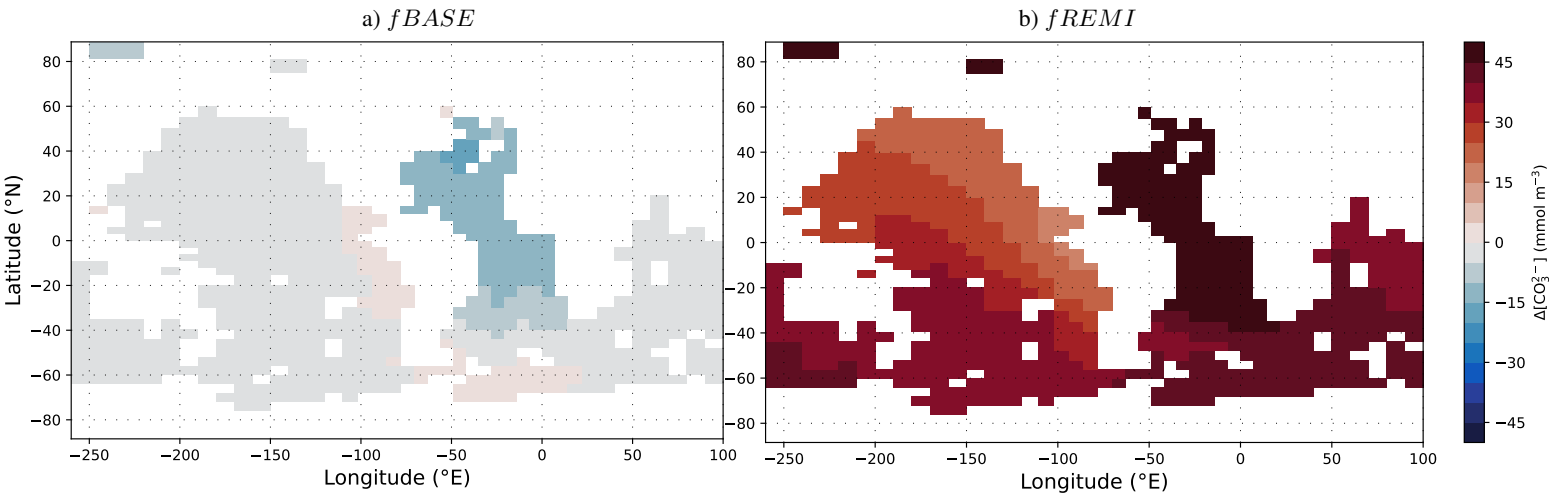

Figure S14. Selected factorial effects on simulated LGM-PI differences in deep CO_3^{2-} (3500 m depth).

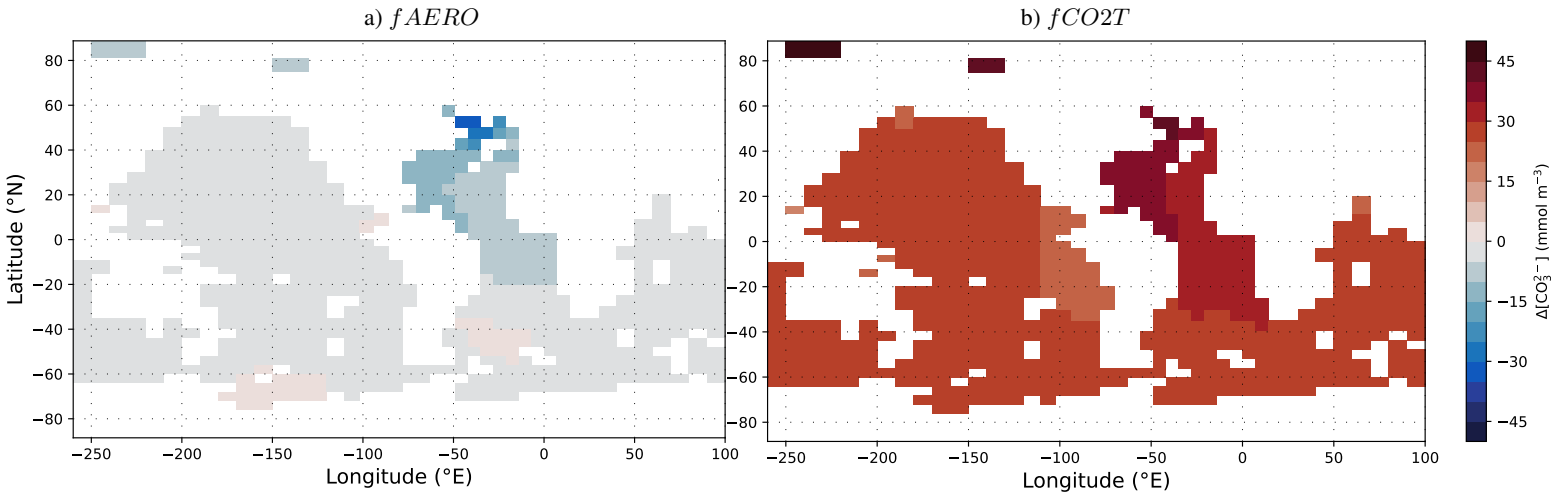

Figure S15. Selected factorial effects on simulated LGM-PI differences in deep CO_3^{2-} (3500 m depth).

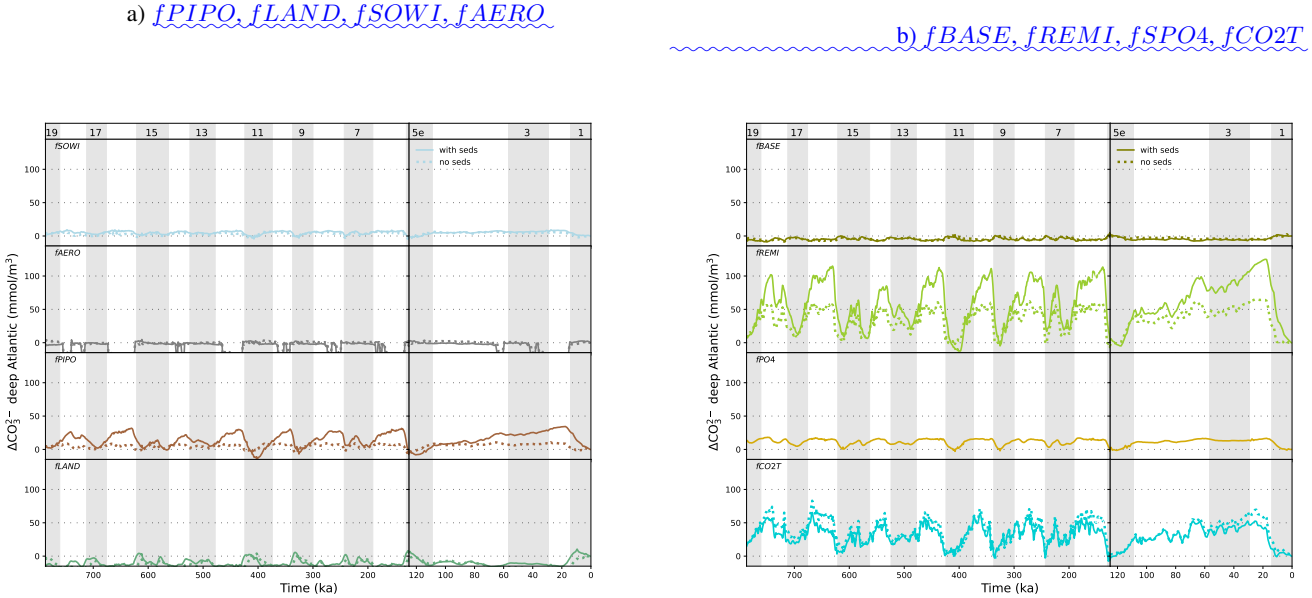

Figure S16. Transient variations of CO_3^{2-} in the deep North Atlantic (40-60 ○N) as simulated in selected simulations.

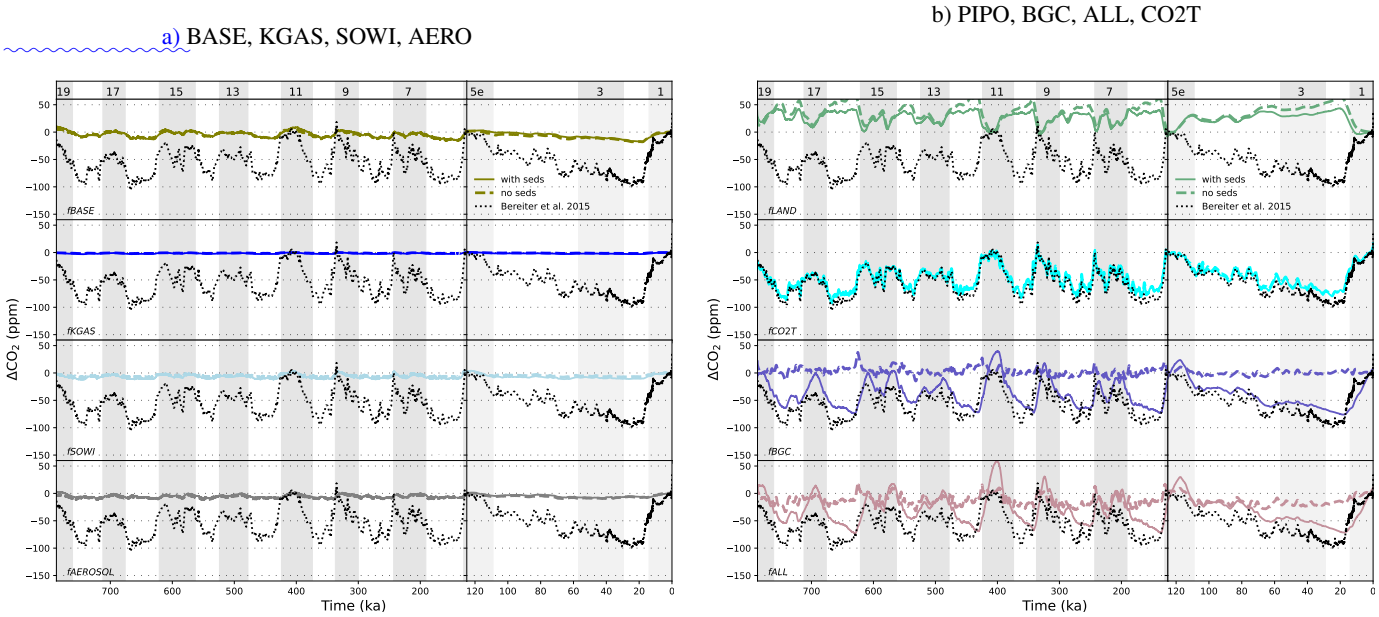

Figure S17. Transient variations of atmospheric CO_2 concentrations as simulated in the simulations not shown in Fig. 5 in the main text, and as reconstructed by Bereiter et al. (2015). Shown is the deviation from the respective pre-industrial value.

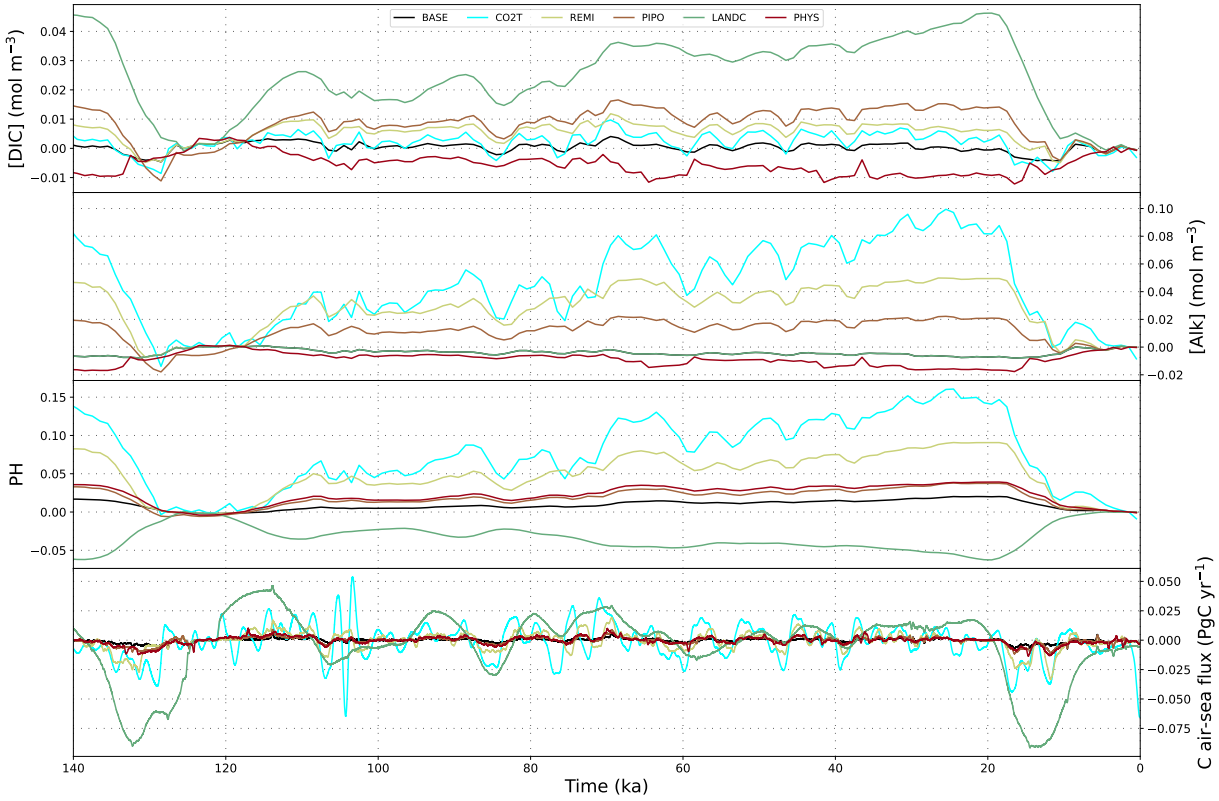

Figure S18. Globally-averaged changes in surface ocean carbonate system parameters in selected simulations without interactive sediments.

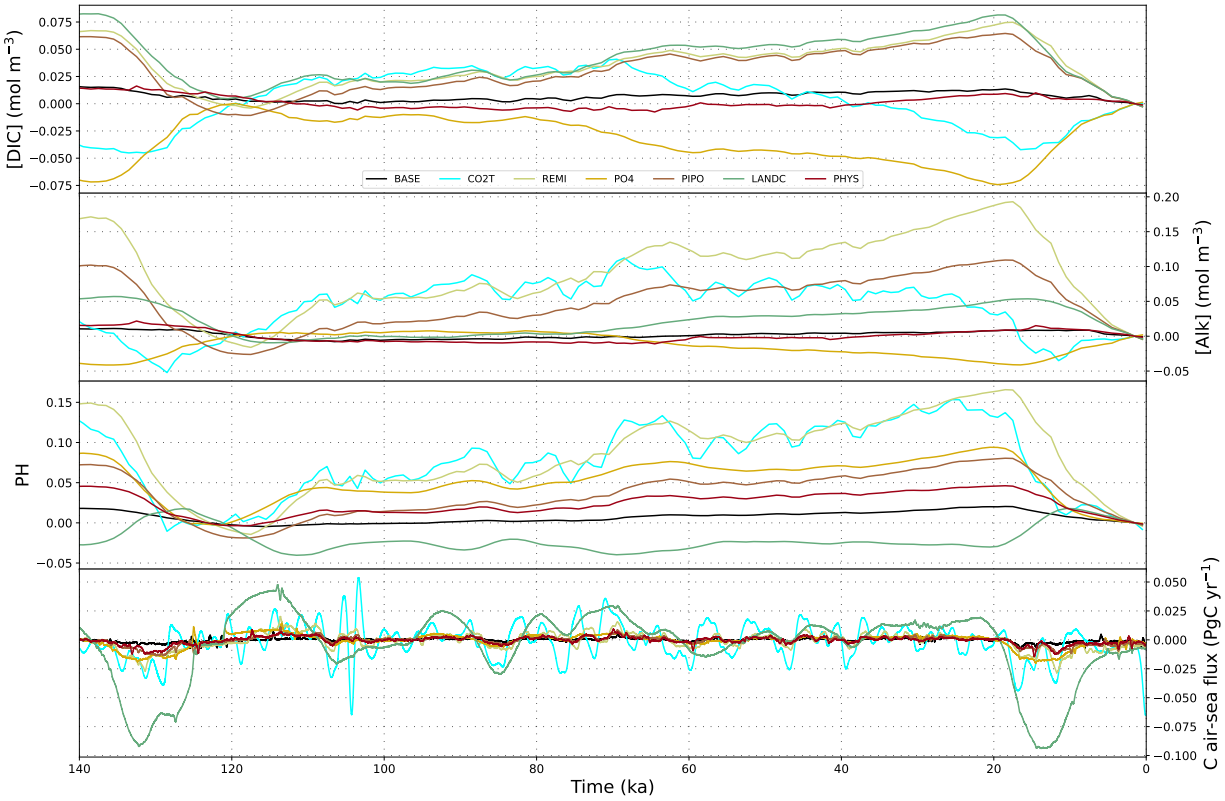

Figure S19. Globally-averaged changes in surface ocean carbonate system parameters in selected simulations with interactive sediments.

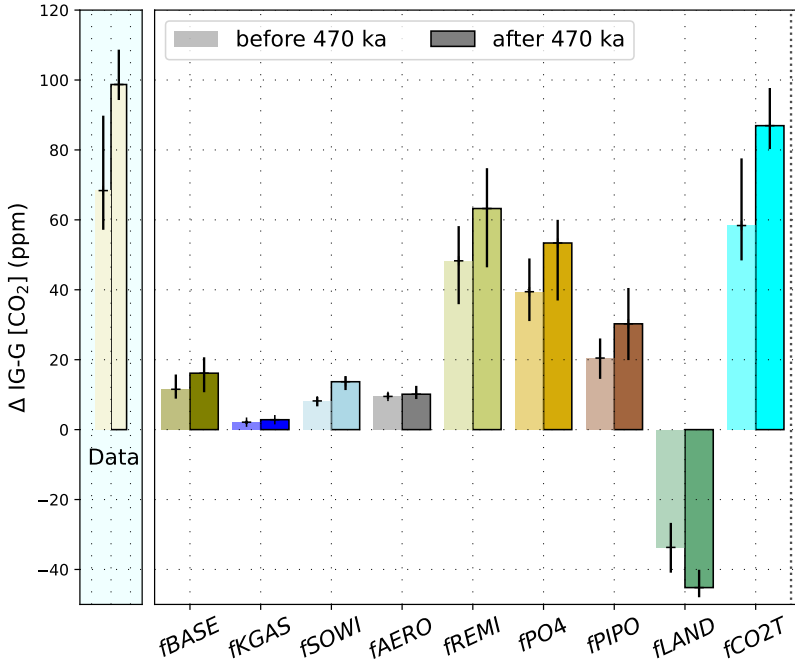

Figure S20. Difference of the glacial-interglacial atmospheric CO_2 amplitude before and after the MBT in our simulations compared to that in the reconstructed CO_2 record (Bereiter et al., 2015). For the results of the simulations without interactive sediments see Fig. S20

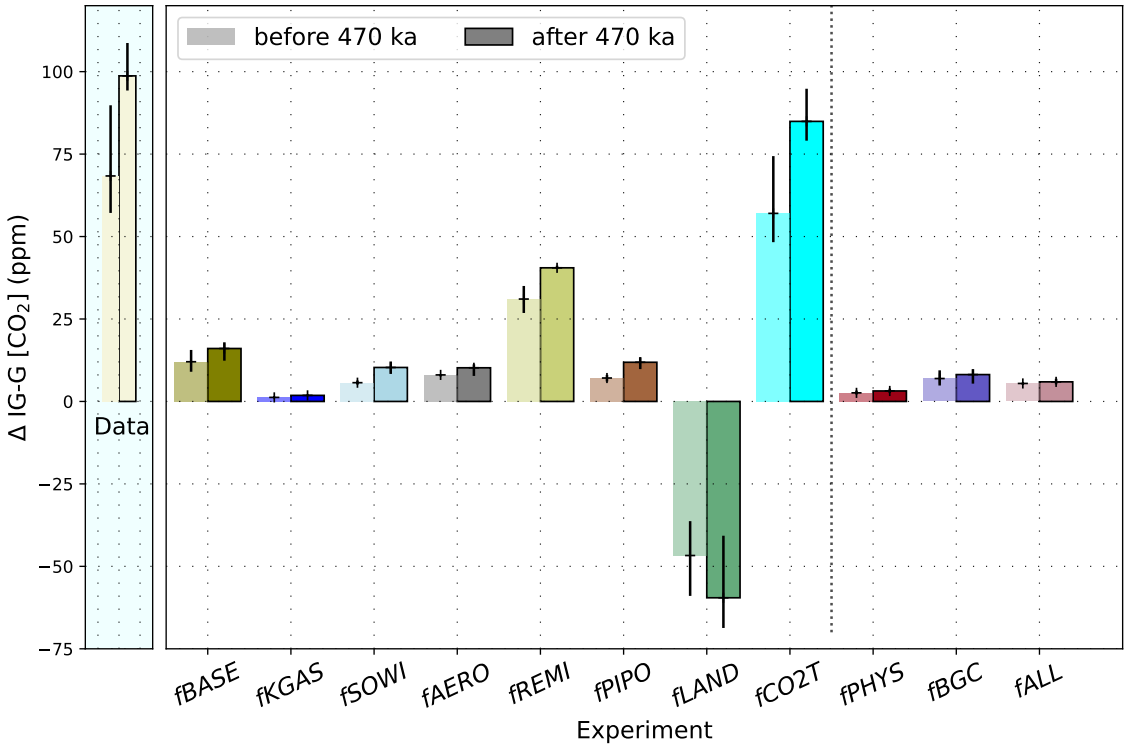

Figure S21. Difference of the glacial-interglacial atmospheric CO_2 amplitude before and after the MBT in our simulations without interactive sediments compared to that in the reconstructed CO_2 record (Bereiter et al., 2015, , horizontal black line).

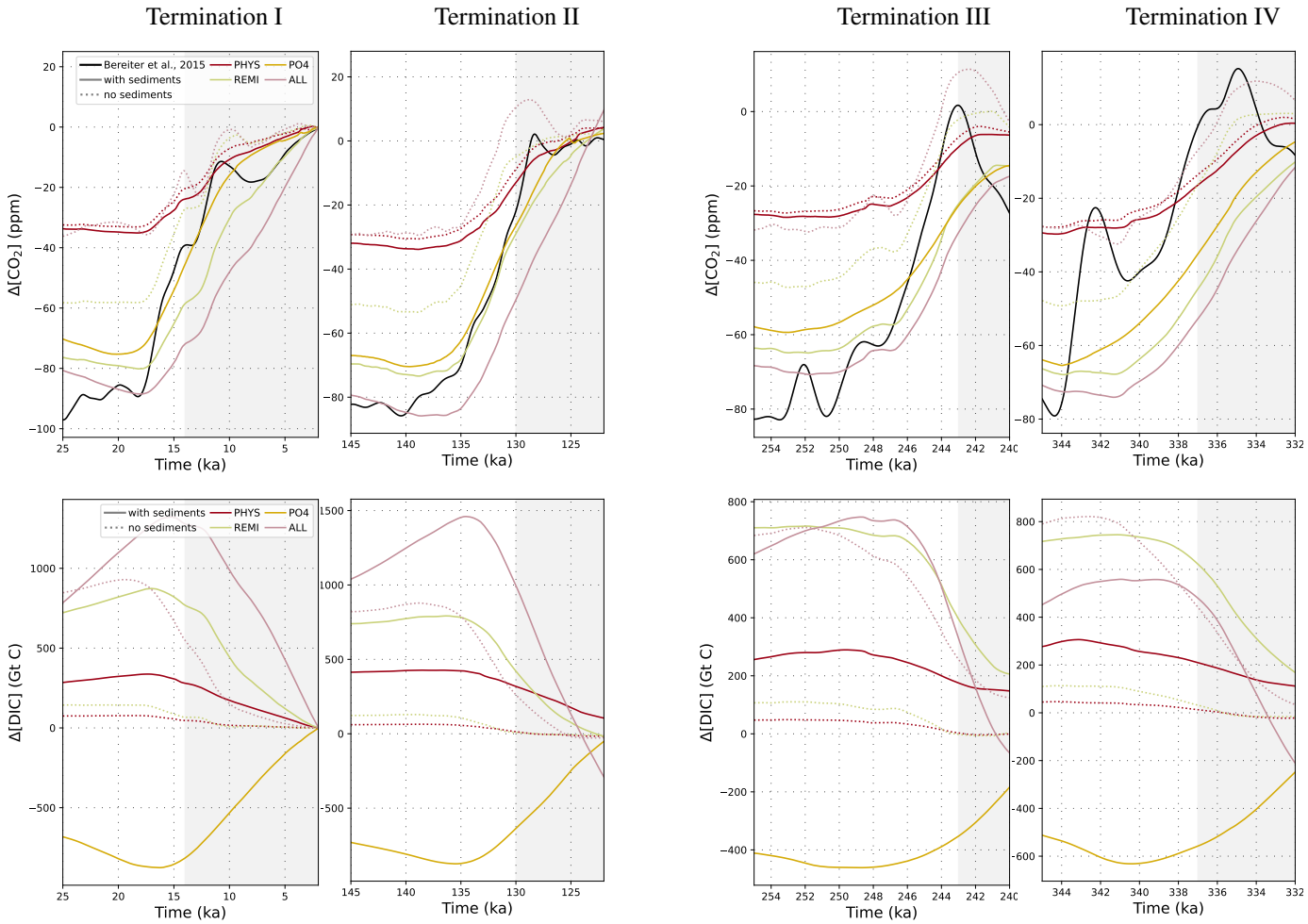

Figure S22. Reconstructed and simulated atmospheric CO_2 changes (upper row) and simulated DIC changes (lower row) across the last four deglaciations.

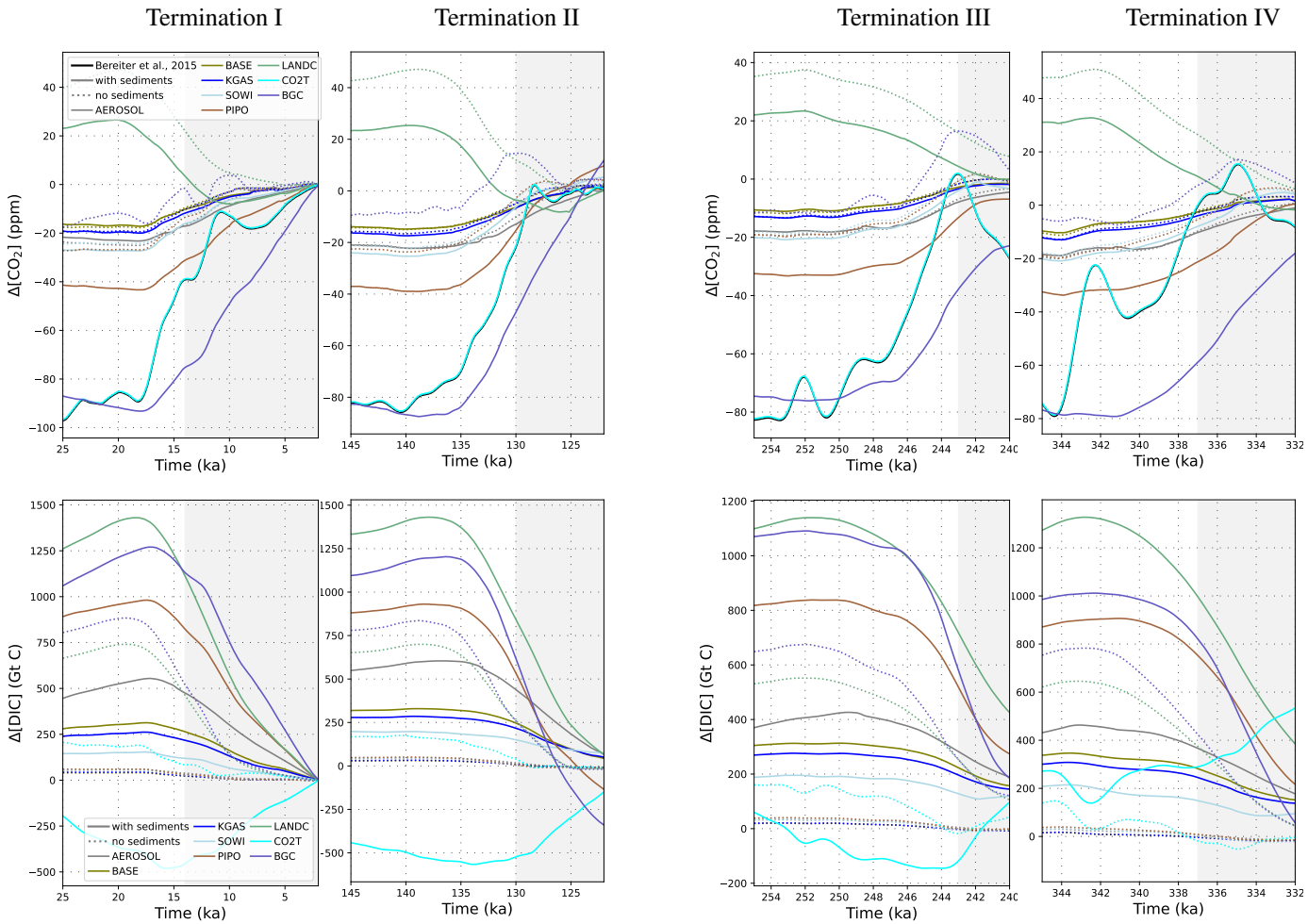

Figure S23. Reconstructed and simulated atmospheric CO_2 changes (upper row) and simulated DIC changes (lower row) across the last four deglaciations.

Table S2. Dynamical geologic carbon cycle imbalances (marine outputs - inputs) at the end of each simulation.

Simulation	DIC (GtC/yr)	ALK (Tmol eq/yr)	PO_4^{3-} (Tmol P/yr)	SiO (Tmol Si/yr)	DI^{13}C (GtC/yr/$^{13}C_{std}$)
BASE	0.017	1.51	0.006	-0.06	0.017
KGAS	0.015	1.32	0.005	-0.06	0.014
SOWI	0.009	0.94	0.003	0.21	0.009
AERO	0.030	2.99	0.008	0.39	0.030
REMI	0.018	4.85	0.006	0.47	0.018
PHOS	-0.045	-3.47	-0.016	-0.13	-0.045
CACO	0.035	4.84	0.005	-0.04	0.035
LAND	0.035	4.66	0.005	-0.04	0.035
CO2T	-0.05	-8.86	0.005	-0.08	-0.05
PHYS	0.016	2.00	0.003	0.28	0.016
BGC	0.028	11.30	-0.026	0.53	0.028
ALL	0.096	22.69	-0.026	1.37	0.097

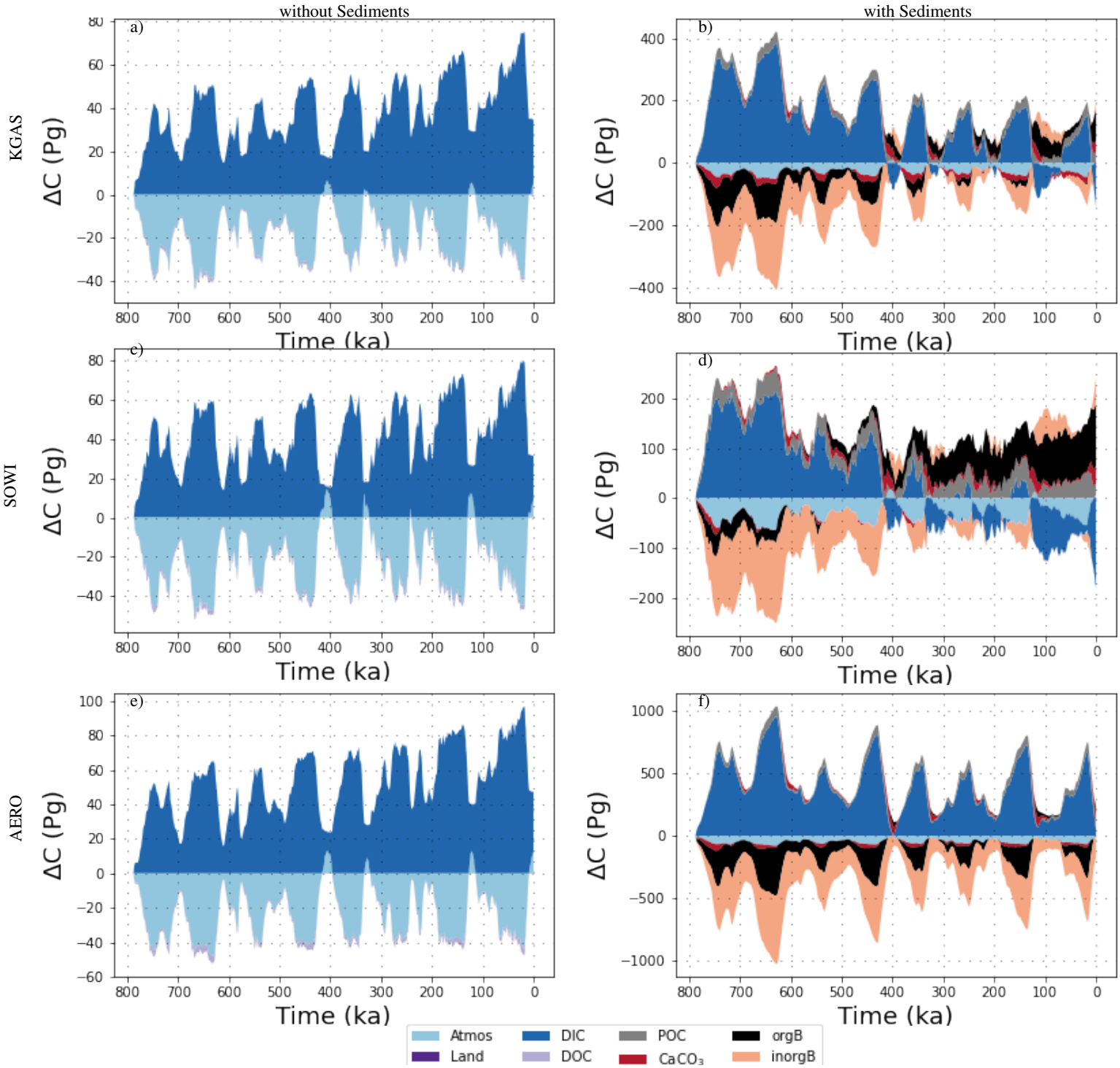

Figure S24. Transient carbon reservoir size changes across the last 780 kyr as simulated in simulations with the standard forcings plus additional physical forcings, left in a closed and right in an open system. Shown are the size changes of atmospheric, terrestrial, marine (DIC and DOC), sedimentary (POC and $CaCO_3$) and lithospheric (organic and inorganic) carbon storage.

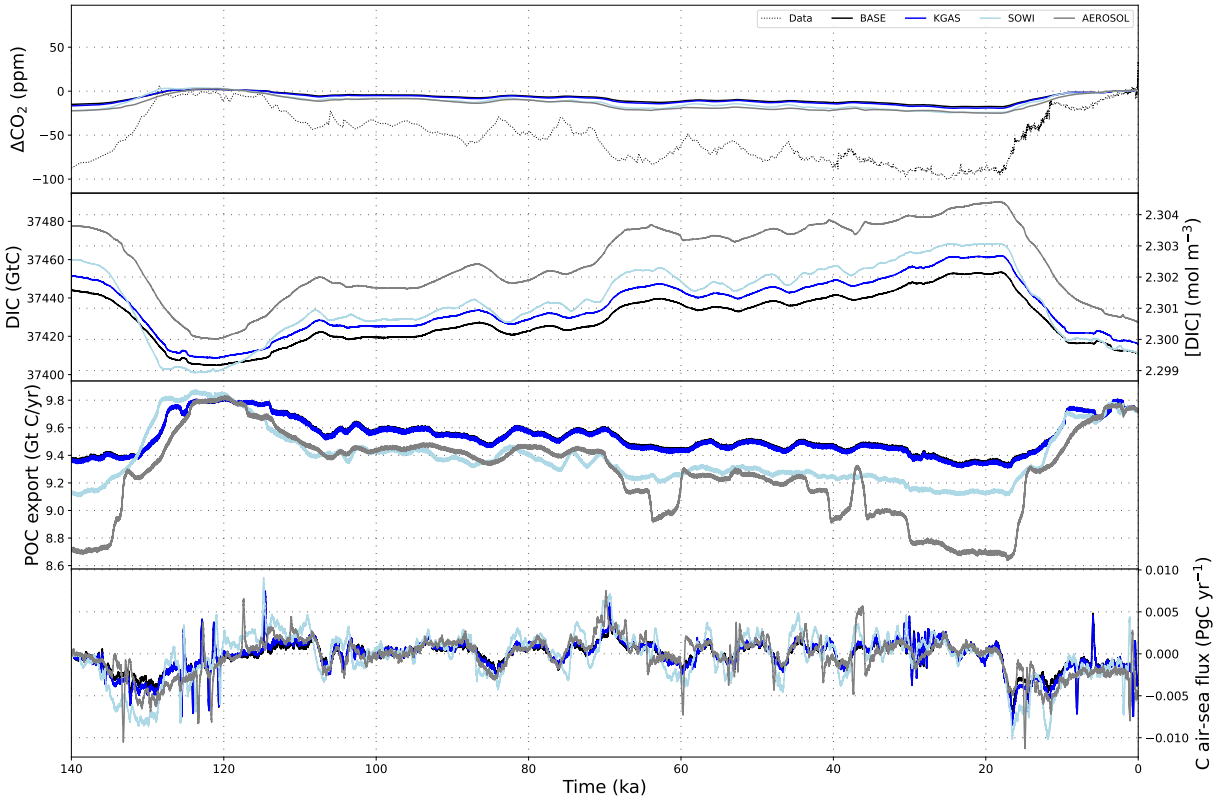

Figure S25. Atmospheric CO_2 concentrations, DIC and carbon fluxes over the most recent full glacial cyle in simulations with additional physical forcings and without dynamic sediments.

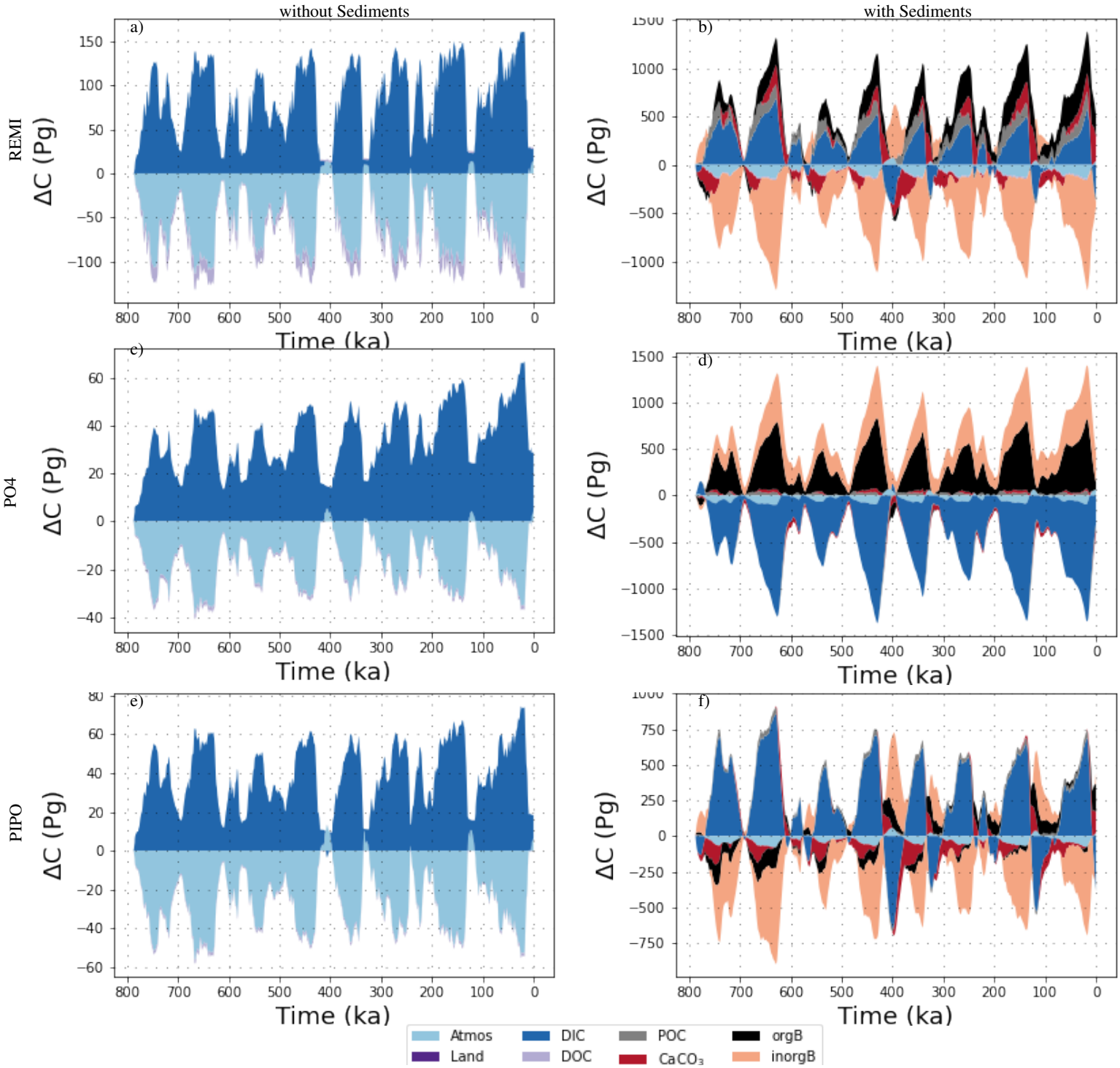

Figure S26. Transient carbon reservoir size changes across the last 780 kyr as simulated in simulations with the standard forcings plus additional biogeochemical forcings, left in a closed and right in an open system. Shown are the size changes of atmospheric, terrestrial, marine (DIC and DOC), sedimentary (POC and $CaCO_3$) and lithospheric (organic and inorganic) carbon storage.

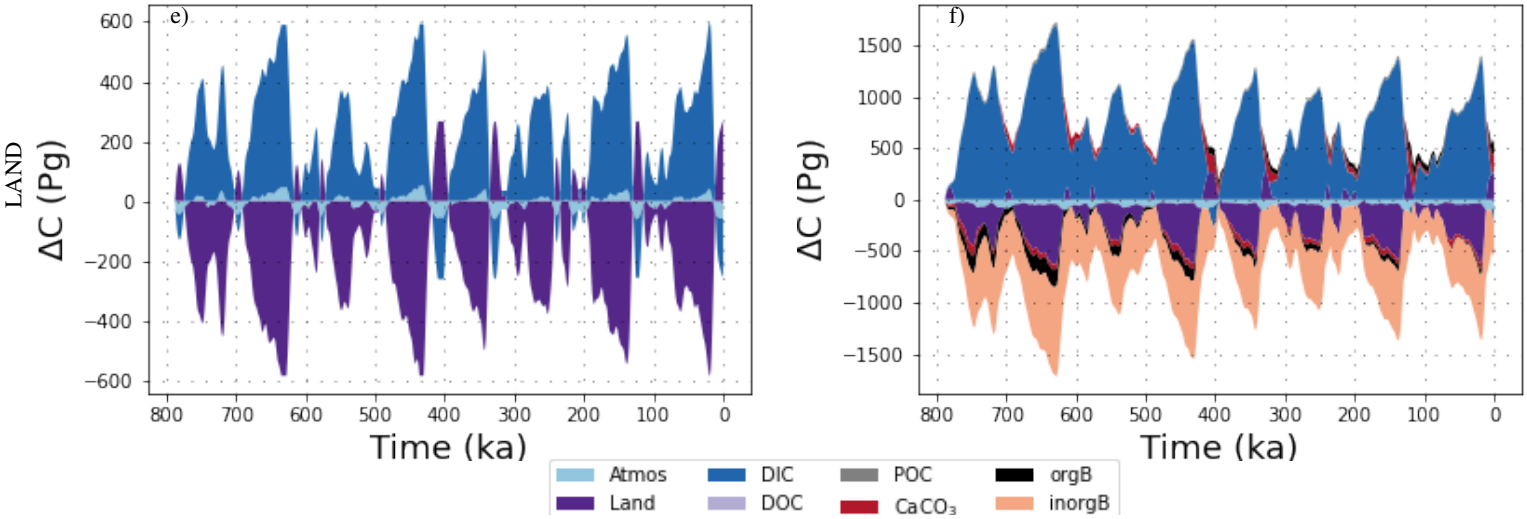

Figure S27. Transient carbon reservoir size changes across the last 780 kyr as simulated in simulations with the standard forcings plus terrestrial ~~C~~ carbon fluxes, left in a closed and right in an open system. Shown are the size changes of atmospheric, terrestrial, marine (DIC and DOC), sedimentary (POC and $CaCO_3$) and lithospheric (organic and inorganic) carbon storage.

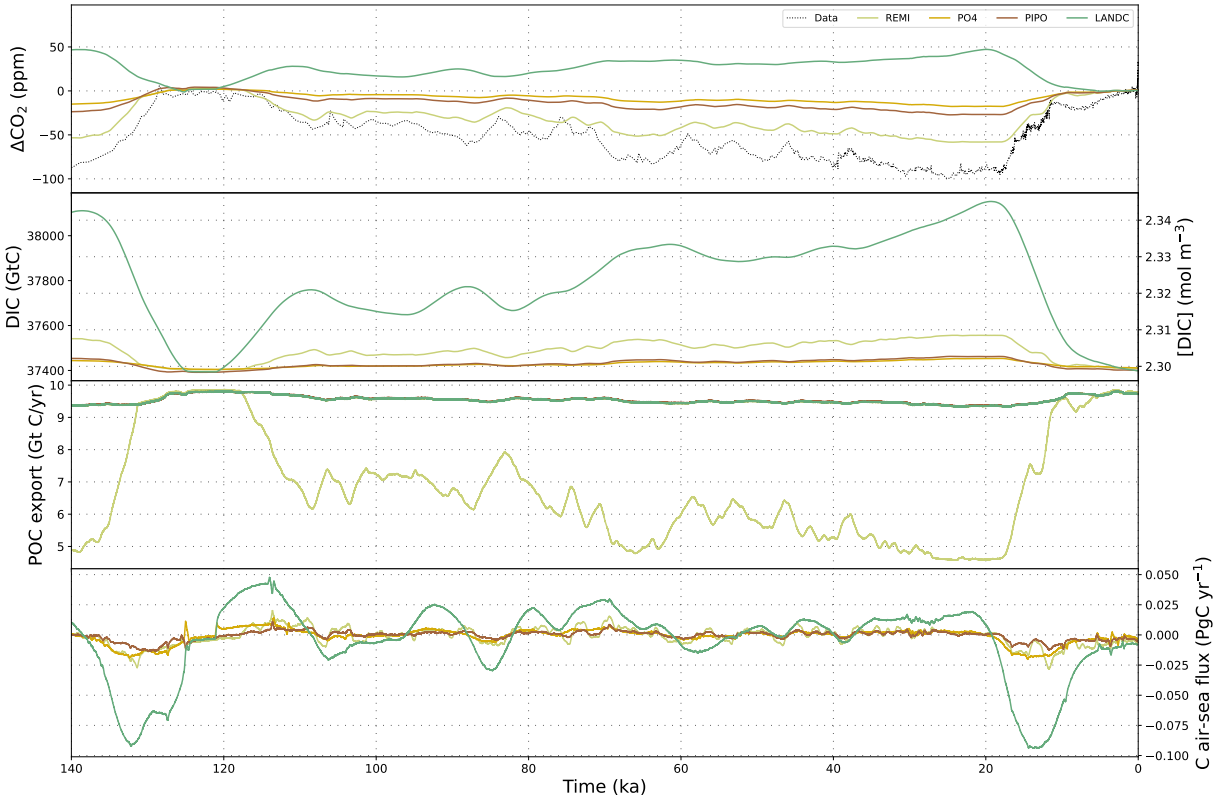

Figure S28. Atmospheric CO_2 concentrations, DIC and carbon fluxes over the most recent full glacial cyle in simulations with additional biogeochemical forcings and without dynamic sediments.

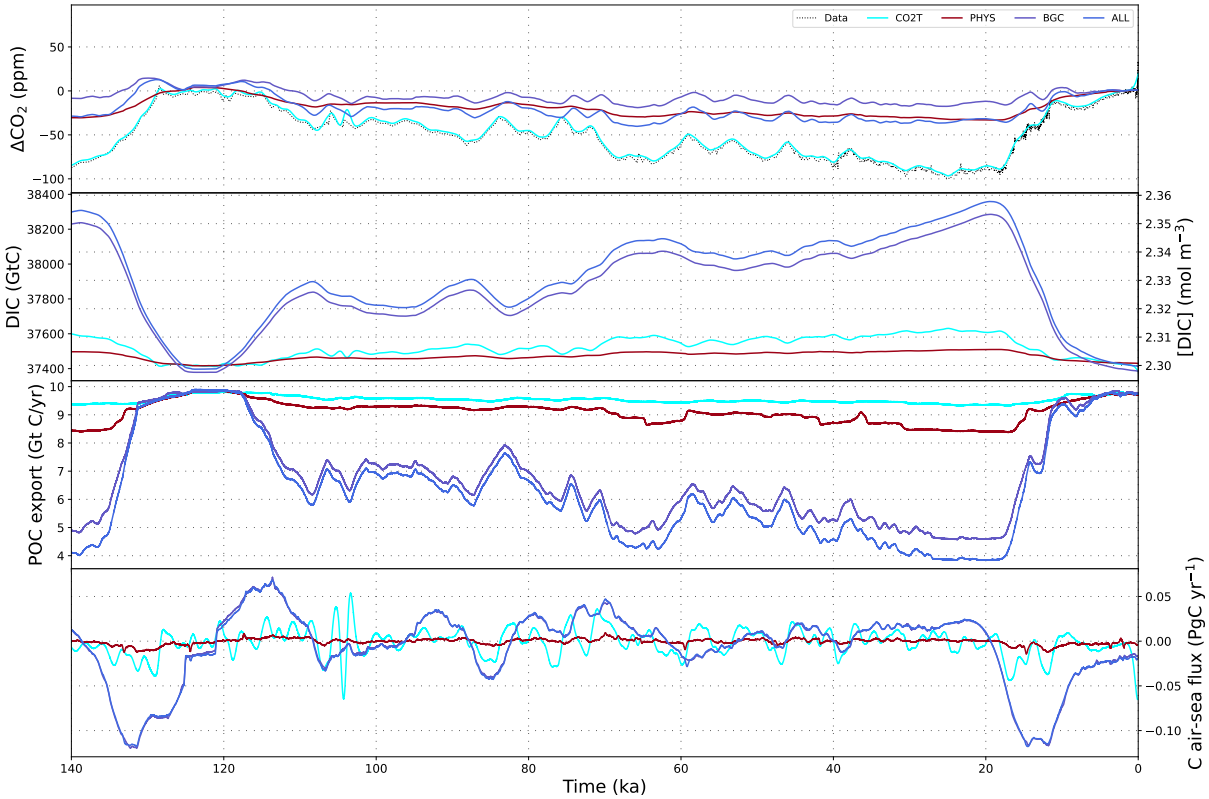

Figure S29. Atmospheric CO_2 concentrations, DIC and carbon fluxes over the most recent full glacial cyle in simulations with combinations of additional forcings and without dynamic sediments.

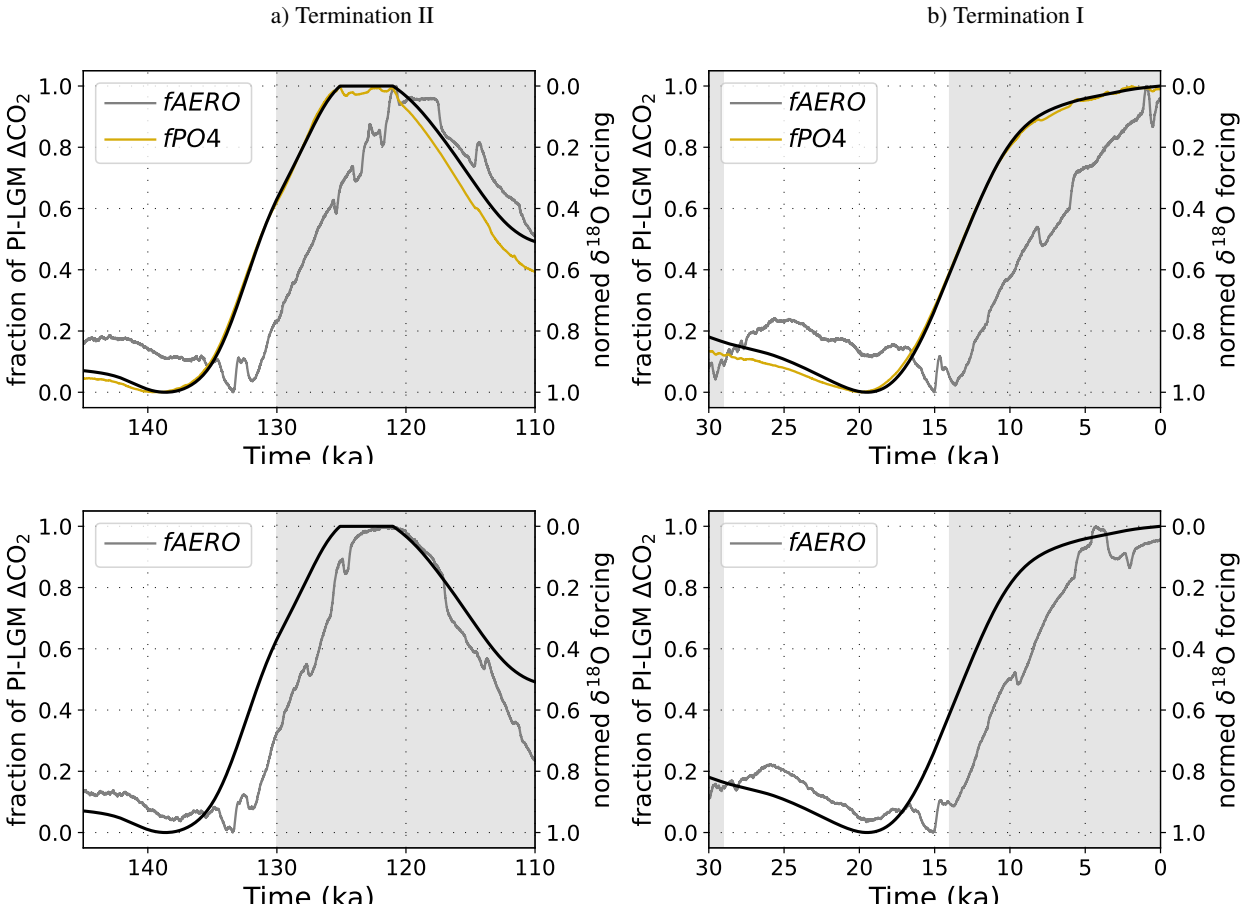

Figure S30. δ^{18}O-derived scaling of the prescribed forcing and the resulting simulated atmospheric CO_2, normalized by the respective PI-LGM CO_2 difference, in selected simulations with interactive sediments (top row) and without interactive sediments (bottom row).

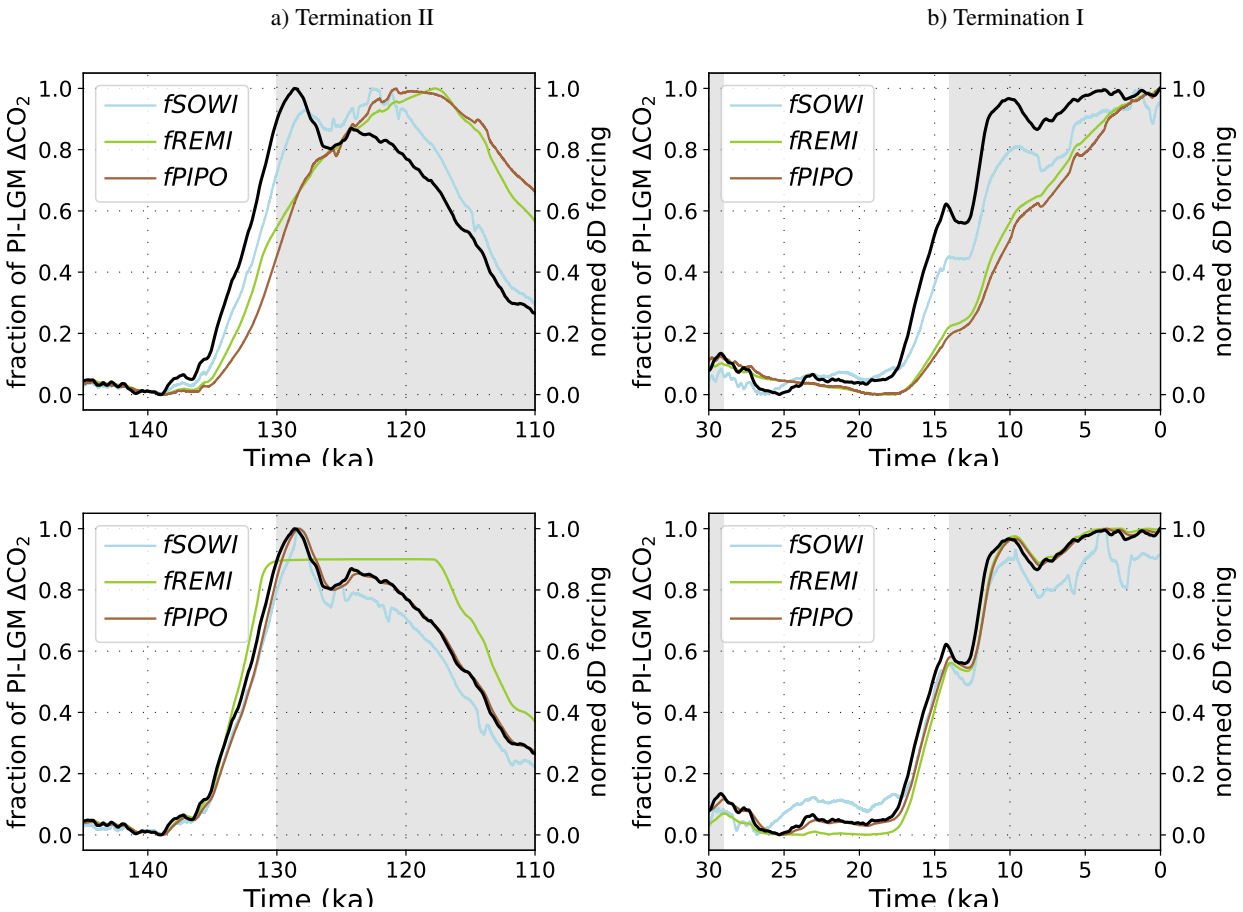

Figure S31. δD-derived scaling of the prescribed forcing and the resulting simulated atmospheric CO_2, normalized by the respective PI-LGM CO_2 difference, in selected simulations with interactive sediments (top row) and without interactive sediments (bottom row).